BI-LAYERED VISCOELASTIC MODEL FOR A STEP CHANGE IN VELOCITY AND A CONSTANT ACCELERATION STIMULUS FOR THE HUMAN OTOLITH ORGANS

by

M. Denise Coggins

Thesis submitted to the Faculty of the Virginia Polytechnic Institute and State University in partial fulfillment of the requirements for the degree of

MASTER OF SCIENCE

IN

ENGINEERING SCIENCE AND MECHANICS

APPROVED BY:

J. Wallace Grant, Chair

Daniel J. Schneck

Brian Love

October 1996

Blacksburg, Virginia

Keywords: *otolith, viscoelastic, gel layer, distributed parameter model, dynamic response*

BI-LAYERED VISCOELASTIC MODEL FOR A STEP CHANGE IN VELOCITY AND A CONSTANT ACCELERATION STIMULUS FOR THE HUMAN OTOLITH ORGANS

by

M. Denise Coggins

Committee Chairman: J. Wallace Grant

Engineering Science and Mechanics

(ABSTRACT)

The otolith organs are commonly modeled as a system consisting of three distinct elements, a viscous endolymph fluid in contact with a rigid otoconial layer that is attached to the skull by a viscoelastic gel layer. However, in this model the gel layer is considered as a bi-layered viscoelastic solid and is modeled as a simple Kelvin-Voigt material. The governing differential equations of motion are derived and nondimensionalized yielding three nondimensional parameters: nondimensional viscosity, nondimensional elasticity and nondimensional density. These nondimensional parameters are derived from experimental research. The shear stresses acting at the interface of the viscoelastic bi-layered gel are nondimensionalized and equated. The governing differential equations are then solved using finite difference techniques on a digital computer for a step change in velocity and a constant acceleration stimulus.

The results indicate that the inclusion of a viscoleastic bi-layered gel is essential for the model to produce greater otoconial layer deflections that are consistent with physiologic displacements. Future mathematical modeling of the otolith organs should include the effects of a viscoelastic bi-layered gel, as this is a major contributor to system damping and response and increased otoconial layer deflections.

Dedicated To:

Irving Coggins, Jr., Mirtis B. Coggins, and Alia L. Coggins

Acknowledgements

I would like to thank the following persons who played a role in the completion of this work:

To Dr. Grant I wish to extend my sincerest thanks for his time, effort and most of all his eternal patience.

Special thanks are given to Dr. Schneck for his guidance throughout my entire Master's program.

I also wish to thank Dr. Love for his constructive comments and for serving on my graduate committee.

Finally, and most importantly, I will always be indebted to my parents and family for their love and support of my continuing and perhaps never ending pursuit of my goals.

Table of Contents

Chapter 1

Introduction

Due mostly to the success of the Space Shuttle and long-term manned space stations, a new generation of space travel and research has emerged. However with the advent of space travel, problems related to exploration of space and debilitating physiologic conditions associated with extended exposure to a weightless environment have arisen. In fact, most passengers of NASA's Space Shuttle have experienced some form of motion sickness during their journey.

These concerns have sparked an increased interest in the function of the vestibular organs. The human vestibular system is located in the non-auditory portion of the inner ear. It is comprised of the semicircular canals and the otolith organs. The semicircular canals sense angular acceleration in three mutually perpendicular planes. The otolith organs sense not only 3-D linear acceleration but also change in gravitational direction relative to the skull.

The intent of this thesis is to present the development of a numerical model to quantify the behavior and response of the otolith organs to a step change in skull velocity and constant acceleration of the skull. An understanding of the anatomical structure and physiologic function of the otolith organ is necessary for the reader to more fully appreciate the model. A concise but complete discussion of pertinent anatomical

considerations is presented in Chapter 1. This chapter includes tests of otolith function. A short review of previous models of the otolith organ is also discussed in this chapter.

Chapter 2 introduces the governing equations presented by Grant [8] and briefly reviews the mathematics upon which these equations are based. Chapter 3 introduces finite difference theory in which the numerical model is developed from which a time dependent solution can be obtained. Discussion of results is subsequently presented in Chapter 4 and arguments are offered that provide endorsement for this work. Conclusions are drawn in Chapter 5. Suggestions are made for the improvement of the present model and for the direction in which future research might proceed. And finally, Chapter 6 provides a summary of the significance of this work.

1.1 Anatomy and Physiology

The human inner ear consists of two distinct sections, the auditory portion responsible for the sense of hearing and the non-auditory vestibular branch whose primary function is to sense and control equilibrium, in addition to visual image fixation. These inner ear sensors and the proprioceptors located throughout the body, enable messages to be sent directly to the Central Nervous System so that the magnitude, location and sense of any external stimulus may be identified and subsequent action taken to insure appropriate maintenance of equilibrium. The human ear is depicted in Figure 1.1a.

The receptors of the inner ear lie within a collection of fluid-filled tubes and chambers referred to as the membranous labyrinth. This membranous labyrinth contains a fluid called endolymph. This fluid is an isotonic solution that is of high potassium and low sodium concentration.

The bony labyrinth is a shell of dense bone that surrounds and protects the membranous labyrinth. It is fused to the surrounding temporal bone. The bony labyrinth, can be subdivided into the semicircular canals, cochlea and the vestibule.

- The semicircular canals enclose slim semicircular ducts. These three canals are stimulated by rotation of the head.
- The bony cochlea contains the cochlear duct of the membranous labyrinth. Receptors within the cochlear duct provide the sense of hearing.
- The vestibule includes a pair of membranous sacs, the saccule and the utricle. Receptors in the saccule and utricle provide sensations of gravity and linear

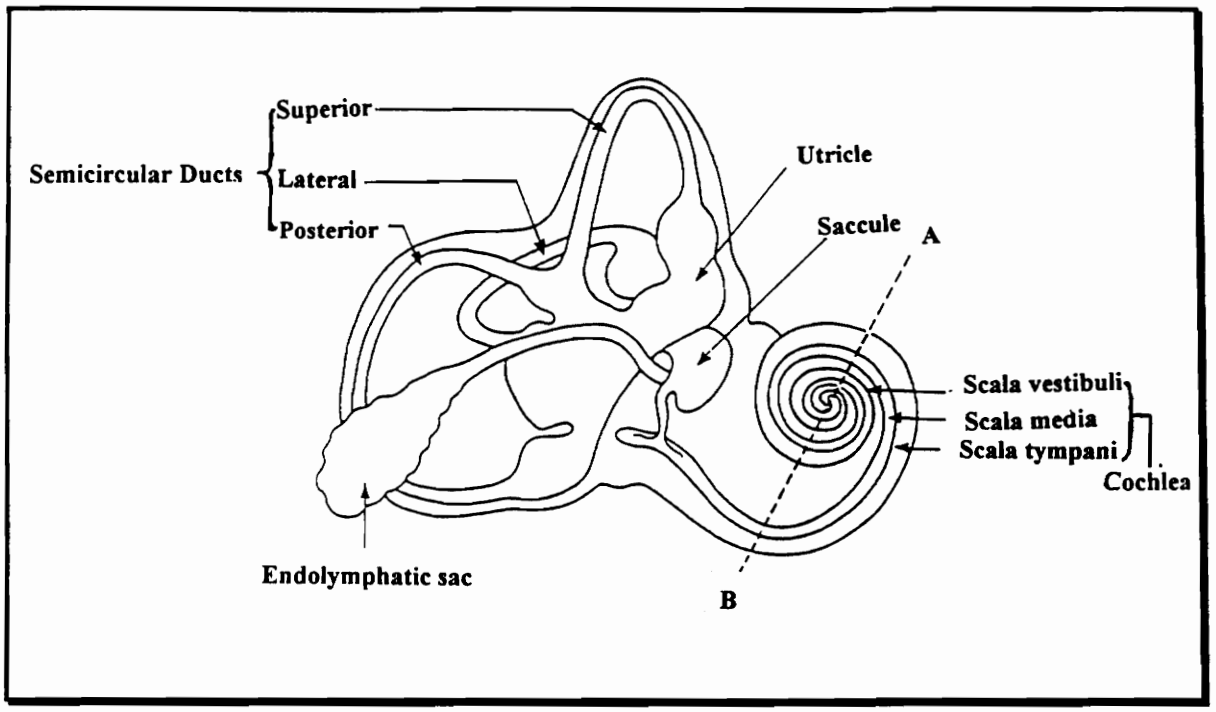

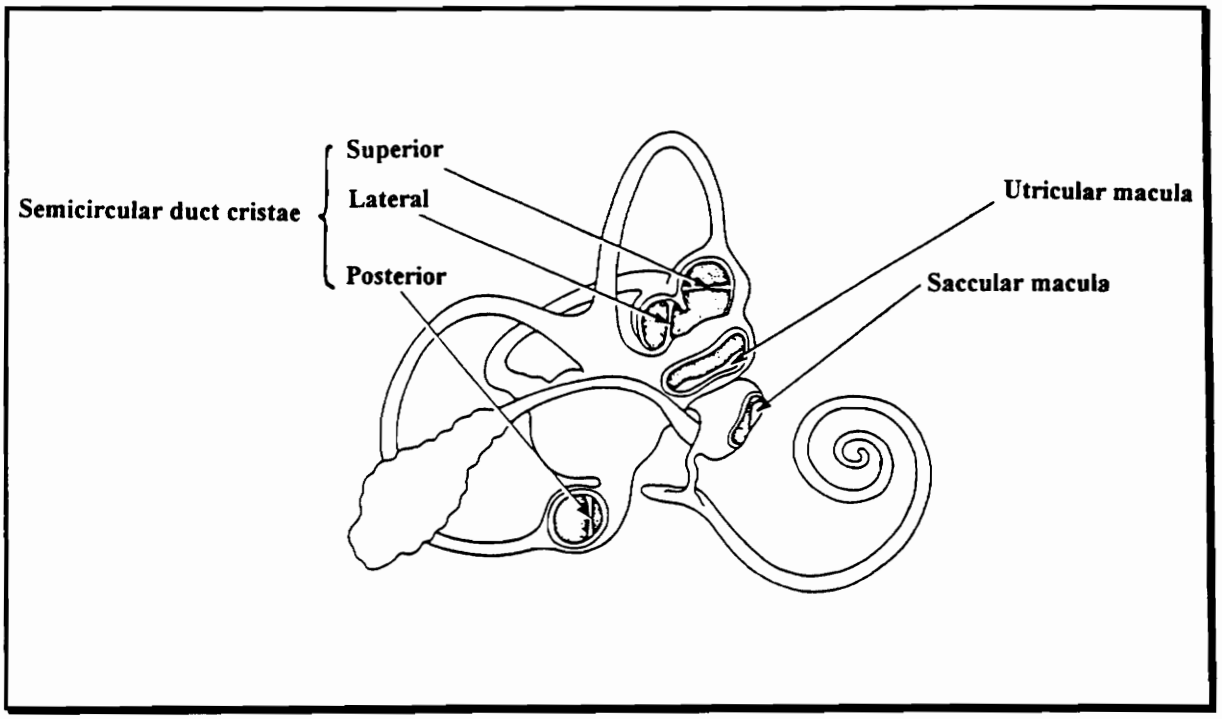

FIGURE 1.1a -**Top Figure**: Schematic drawing of the inner ear
Bottom Figure: The vestibular sensory epithelia: cristae in the semicircular ducts; maculae in the utricle and saccule, Reproduced from [1].

acceleration.

Two otolith organs are found in each human ear. These organs are contained in saclike vessels filled with endolymph and are situated in the vestibule of the bony labyrinth. The macula contained in the utricle is called the utricular macula. It lies on the floor of the vessel in a plane parallel to that of the lateral (horizontal) semicircular canal. The utricular macula sends nervous impulses to the upper portion of the vestibular nerve. The saccular macula, situated in the saccule, lies in a plane orthogonal to the utricular macula. The saccular macula sends nervous impulses to the lower portion of the vestibular nerve. This perpendicular structure enables the otolith system to effectively sense motion and gravity in each of three mutually orthogonal axes. This system is illustrated in Figure 1.1b.

The composition of each otolith consists of three distinct constituents; the otoconial membrane, the gelatinous membrane, and the endolymph fluid. The human otolith organ is depicted in Figure 1.1c. The otoconial membrane is an aggregation of stone-shaped calcium carbonate crystals, referred to as otoconia. The density of these calcium carbonate crystals is 2.71 gm/cm^3 [2]. The otoconial membrane has an approximate thickness of 20 to 30 microns [12]. It has an approximate surface area of $2mm^2$ [6]. This membrane is bounded on its top surface by endolymph fluid (ρ=1.0002) and underneath by a very elastic deformable gelatinous material, the gelatinous membrane or gel layer.

This gelatinous membrane is formed of amorphous and fibrillar material [13]. This gelatinous material is rigidly attached to the wall of the utricle or saccule which is secured

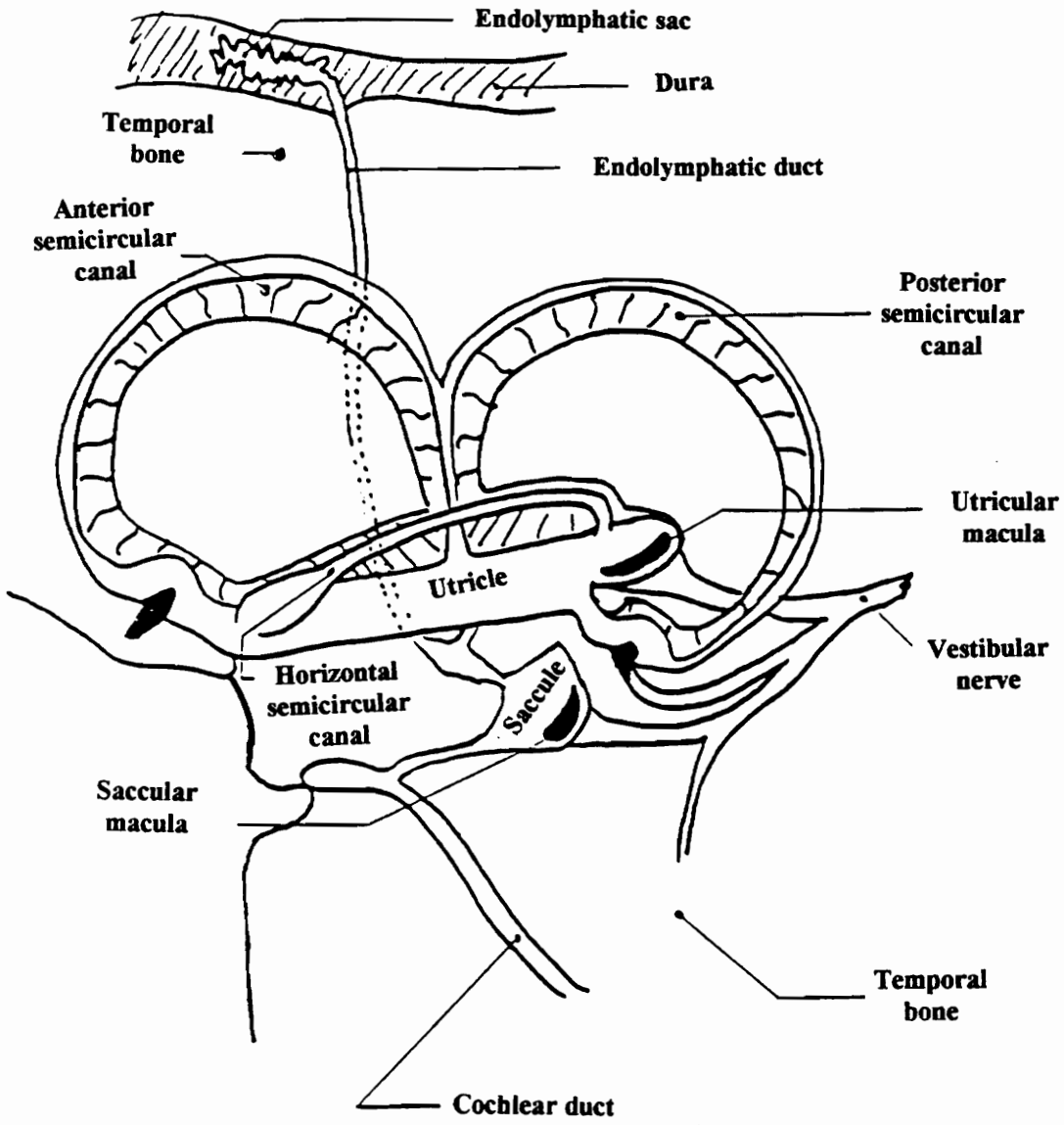

FIGURE 1.1b - Schematic of inner ear, showing locations of maculae, Reproduced from after de Burlet, 1929.

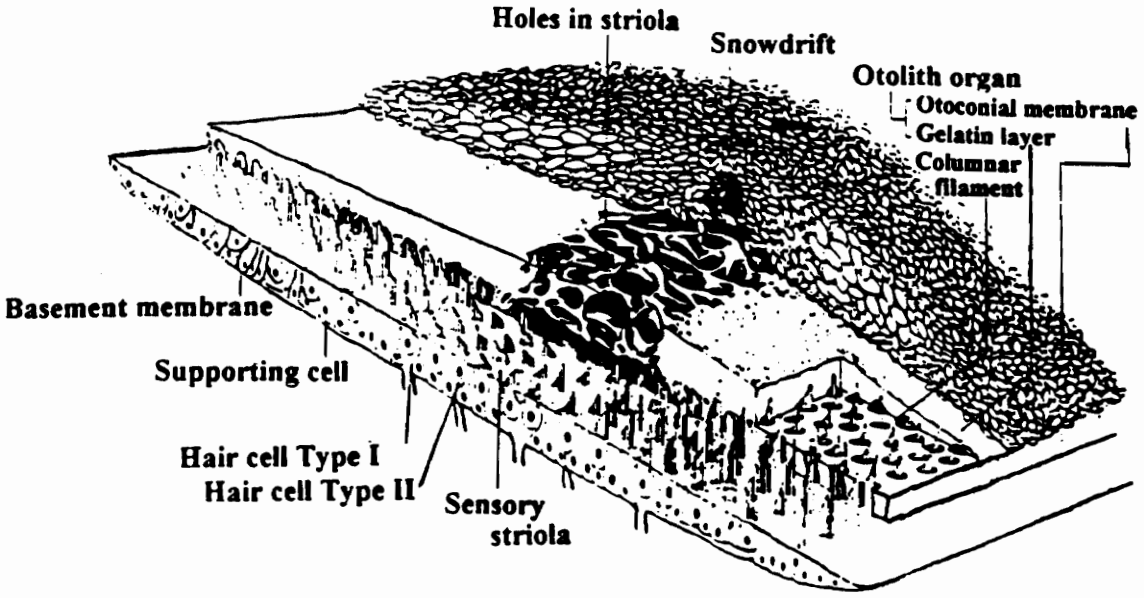

FIGURE 1.1c - Artist's view of a cross-section of the saccule showing the substructures of the otolith organ, Reproduced from [13].

to the temporal bone of the skull. The gelatinous membrane consists of two discrete parts; the upper portion (gelatin layer) to which the otoconia are attached and the lower portion (columnar filament) which houses the tall ciliary bundles of the sensory cell base. This sensory cell base is composed of specialized sensory cells which sense the deformation of the gelatinous membrane. The sensory cell base and membranous tissues are rigidly attached to the skull and move with any motion of the head. The work of Kachar, et. al. [12] suggests that the columnar filament has a more loosely arranged meshwork than the gelatin layer. This columnar filament has an approximate thickness of 5 to 8 microns [12]. The thickness of the gelatin layer is approximately 15 to 22 microns.

The sensory hair bundles project outward from the utricular and saccular walls into the gelatinous membrane. When there is no skull motion, these hair bundles generate a resting action potential [19]. During changes in acceleration, such as an external disturbance, the differences in densities between the endolymph fluid, gelatinous membrane and the otoconial membrane cause a shearing of the gelatinous membrane. The denser otoconial membrane mass tends to lag behind the sensory cell base due to its inertia and this relative motion results in deforming the gelatinous membrane in shear. Similarly, any tilting of the skull with respect to the gravity vector will result in the weight of the otoconial membrane producing a shearing deformation of the gelatinous membrane. This shearing of the gelatinous membrane bends the hair bundles, altering their firing rates. The hair bundles transduce the deformation into two different types of signals depending upon their location in the sensory cell base. As illustrated in Figure 1.1d, the sensory cells

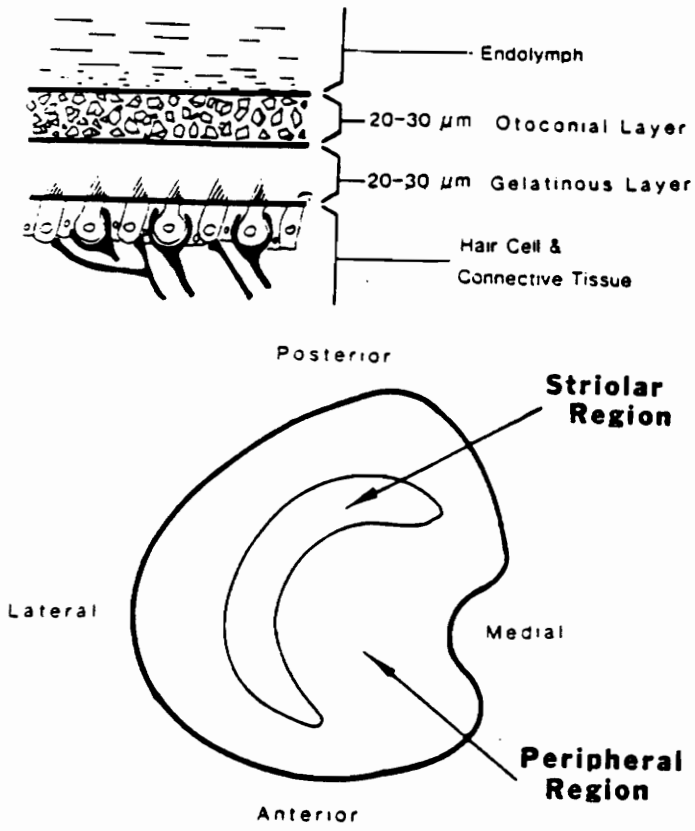

FIGURE 1.1d - **Top figure:** Otolith organ shown in cross section. **Bottom Figure:** Top view of the utricular otolithic membrane showing peripheral and striolar regions, Reproduced from [6].

in the peripheral region generate nervous signals which are proportional to the relative displacement of the otoconial membrane measured with respect to the sensory cell base. Sensory cells in the striolar region produce a nervous signal proportional to the velocity of the otoconial layer measured with respect to the sensory cell base [6]. The sensory cells in this region are also illustrated in Figure 1.1d. These two types of sensory signals are then transmitted to the central nervous system. Peripheral cells consist primarily of histologic Type II cells and striolar cells consist primarily of histologic Type I cells [6]. These altered nerve action potentials are sent through the Central Nervous System to the brain, where the two types of sensory signals are utilized to provide changes in visual fixation and postural control. The work of Wersäll and Lundquist [19] shows that each hair bundle is directionally sensitive, so that different shearing directions produce different action potentials in different hair bundles. The approximate directionality at various locations on each macula is illustrated in Figure 1.1e. The directionally sensitive hair bundles and the two mutually orthogonal maculae enable the otolith system to sense motion in three perpendicular planes.

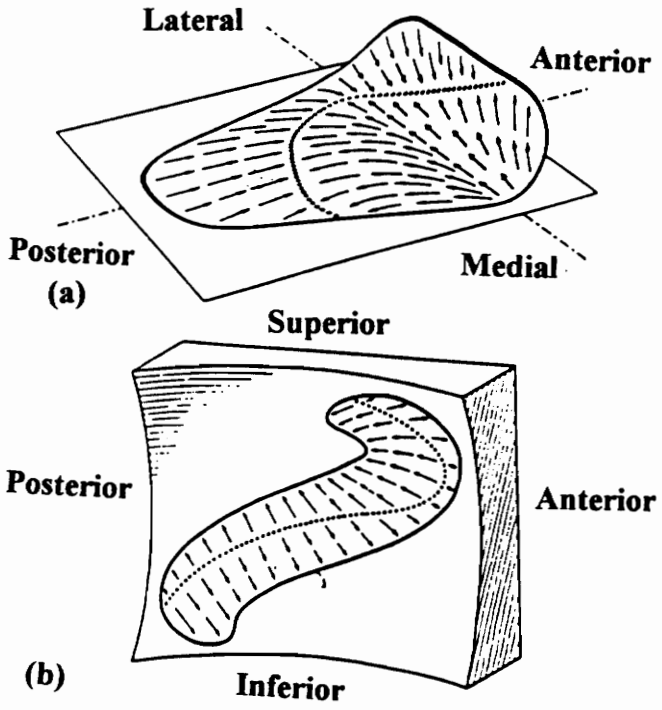

FIGURE 1.1e - Schematic representation of the direction of the sensory hairs. **(a)** In the macula utriculi; and **(b)** in the maculi sacculi, Reproduced from [17].

1.2 *Tests for Otolith Function*

Both sensations and reflexes are used to test otolith function in humans for clinical purposes or to determine the degree of normality of the vestibular system. Two functional tests of the otolith organs are discussed in this section: oculogravic illusion and ocular counterolling. In these tests, natural mechanisms and reflex pathways are used. There is no decrease in thresholds of response or to adaptation effects in these tests [9].

Oculogravic illusion is defined as an apparent movement and displacement of the visual field when a person is exposed to a change in direction of the gravitational-inertial force environment relative to himself [10]. It is known that persons who have healthy otolith organs may perceive the illusion [14]. Failure to perceive the illusion has been ascribed to loss of function of the otolith organ [19]. However, few studies are carried out on subjects with labyrinthine defects, and very few quantitative data are available [10]. In this functional test, a person is subjected to a change in direction of the gravitoinertial vertical with reference to himself, this circumstance is rightly interpreted as body tilt away from the upright [11]. A person with closed eyes is seated facing the direction of rotation. The person is exposed to a centripetal force of 1.0G. With eyes closed the person interprets the counterclockwise rotation of the environment as the clockwise rotation. The person has a sensation of being tilted in a rightward direction in a room that is upright. With opened eyes, the fixation target will appear to have rotated to position 1 in Figure 1.2. If the person is requested to set the line of the fixation target to

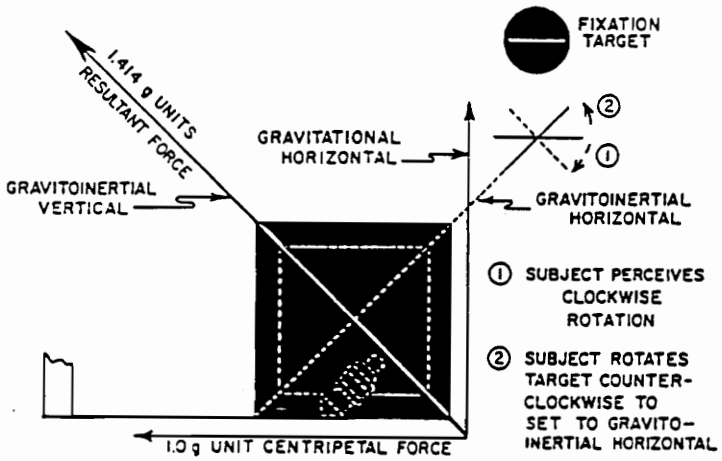

FIGURE 1.2 - Subject in the dark facing away from direction of rotation fixating a luminous line regards himself as tilted in an upright room, Reproduced from [11].

the earth's horizontal, the individual will rotate it counterclockwise from its original setting toward the gravitoinertial horizontal (position 2).

Ocular counterolling can be defined as the involuntary conjugate rolling movement of the eyes around their lines of sight in the direction opposite to the leftward or rightward tilted position of the head (and body) relative to the gravitational or gravitoinertial upright [9]. Ocular counterolling measurements can be made from photographs of iris landmarks obtained in the upright and tilt positions. The person must focus on a dim light in darkness prior to recordings of an electronic flash. The amount of roll is measured in minutes of arc and often expressed as an index [15] defined as one half the sum of the maximum roll associated with the range of leftward and rightward tilt employed. In persons with labyrinth defects, there is very little ocular counterolling [16]. The oculogravic illusion and ocular counterolling tests can determine the absence or presence of otolithic function.

1.3 Previous Models

Grant, Best, and LoNigro [5] developed a distributed parameter model representing otoconial layer displacement in response to inertia of the skull and gravity. These authors modeled the otolith organs as a system of three homogeneous isotropic materials: the endolymph fluid, the otoconial layer and the gel layer. The height of each material remained constant. The otoconial layer was treated as a rigid body. Because the width and length of the otoconial membrane were assumed to be several orders of magnitude larger than the height, the end effects on the plate were neglected. This simplified model is shown in Figure 1.3. In this work, the gel layer was modeled as a linear elastic material. The material was in simple shear, which produced a linear displacement profile when it was deformed.

This model yielded displacements that greatly exceeded expected results. The otoconial layer displaced several times its thickness for reasonable values of gel elasticity. These large displacements would definitely cause permanent damage to the material. When the elasticity increased to provide smaller displacements, the otoconial layer returned to its equilibrium position too quickly which caused the system to oscillate. DeVries' [4] discovery suggested that the system is overdamped which would indicate that the otolith organ has a velocity sensing capability. Human sensation of motion is not oscillatory. Subsequently, the oscillatory response is incorrect.

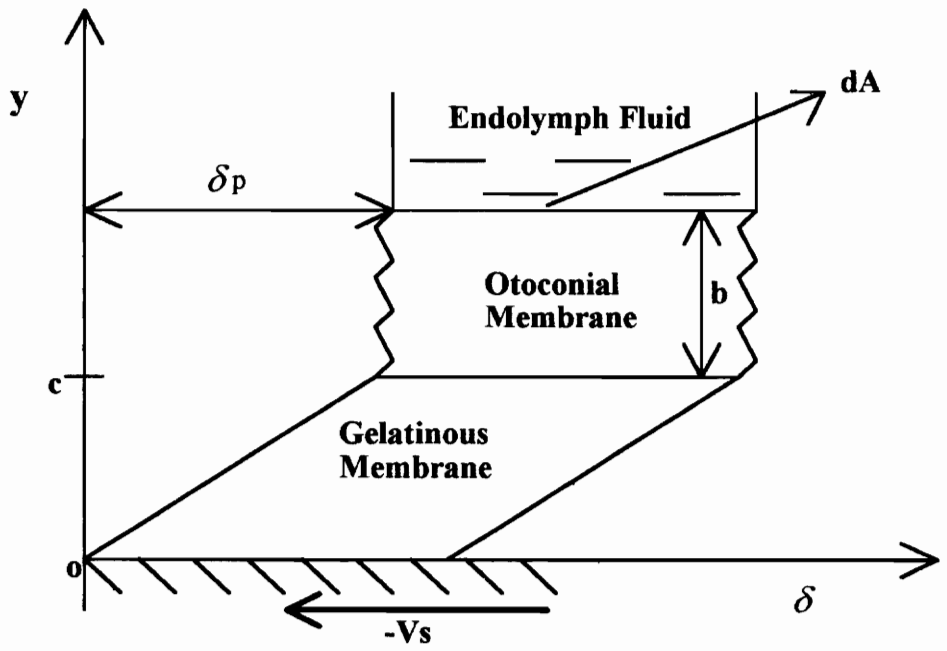

FIGURE 1.3 - Simplified model of the otolith with surface area dA which is perpendicular to the plane of cross section. The displacement of otoconial membrane in x direction with respect to the skull is represented as $\delta_p(t)$. The thickness of the otoconial layer is b and the gelatinous layer has thickness c.

The solution of this error is to include the viscous effects of the solid. Therefore, the gel layer material must be viscoelastic, having both elastic and viscous characteristics. By considering the gel as a viscoelastic material, the short time displacements are reduced and the long-term effects are extended further in time. In addititon, the elastic modulus may be increased without system oscillation. By treating the gel as a viscoelastic material instead of an elastic one, the motion of the system is damped and the model more closely resembles reality.

Chapter 2

Governing Equations

Experimental data [2,20,21] indicate that the phenomenological behavior of the human otolith organ is a highly overdamped, second-order mechanical system with an inertially active mass whose dynamic response is a combination of two distinct phases: short time (τ_s) and the long time (τ_l). The short time constant is approximately 0.0002s using a maximum mechanical displacement criterion for the otoconial layers. The long time constant has been experimentally measured at 10s. With these two values determined, the system dynamic response indicates that, between the two system corner frequencies, the peripheral sensory cells, (primary Type II cells) report skull velocity information to the central nervous system. Below the lower corner frequency, peripheral sensory cells report skull acceleration information to the central nervous system, and striolar sensory cells report rate of change of acceleration information to the central nervous system.

The concept of overdamping implies that following a sudden positive change in linear velocity the maximum displacement of the otoconial membrane would occur quickly. Then, during the corresponding return phase, upon reaching equilibrium, there would be no rapid oscillation. DeVries [4] who in 1950 used x-ray methods to measure the movements of the otoconial membrane in fish, first postulated the critically

overdamped model. Young et. al [21] have also demonstrated this behavior in humans further strengthening the idea of an overdamped system.

A two-dimensional cross-sectional view of the otolith geometry used in this study is illustrated in Figure 2.0a. For this analysis the otolith organ has been divided into three separate distinct elements: 1) The Fluid (Endolymph), 2) The Rigid Plate (Otoconial Membrane), and 3) The Elastic Deformable Base (Gelatinous Membrane). The free body diagram of each element with their associated forces is illustrated in Figure 2.0b. It is necessary to note that the element is coupled to the plate element by τ_f (fluid shear) as well as coupled to the elastic element by τ_e (elastic shear).

The governing equations of motion for this system have already been derived by Grant et. al. [5] . However, a concise review is presented with the introduction of the gelatinous membrane as a bi-layered viscoelastic structure. The addition of this bi-layered viscoelastic element is the significance of this work. Perhaps problems of previous models will be remedied.

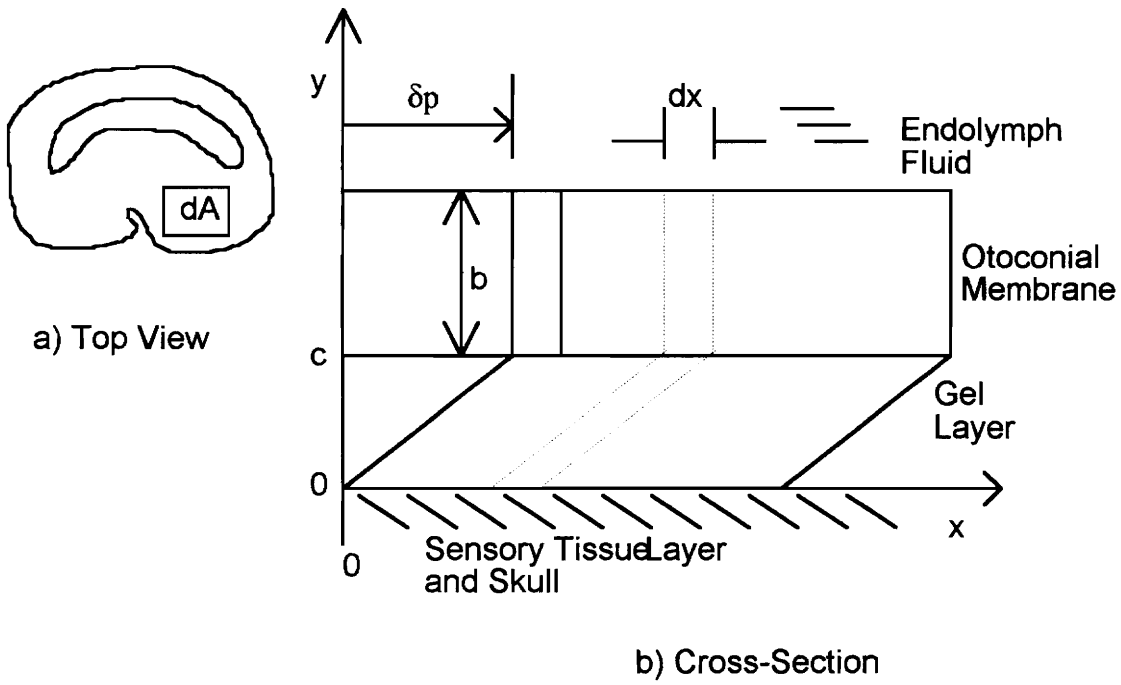

FIGURE 2.0a - Schematic of the otolith organ: (a) **Top view** showing the peripheral region with differential area dA where the model is developed. (b) **Cross-section** showing the layered structure where dx is the width of the differential area dA shown in the top view at the left.

Endolymph Fluid Layer - The spatial coordinate in the vertical direction is y_f, and the velocity of the endolymph fluid is $u(y_f,t)$, a function of the fluid depth y_f and time t.

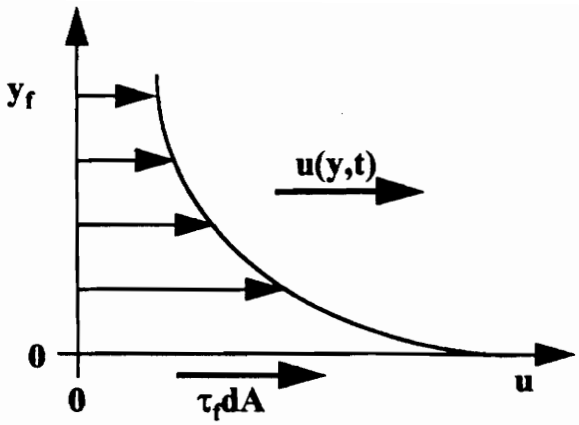

Otoconial Layer - The otoconial layer with thickness b and at a height b above the gel layer vertical coordinate origin. The velocity of the otoconial layer is v(t), which is a function of time only.

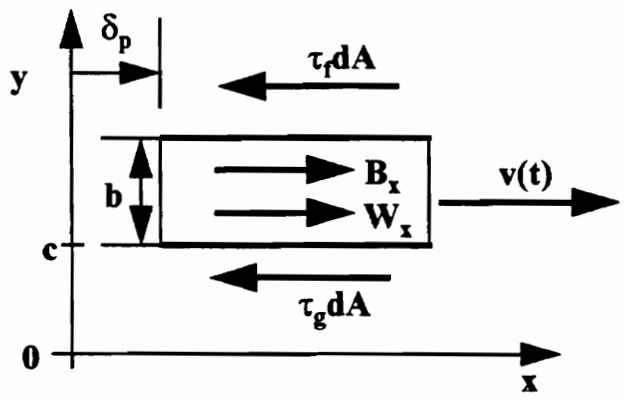

Gel Layer - Gel layer of thickness c, vertical coordinate y_g, and horizontal coordinate δ_g the gel deflection. The gel deflection is a function of both y_g and time t. The velocity of the gel is $w(y_g,t)$, a function of y_g and t.

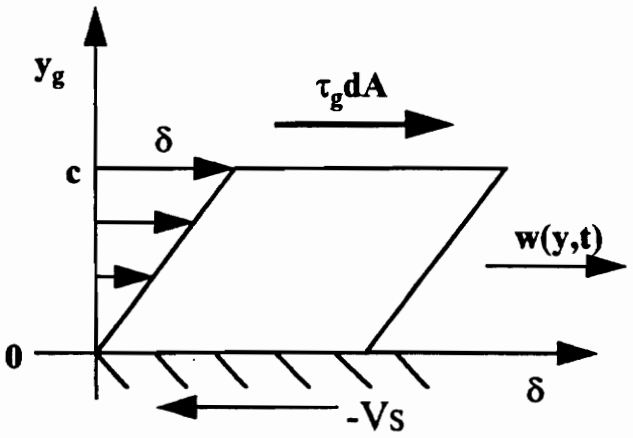

FIGURE 2.0b - The free-body diagrams of each layer of the otolith with the forces that act on each layer. The interfaces are coupled by shear stress of equal magnitude that act in opposite directions at each surface. The τ_g shear stress acts between the gel-otoconial layer, and the τ_f acts between the fluid-otoconial layer. The forces acting at these interfaces are the product of the shear stress τ and area dA. The B_x and W_x forces are respectively the components of the buoyant and weight forces acting in the plane of the otoconial layer.

2.1 Otoconial Membrane (rigid plate)

From Figure 2.1 and applying Newton's Second Law, F=ma;

$$\tau_g dA - \tau_f dA + W_X + B_X = \rho_o (bdA) \frac{\partial V_I}{\partial t} \qquad \textbf{[2.1.1]}$$

where

m = Mass of the otoconial membrane = ρ_o(bdA)

dA = Cross-sectional area of the otoconial membrane

τ_g = Gelatinous shear = $G \int_0^t \frac{\partial w}{\partial y_g} dt + \mu_g \frac{\partial w}{\partial y_g}$

μ_g = Viscosity of the gelatinous membrane

G = Shear modulus of the gel material = $\frac{1}{2}\left(\frac{E}{1+\nu}\right)$

E = Young's modulus of the gelatinous membrane material

ν = Poisson's ratio of the gelatinous membrane material

τ_e = Elastic shear = $G \int_0^t \frac{\partial w}{\partial y_g} dt$

τ_v = Viscous shear = $\mu_g \frac{\partial w}{\partial y_g}$

τ_f = Fluid shear = $\mu \frac{\partial u}{\partial y}$

W_x = Weight component in x direction = ρ_o(bdA)g_x

ρ_o = Density of the otoconial membrane

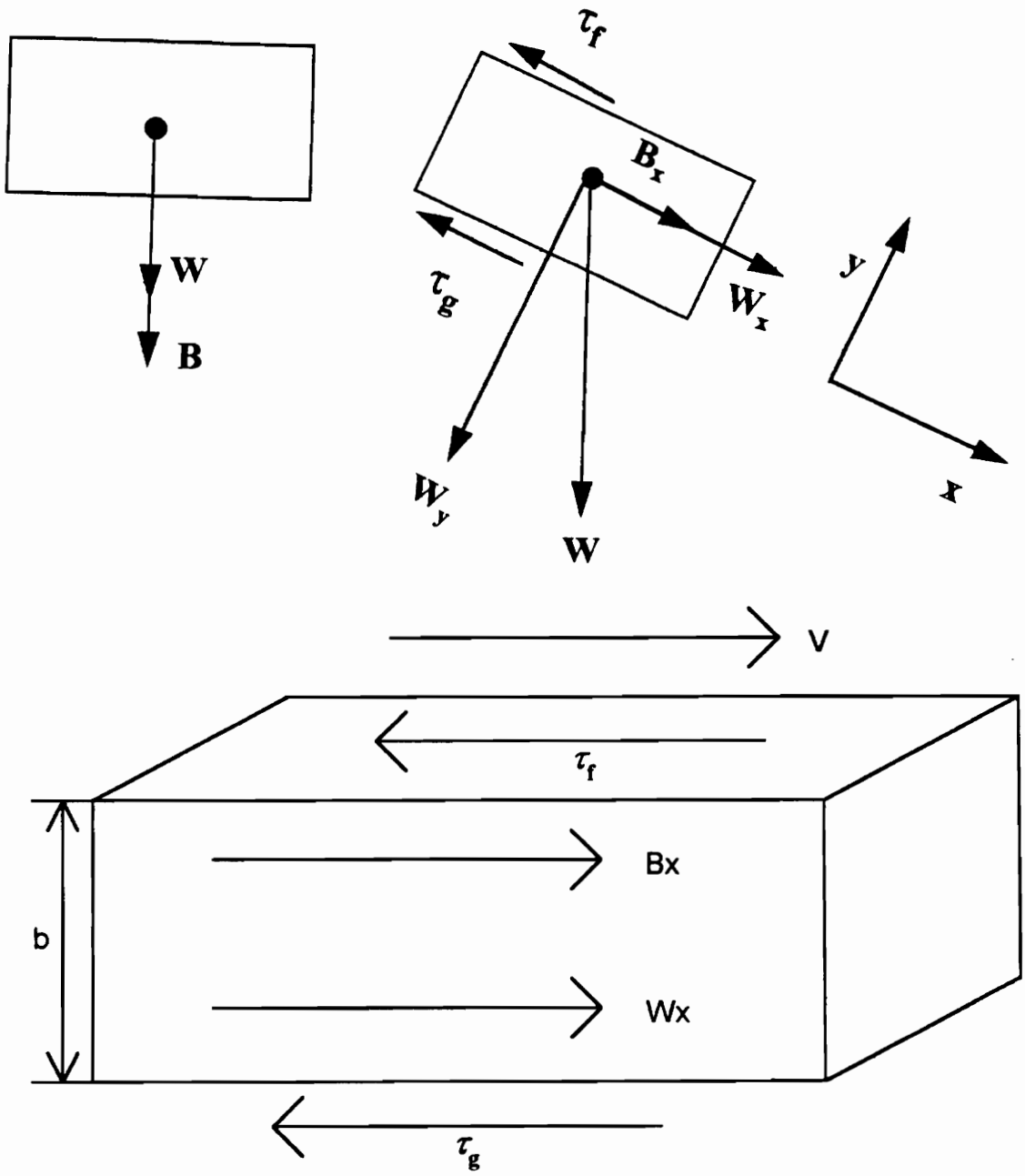

FIGURE 2.1 - **Top Left Figure:** The free body diagram of the otoconial membrane when the skull is at rest. **Top Right Figure:** The otoconial membrane when the skull is tilted where x is the coordinate direction of the skull. **Bottom Figure:** Free body diagram of the forces acting on the otoconial membrane in the x direction.

B_x = Buoyant force in x direction = $\rho_f (bdA)\left[\frac{\partial Vs}{\partial t} - g_x\right]$

ρ_f = Density of the endolymph fluid

V_I = Velocity of the otoconial membrane in x direction with respect to an inertial reference frame = $V_s + V$

V_s = Velocity of the skull in x direction with respect to an inertial reference frame

V = Velocity of the otoconial membrane in x direction with respect to the skull

ν = Poisson's ratio

μ_f = Viscosity of the endolymph fluid

b = Thickness of the otoconial membrane

w = Velocity of the gelatinous membrane in x direction with respect to the skull

Substituting the above quantities into equation 2.1.1 yields the governing equation for the otoconial membrane:

$$\left[-G\int_0^t \frac{\partial w}{\partial y_g} dt - \mu_g \frac{\partial w}{\partial y_g} + \mu_f \left(\frac{\partial u}{\partial y_f}\right)\right] dA =$$

$$\rho_o (bdA)\frac{\partial V}{\partial t} + (\rho_o - \rho_f)(bdA)\left[\frac{\partial V_s}{\partial t} - g_x\right]. \qquad \textbf{[2.1.2]}$$

2.2 Endolymph (fluid)

The fluid is assumed to be Newtonian in behavior so the governing equation becomes the Navier-Stokes equation:

$$\rho_f \frac{\partial u_I}{\partial t} = \rho_f g_x - \frac{\partial P}{\partial x} + \mu_f \frac{\partial^2 u_I}{\partial y_f^2} \qquad \textbf{[2.2.1]}$$

where

u_I = Velocity of the fluid in x direction with respect to an inertial reference frame = $V_s + u$

V_s = Velocity of the skull in x direction with respect to an inertial reference frame

u = Velocity of the fluid with respect to the skull

$\frac{\partial P}{\partial x}$ = Fluid Pressure Gradient = $\rho_f \left[g_x - \frac{\partial V_s}{\partial t} \right]$

Upon substitution of the pressure gradient and inertial velocity into equation 2.2.1, the governing equation for the endolymph fluid becomes

$$\rho_f \frac{\partial u}{\partial t} = \mu_f \left(\frac{\partial^2 u}{\partial y_f^2} \right) \qquad \textbf{[2.2.2]}$$

with the necessary boundary conditions

$$u(o,t) = V(t) \qquad \text{and} \qquad u(\infty,t) = 0.$$

The fluid velocity at the otoconial membrane (plate) surface is equal to the velocity of the plate. Therefore, the plate initiates fluid motion. The velocity at infinity is equal to zero. The assumption of large fluid depth above the plate in relation to its small displacement justifies this boundary condition.

2.3 Gelatinous Membrane (viscoelastic gel)

Figure 2.3a is the free body diagram of an element of the viscoelastic gel in shear. The forces acting on the element are the shear forces on the top and bottom layers, $\tau_y + d\tau_y$ and τ_y, the pressure on each side of the element, P_x and P_x and $d P_x$, and the body force on the element due to the component of gravity in the x direction, g_x. Utilizing Newton's Law, F=ma, the gelatinous membrane equation becomes

$$\rho_g dV \frac{\partial w_I}{\partial t} = (\tau_y + d\tau_y - \tau_y)dA + (P_x - P_x + d P_x)dydz + dV\rho_g g_x \qquad \textbf{[2.3.1]}$$

where

ρ_g = Density of the Gelatinous Membrane = ρ_f

w_I = Velocity of the Gelatinous membrane in x direction with respect to an inertial reference frame = $V_s + w$

By dividing the equation [2.3.1] by space coordinates and using differential substitution for the differences in shear and pressure in addition to equating the endolymph fluid density to the gel density, $\rho_g = \rho_f$, the final equation becomes

$$\rho_g \frac{\partial w_I}{\partial t} = \rho_g g_x - \frac{\partial P}{\partial x} + \frac{\partial \tau}{\partial y}$$

where

$\frac{\partial P}{\partial x}$ = Fluid Pressure Gradient = $\rho_f \left[g_x - \frac{\partial V_s}{\partial t} \right]$

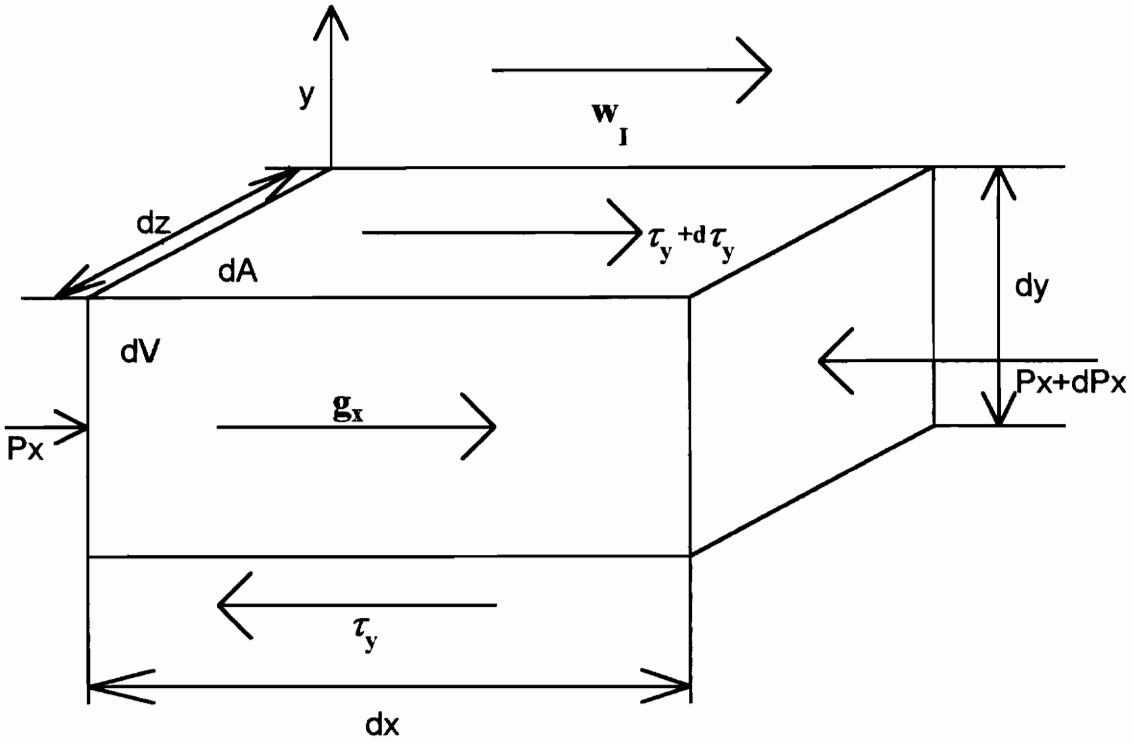

FIGURE 2.3a - Free body diagram of an element within the gel layer of the otolith organ.

w_I = Velocity of the gelatinous membrane in x direction with respect to an inertial reference frame = $V_s + w$

V_s = Velocity of the skull in x direction with respect to an inertial reference frame

After substituting for the pressure gradient and the gel velocity with respect to the skull, w, the equation becomes

$$\rho_g \frac{\partial w_I}{\partial t} = \frac{\partial \tau}{\partial y} . \qquad \textbf{[2.3.2]}$$

Treating the gel as a viscoelastic material produces damped motion and the model more closely resembles reality [7]. Therefore the Kelvin-Voigt model for viscoelastic materials may be used for this model. Shear stress is a function of both velocity and displacement. This model is described as a spring and a dashpot connected in parallel. The shear stress is then expressed as

$$\tau_{xy} = G\frac{\partial \delta}{\partial y} + \mu_g \frac{\partial w}{\partial y} \qquad \textbf{[2.3.3]}$$

where

G = Shear modulus = $\frac{1}{2}\left(\frac{E}{1+\nu}\right)$

μ_g = Viscosity of the gelatinous membrane

δ = $\int_0^t w(y_g, t)\, dt$

$\frac{\partial \delta}{\partial y}$ = $\int_0^t \frac{\partial w}{\partial y_g} dt$

Substituting these values into equation 2.3.3 yields

$$\tau_{xy} = G \int_0^t \frac{\partial w}{\partial y_g} dt + \mu_g \frac{\partial w}{\partial y_g}.$$

Then substituting this result into equation 2.3.2, it becomes

$$\rho_f \frac{\partial w}{\partial t} = G \int_0^t \frac{\partial^2 w}{\partial y_g^2} dt + \mu_g \frac{\partial^2 w}{\partial y_g^2}. \qquad \textbf{[2.3.4]}$$

The boundary conditions for this field equation are $w(c,t) = v(t)$ and $w(o,t) = 0$. The velocity of the gelatinous material is equal to that of the otoconial membrane at their interface. The velocity of the gelatinous layer is equal to zero at the skull.

Now consider the bi-layered viscoelastic structure which is demonstrated in Figure 2.3b. The governing equation for gel layer 1 is

$$\rho_f \frac{\partial w_1}{\partial t} = G_1 \int_0^t \frac{\partial^2 w_1}{\partial y_1^2} dt + \mu_1 \frac{\partial^2 w_1}{\partial y_1^2}$$

and has boundary conditions of $w_1(R,t) = w_2(t)$ and $w_1(o,t) = 0$. The velocity of gel layer 1 is equal to that of gel layer 2 at their interface. The velocity of gel layer 1 is equal to zero at the skull. Similarly, the governing equation for gel layer 2 yields

$$\rho_f \frac{\partial w_2}{\partial t} = G_2 \int_0^t \frac{\partial^2 w_2}{\partial y_2^2} dt + \mu_2 \frac{\partial^2 w_2}{\partial y_2^2}$$

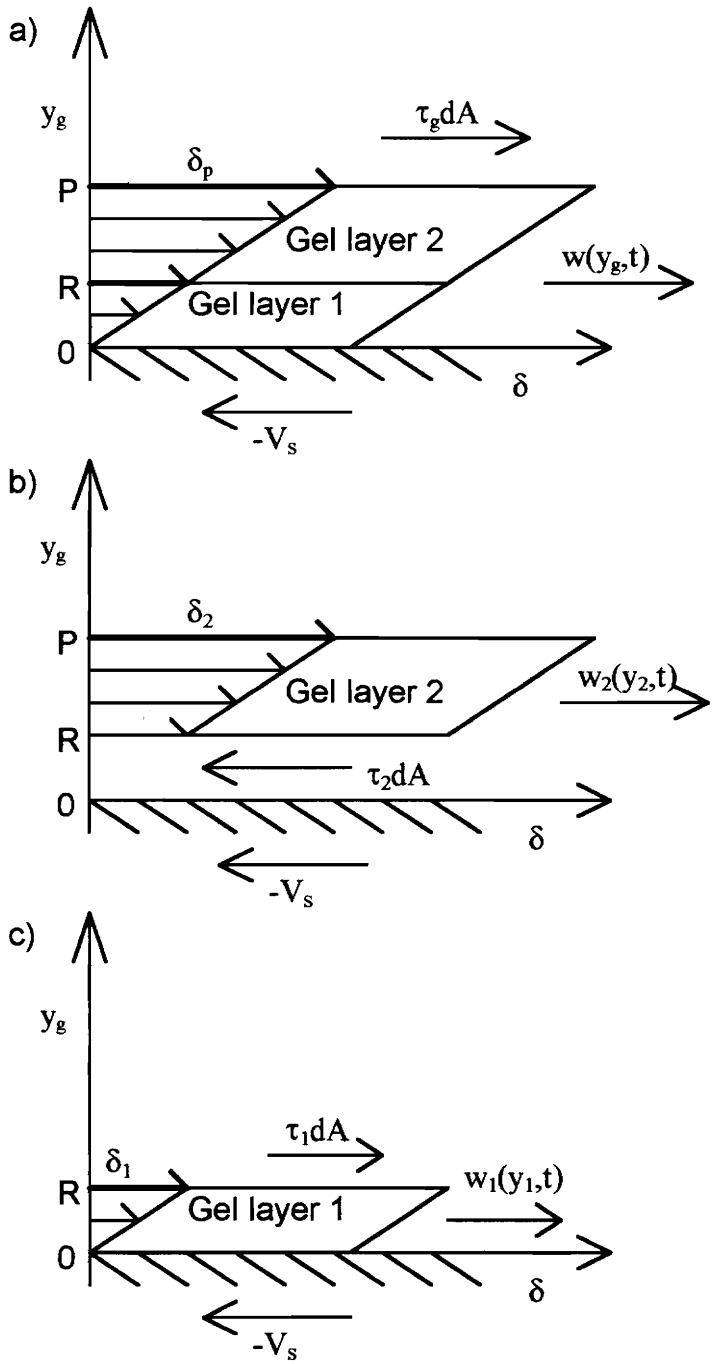

FIGURE 2.3b - a) Free body diagrams of bi-layered structure of viscoelastic gel having thickness c, vertical coordinate y_g, and horizontal coordinate δ, the gel deflection. This deflection is a function of both y_g and time t. The velocity of the gel is $w(y_g,t)$, a function of y_g and t. Point P is the plate location which is above gel layer 2 and point R is the interface of gel layer 1 and gel layer 2. b) Free body diagram of gel layer 2 having a thickness c_2, velocity $w_2(y_g,t)$, and deflection δ_2. c) Free body diagram of gel layer 1 having a thickness c_1, velocity $w_1(y_g,t)$ and deflection δ_1 for the gelatinous membrane.

and has boundary conditions of $w_2(R,t) = w_1(t)$ and $w_2(P,t) = v(t)$. The velocity of gel layer 2 is equal to that of gel layer 1 at their interface. The velocity of gel layer 2 is equal to the velocity of the otoconial plate.

2.4 *Nondimensionalization*

These equations can be nondimensionalized by substitution of the following variables where the bars indicate the nondimensionalized variables:

$$\bar{y}_g = \frac{y_g}{b} \qquad \bar{y} = \frac{y}{b} \qquad \bar{t} = \frac{\mu}{\rho_o b^2} t \qquad \bar{u} = \frac{u}{V} \qquad \bar{w} = \frac{w}{V} \qquad \bar{v} = \frac{v}{V} \qquad \bar{v}_S = \frac{v_S}{V}$$

and V is some characteristic velocity in the problem [7]. This leads to three nondimensional governing equations for the behavior of the Human Otolith organs:

for the fluid,

$$R\frac{\partial \bar{u}}{\partial \bar{t}} = \frac{\partial^2 \bar{u}}{\partial \bar{y}_f^{\,2}} \qquad \textbf{[2.4.1]}$$

and for the plate,

$$\frac{\partial \bar{v}}{\partial \bar{t}} + (1-R)\left[\frac{\partial \bar{V}_S}{\partial \bar{t}} - \bar{g}_x\right] = \frac{\partial \bar{u}}{\partial \bar{y}_f} - \varepsilon \int_o^{\bar{t}} \frac{\partial \bar{w}}{\partial \bar{y}_g} d\bar{t} - M\frac{\partial \bar{w}}{\partial \bar{y}_g} \qquad \textbf{[2.4.2]}$$

$$R\frac{\partial \bar{w}}{\partial \bar{t}} = \varepsilon \int_o^{\bar{t}} \frac{\partial^2 \bar{w}}{\partial \bar{y}_g^{\,2}} d\bar{t} + M\frac{\partial^2 \bar{w}}{\partial \bar{y}_g^{\,2}} \qquad \textbf{[2.4.3]}$$

where

$$R = \frac{\rho_f}{\rho_o}, \quad M = \frac{\mu_g}{\mu_f} \quad \text{and} \quad \varepsilon = G\left[\frac{b^2}{\mu_f^{\,2}}\right]\rho_o.$$

Now consider the bi-layered gel, the nondimensionalized equations become for gel layer 1

$$R\frac{\partial \bar{w}_1}{\partial \bar{t}} = \varepsilon_1 \int_o^{\bar{t}} \frac{\partial^2 \bar{w}_1}{\partial \bar{y}_1^2}\, d\bar{t} + M_1 \frac{\partial^2 \bar{w}_1}{\partial \bar{y}_1^2} \qquad \textbf{[2.4.4]}$$

and for gel layer 2

$$R\frac{\partial \bar{w}_2}{\partial \bar{t}} = \varepsilon \int_o^{\bar{t}} \frac{\partial^2 \bar{w}_2}{\partial \bar{y}_2^2}\, d\bar{t} + M\frac{\partial^2 \bar{w}_2}{\partial \bar{y}_2^2}. \qquad \textbf{[2.4.5]}$$

Chapter 3

Problem Formulation

The otoconial membrane is considered as a rigid flat plate of thickness band density ρ_o, and having infinite extent. The edge effects of the actual organ, which has finite extent, can be shown to be negligible due to the small thickness b (15 μm) in relation to its flat plane area (2 mm^2). For the present formulations only a small elemental surface area dA of the plate is considered. This plate is in contact with the endolymph fluid above and the gelatinous bi-layer below it. The governing equations derived in the previous chapter are solved for a step change in skull velocity and a constant acceleration stimulus. A solution for a step change in linear velocity of the skull is useful in establishing numerical values for the short and long time constants and in determining the system dynamics. A solution for constant linear acceleration is similar to tilting the skull with respect to the gravity vector. The entire system is considered such that time starts at zero, t=0, and the skull is given a step change in velocity of V_S. The endolymph fluid and gel material begin at rest at time equal to zero and eventually are accelerated to the skull velocity. The otoconial membrane also starts from rest. Due to its inertia, the otoconial membrane is accelerated to the skull velocity producing a relative displacement of the otoconial membrane, shearing the gel layer. Since the velocities in the governing equations are measured with respect to the skull and the fluid portion is in a closed volume of equal density material, the effects are considered as the plate being given a step change

in velocity equal, but opposite, to that of the skull, while the skull and surrounding gel and endolymph fluid remain at rest. At infinite time, $t=\infty$, all the transient terms in the governing equation for the plate are lost. The results yield the gravitational acceleration term equaling the elastic term.

Several approaches are used to arrive at the correct solution. One attempt is made to take the derivative of the nondimensionalized gel stress equation. As a result, the elasticity and viscosity become functions of depth. The displacement calculation in which the present velocity and the velocity at one time step ahead are averaged did not provide a solution. Using first order correct derivatives for the governing equations of the endolymph fluid, otoconial membrane and gelatinous membrane are also unsuccessful. These failed attempts prove that the boundary condition of the bi-layered gelatinous membrane is, in fact, the nondimensionalized shear stresses of gel layer 1 and gel layer 2 equal in magnitude and opposite in direction. The omission of this step results in discontinuities within the velocity field.

3.1 Finite Difference Solution

The differential terms of the governing equations are expressed as finite difference analogues. The results are coded into Matlab for a solution by digital computer. The solution space, which extends spatially from the skull-gel interface, $y=0$, up through the bi-layered gel interface $y=R$ (the boundary of the two gel layers), the plate, $y=P$, to the fluid boundary, $y=Q$, and includes time from $t=0$ to $t=\infty$, is shown in Figure 3.1. This solution

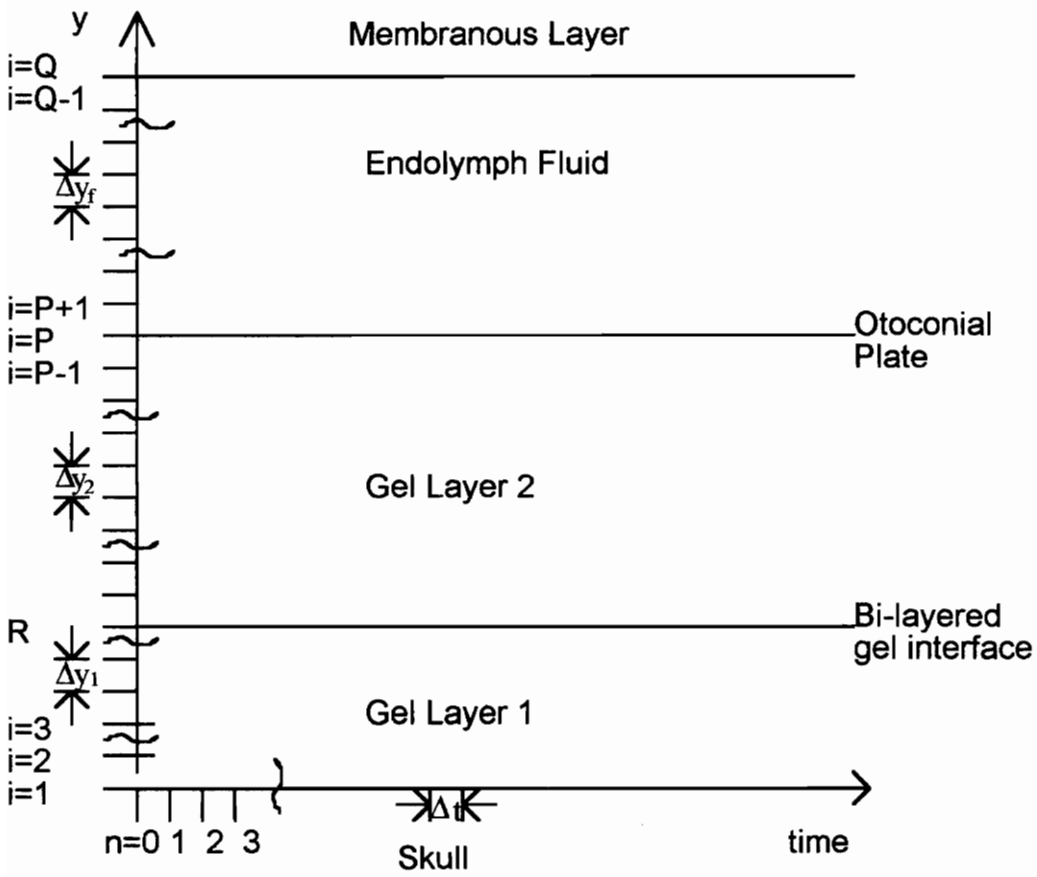

FIGURE 3.1 - Solution space for Numerical Model.

space is partitioned by discrete spatial and time steps Δy and Δt.

In this model, separate values for the fluid, plate and gel are not considered. Therefore, the following derivations consider a uniform Δy. Hence, all results presented have $\Delta y=\Delta y_g=\Delta y_f$. The velocities of fluid, plate, and gel are no longer designated by the separate variables $\bar{u}, \bar{v}$, and $\bar{w}$, but rather by the single variable $U_{i,n}$. The velocity of the material is determined by the spatial subscript i and time as n.

3.2 Time and Space Derivatives

The backward-finite difference method is used because it allows for unconditional stability and first order accuracy on first order time derivatives. The derivatives for the terms in the differential equations are found by changing the values of these parameters at node points or at adjacent points. The graphical representation of this method is illustrated in Figure 3.2. The subscripts n correspond to time t and n+1 corresponds to time t+Δt. The first time derivative is defined as

$$\left(\frac{\partial U}{\partial t}\right)_{i,n+1} = \frac{U_{i,n+1} - U_{i,n}}{\Delta t} + O(\Delta t),$$

and the first and second order space derivatives are

$$\left(\frac{\partial U}{\partial y}\right)_{i,n+1} = \frac{U_{i+1,\,n+1} - U_{i-1,n+1}}{2\Delta y} + O(\Delta y^2)$$

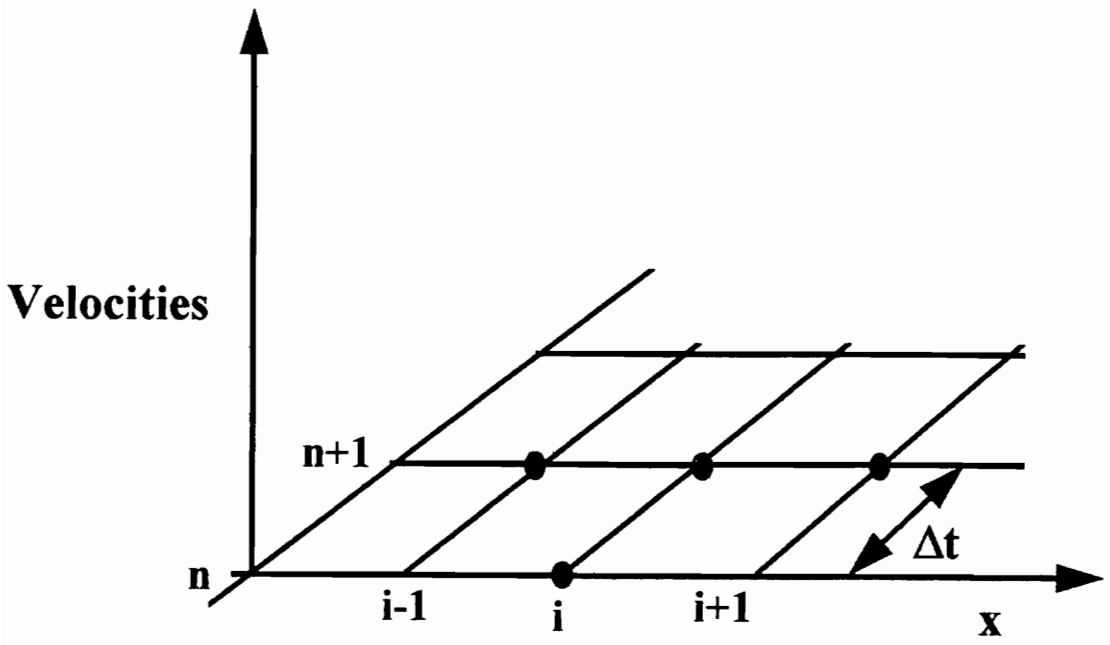

FIGURE 3.2 - Grid points used for backward difference equation.

and

$$\left(\frac{\partial^2 U}{\partial y^2}\right)_{i,n+1} = \frac{U_{i+1,n+1} - 2U_{i,n+1} + U_{i-1,n+1}}{\Delta y^2} + O(\Delta y^2).$$

The higher order derivatives are neglected. The above formulas are used for displacements by substituting δ for U.

3.3 Displacement Calculations

Simpson's rule is used to calculate displacement, δ. According to the formula, displacement at all points are calculated using velocity at one time step ahead along with the present displacement. The formula reads

$$\delta_{i,n+1} = \delta_{i,n} + U_{i,n+1}\Delta t .$$

The method is graphically depicted in Figure 3.3.

3.4 Finite Difference Governing Equations

The previously derived equations are as follows:

for the endolymph fluid

$$\rho_f \frac{\partial u}{\partial t} = \mu_f \left(\frac{\partial^2 u}{\partial y_f^2}\right),$$

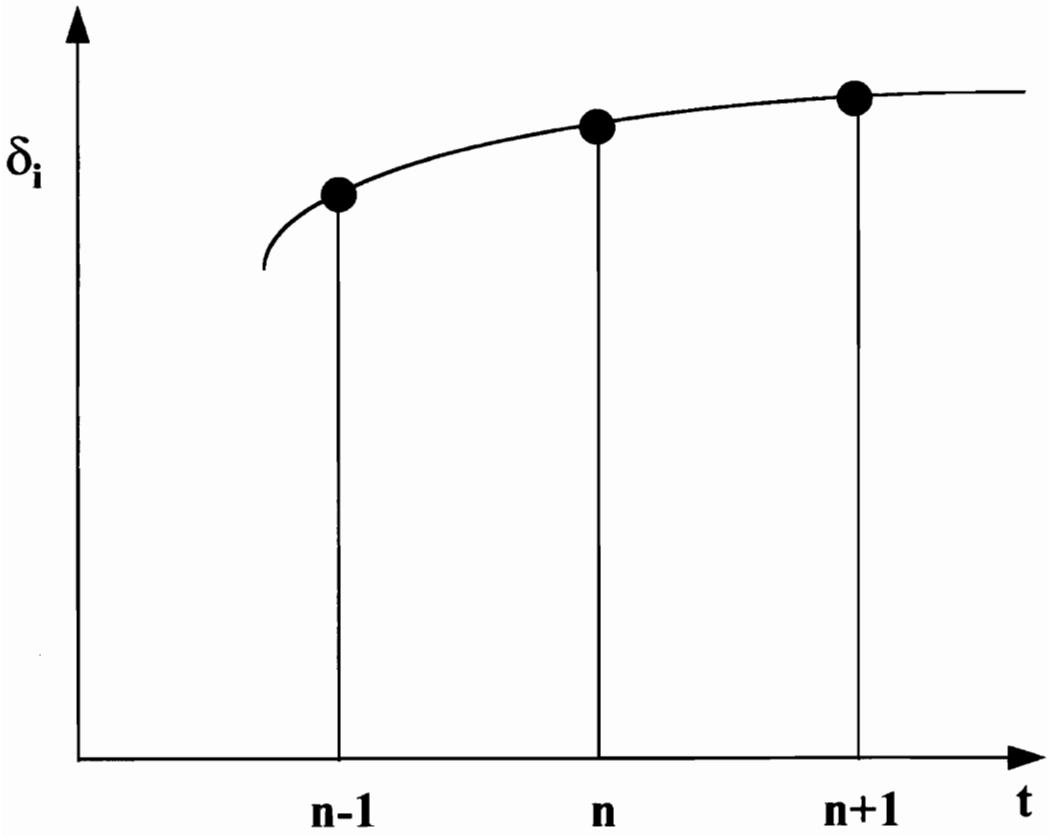

FIGURE 3.3 - Graphical Example of Displacement Calculations.

for the otoconial membrane

$$\left[-G\int_0^t \frac{\partial w}{\partial y_g}dt - \mu_g \frac{\partial w}{\partial y_g} + \mu_f\left(\frac{\partial u}{\partial y_f}\right)\right]dA =$$

$$\rho_o(bdA)\frac{\partial V}{\partial t} + \left(\rho_o - \rho_f\right)(bdA)\left[\frac{\partial V_s}{\partial t} - g_x\right],$$

and for the gelatinous membrane

$$\rho_f \frac{\partial w}{\partial t} = G\int_0^t \frac{\partial^2 w}{\partial y_g^2}dt + \mu_g \frac{\partial^2 w}{\partial y_g^2}.$$

These equations are substituted into the governing differential equations and algebraically manipulated to separate unknown from known quantities, or n+1 time subscripts from n, n-1, etc. subscripts. The finite difference equations then become the following:

for the fluid,

$$-U_{i-1,n+1} + R\left(\frac{\Delta y^2}{\Delta t}\right) + 2)U_{i,n+1} - U_{i+1,n+1} = R\left(\frac{\Delta y^2}{\Delta t}\right)U_{i,n}$$

for the plate,

$$(M + \varepsilon\ \Delta t - 1)U_{i-1,n+1} + \left(2\frac{\Delta y}{\Delta t}\right)U_{i,n+1} - (M + \varepsilon\ \Delta t - 1)U_{i+1,n+1}$$

$$= 2\frac{\Delta y}{\Delta t}U_{i,n+1} - \varepsilon\left(\delta_{i+1,n} - \delta_{i-1,n}\right).$$

and for the gelatinous membrane,

$$-(M+\varepsilon\,\Delta t)U_{i-1,n+1}+\left(R\frac{\Delta y^2}{\Delta t}+2\varepsilon\,\Delta t+2M\right)U_{i,n+1}-(M+\varepsilon\,\Delta t)U_{i+1,n+1}$$

$$=R\frac{\Delta y^2}{\Delta t}U_{i,n}-\varepsilon\left(\delta_{i-1,n}-2\delta_{i,n}+\delta_{i-1,n}\right).$$

Now the bi-layered gel is considered. To determine the finite difference equation for gel layer 1, gel layer 2 and the intermediate (i=R) layer, the shear stresses acting on the interface must be nondimensionalized and equated. Figure 3.4 provides a graphical illustration. The nondimensionalized stress for the gel is

$$\bar{\tau}_g=\bar{\varepsilon}\frac{\partial\bar{\delta}}{\partial\bar{y}_g}+\bar{M}\frac{\partial\bar{w}}{\partial\bar{y}_g}.$$

The nondimensionalized stress equations become the following:

for gel layer 1

$$\bar{\tau}_1=\bar{\varepsilon}_1\frac{\partial\bar{\delta}_1}{\partial\bar{y}_1}+\bar{M}_1\frac{\partial\bar{w}_1}{\partial\bar{y}_1},$$

for gel layer 2

$$\bar{\tau}_2=\bar{\varepsilon}_2\frac{\partial\bar{\delta}_2}{\partial\bar{y}_2}+\bar{M}_2\frac{\partial\bar{w}_2}{\partial\bar{y}_2},$$

and for the gel layer at point R

$$\bar{\tau}_R=\bar{\varepsilon}_R\frac{\partial\bar{\delta}_R}{\partial\bar{y}_R}+\bar{M}_R\frac{\partial\bar{w}_R}{\partial\bar{y}_R}.$$

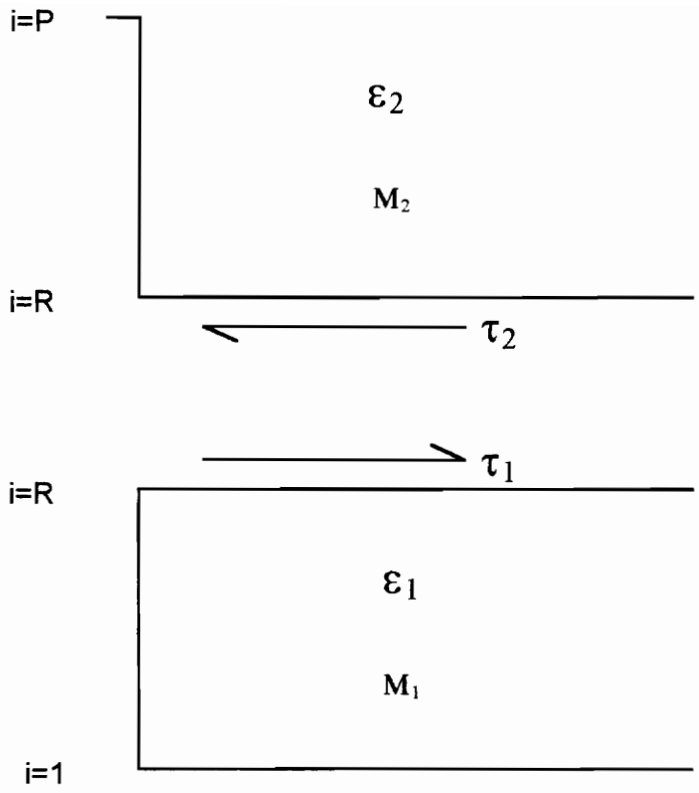

FIGURE 3.4 - Shear stresses acting at the interface, i=R, of the bi-layered gel.

The finite difference equations are as follows:

for gel layer 1

$$\varepsilon_1\left(\frac{\delta_{r+1,n+1} - \delta_{r-1,n+1}}{2\Delta y_g}\right) + M_1\left(\frac{u_{r+1,n+1} - u_{r-1,n+1}}{2\Delta y_g}\right),$$

for gel layer 2

$$\varepsilon_2\left(\frac{\delta_{r+1,n+1} - \delta_{r-1,n+1}}{2\Delta y_g}\right) + M_2\left(\frac{u_{r+1,n+1} - u_{r-1,n+1}}{2\Delta y_g}\right),$$

and for the gel layer at point R

$$\varepsilon_R\left(\frac{\delta_{r+1,n+1} - \delta_{r-1,n+1}}{2\Delta y_g}\right) + M_R\left(\frac{u_{r+1,n+1} - u_{r-1,n+1}}{2\Delta y_g}\right).$$

After equating $\bar{\tau}_1 = \bar{\tau}_2$, the finite difference equation becomes

$$\varepsilon_1\left(\frac{\delta_{r+1,n+1} - \delta_{r-1,n+1}}{2\Delta y_g}\right) + M_1\left(\frac{u_{r+1,n+1} - u_{r-1,n+1}}{2\Delta y_g}\right) = \varepsilon_2\left(\frac{\delta_{r+1,n+1} - \delta_{r-1,n+1}}{2\Delta y_g}\right) + M_2\left(\frac{u_{r+1,n+1} - u_{r-1,n+1}}{2\Delta y_g}\right). \quad \textbf{[3.4.1]}$$

The nondimensionalized governing equation for the gelatinous membrane is

$$R\frac{\partial \bar{w}}{\partial \bar{t}} = \varepsilon \int_o^{\bar{t}} \frac{\partial^2 \bar{w}}{\partial \bar{y}_g^{\,2}}\, d\bar{t} + M\frac{\partial^2 \bar{w}}{\partial \bar{y}_g^{\,2}},$$

for gel layer 1

$$R\frac{\partial \bar{w}_1}{\partial \bar{t}} = \varepsilon_1 \int_o^{\bar{t}} \frac{\partial \bar{w}_1}{\partial \bar{y}_1^2}\, d\bar{t} + M_1 \frac{\partial^2 \bar{w}_1}{\partial \bar{y}_1^2},$$

and for gel layer 2

$$R\frac{\partial \bar{w}_2}{\partial \bar{t}} = \varepsilon \int_o^{\bar{t}} \frac{\partial \bar{w}_2}{\partial \bar{y}_2^2}\, d\bar{t} + M\frac{\partial^2 \bar{w}_2}{\partial \bar{y}_2^2}.$$

The finite difference analogues for these equations become

$$R\left(\frac{u_{i,n+1} - u_{i,n}}{\Delta t}\right) = \varepsilon \left(\frac{\delta_{i+1,n+1} - 2\delta_{i,n+1} + \delta_{i-1,n+1}}{\Delta y_g^2}\right) + M\left(\frac{u_{i+1,n+1} - 2u_{i,n+1} + u_{i-1,n+1}}{\Delta y_g^2}\right),$$

for gel layer 1

$$R\left(\frac{u_{i,n+1} - u_{i,n}}{\Delta t}\right) = \varepsilon_1 \left(\frac{\delta_{i+1,n+1} - 2\delta_{i,n+1} + \delta_{i-1,n+1}}{\Delta y_g^2}\right) + M_1\left(\frac{u_{i+1,n+1} - 2u_{i,n+1} + u_{i-1,n+1}}{\Delta y_g^2}\right),$$

and for gel layer 2

$$R\left(\frac{u_{i,n+1} - u_{i,n}}{\Delta t}\right) = \varepsilon_2 \left(\frac{\delta_{i+1,n+1} - 2\delta_{i,n+1} + \delta_{i-1,n+1}}{\Delta y_g^2}\right) + M_2\left(\frac{u_{i+1,n+1} - 2u_{i,n+1} + u_{i-1,n+1}}{\Delta y_g^2}\right).$$

These equations are solved for $\delta_{r+1,n+1}$ and $u_{r+1,n+1}$ in gel layer 1 and $\delta_{r-1,n+1}$ and $u_{r-1,n+1}$ in gel layer 2. These quantities are substituted into equation 3.4.1. The like terms of $u_{r-1,n+1}$, $u_{r,n}$ and $u_{r,n+1}$ are collected and placed on the left side of the equation. The finite difference equations become the following:

for gel layer 1

$$[-\varepsilon_1 \Delta t - M_1]u_{r-1,n+1} + \left[\frac{\Delta y_g^2}{\Delta t}R + \Delta t(\varepsilon_1 + \varepsilon_1) + (M_1 + M_1)\right]u_{r,n+1}$$

$$- [M_1 + \varepsilon_1 \Delta t]u_{r+1,n+1} = \left[\frac{\Delta y_g^2}{\Delta t}R\right]u_{r,n} - [\varepsilon_1 + \varepsilon_1]\delta_{r,n}$$

$$+ \varepsilon_1 \delta_{r-1,n} + \varepsilon_1 \delta_{r+1,n} ,$$

and for gel layer 2

$$[-\varepsilon_2 \Delta t - M_2]u_{r-1,n+1} + \left[\frac{\Delta y_g^2}{\Delta t}R + \Delta t(\varepsilon_2 + \varepsilon_2) + (M_2 + M_2)\right]u_{r,n+1}$$

$$- [M_2 + \varepsilon_2 \Delta t]u_{r+1,n+1} = \left[\frac{\Delta y_g^2}{\Delta t}R\right]u_{r,n} - [\varepsilon_2 + \varepsilon_2]\delta_{r,n}$$

$$+ \varepsilon_2 \delta_{r-1,n} + \varepsilon_2 \delta_{r+1,n} .$$

The finite difference equation for the intermediate layer, i=R, is

$$\left[2\left(-\varepsilon_1 \Delta t - M_1\right)\right]u_{r-1,n+1} + \left[2\frac{\Delta y_g^2}{\Delta t}R + 2\Delta t(\varepsilon_1 + \varepsilon_1) + 2(M_1 + M_1)\right]u_{r,n+1}$$

$$- 2[M_2 + \varepsilon_2 \Delta t]u_{r+1,n+1} = \left[2\frac{\Delta y_g^2}{\Delta t}R\right]u_{r,n} + 2[-\varepsilon_1 - \varepsilon_2]\delta_{r,n}$$

$$+ 2\varepsilon_1 \delta_{r-1,n} + 2\varepsilon_2 \delta_{r+1,n}.$$

3.5 *Solution Strategy*

For a step change in skull velocity, the above equations are solved by establishing the initial condition that all relative velocities are zero, except for the plate which is given a velocity of (1-R). All initial displacements equal zero. The solution to the group of equations is

$$[C_{i,j}][U_i] = [D_j],$$

where $[C_{i,j}]$ is a tri-diagonal matrix whose values are found in the above equations. The solution to the above equation is found by using the Thomas algorithm [18]. From this result the next values of velocity are obtained and the displacements are solved and then moved ahead one more time step and the procedure is repeated.

However, for a constant acceleration stimulus, the initial condition of relative velocities are equal to zero and the plate velocity is also equal to zero. All initial displacements still equal zero. The above procedure can then be followed. The problem solving technique is detailed in Figure 3.5.

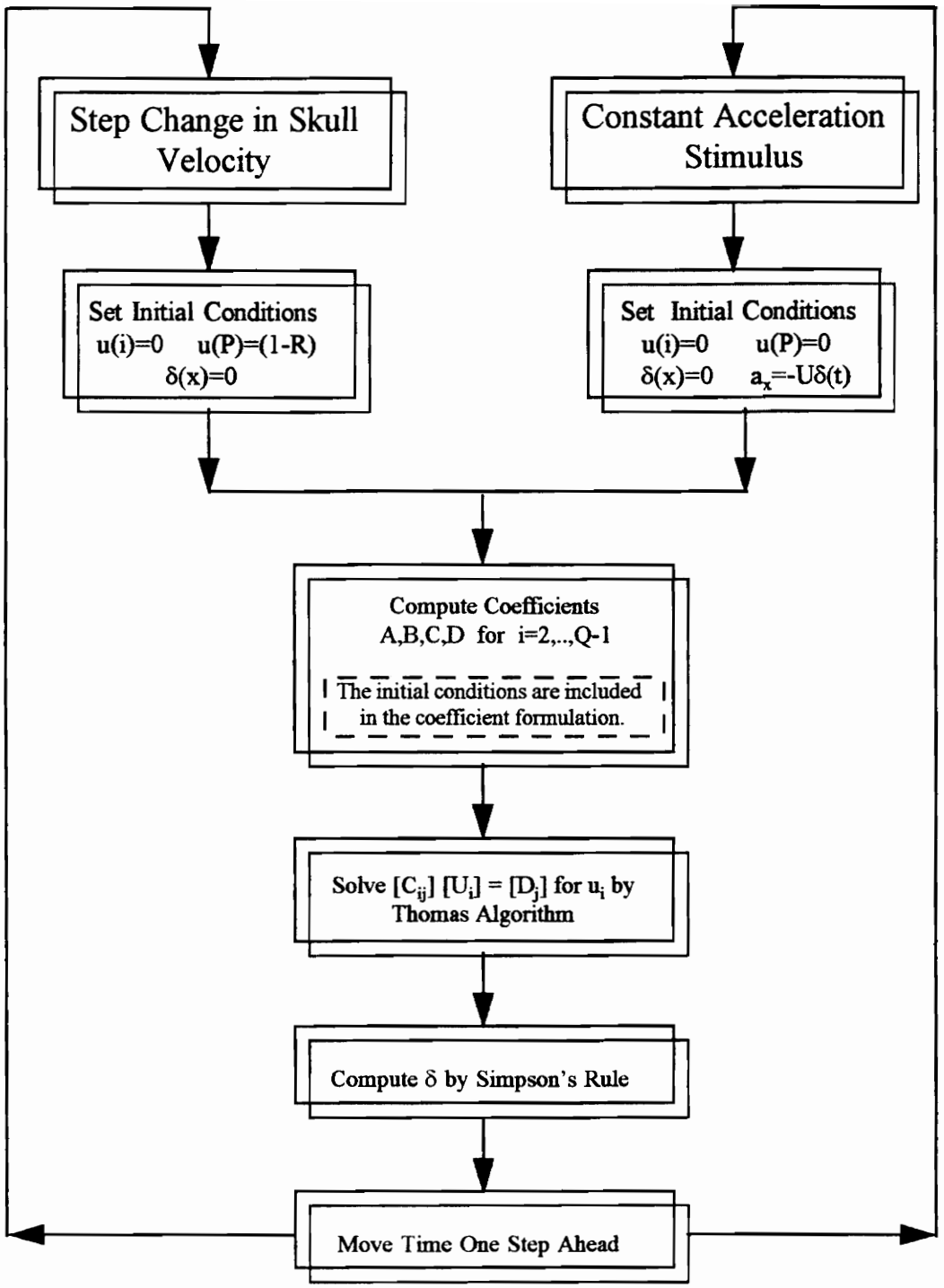

Figure 3.5: Flow Chart of Problem Solving Techniques

Chapter 4

Results and Discussion

In this study, a nondimensional parameter either ε_r or M_r is varied while one remains constant. These parameters are expressed as ratios. The parameter ε_r relates the elasticity of the lower layer to the upper layer whereas the parameter M_r is the relation of the viscosity of the lower layer to the upper layer. The work of Grant and Cotton [7] considers ε=0.0 to 10. Their findings suggest that ε values from 1 to 10 made the system so elastic that significant oscillation is produced. Therefore, the ε values range from .01 to .2 which yields ε_r values varying from 1 to 10.

Now let's consider the relative sizes of the gel layer and the fluid layer. The height of the gel is expressed as $h_p=(P-1)\Delta y$. Increasing P raises the gel height. Similarly, the fluid height is given by $h_q=(Q-P)\Delta y$ and the height is controlled by Q. These heights are illustrated in Figure 4.0a. The work of Kachar, et. al. [12] suggests that the otoconial layer has a thickness of 20 to 30 μm and the lower portion of the gelatinous layer also referred to as the columnar filament layer has thickness of 5 to 8 μm. The upper layer of the gel which is known as the gelatin layer has a thickness between 15-22 μm. Using otoconial layer thickness of 25 μm and the columnar filament to be 7 μm, yields a P value of 26 and a R value of 8.

The Q value is ideally supposed to be set at infinity. In this solution presented here

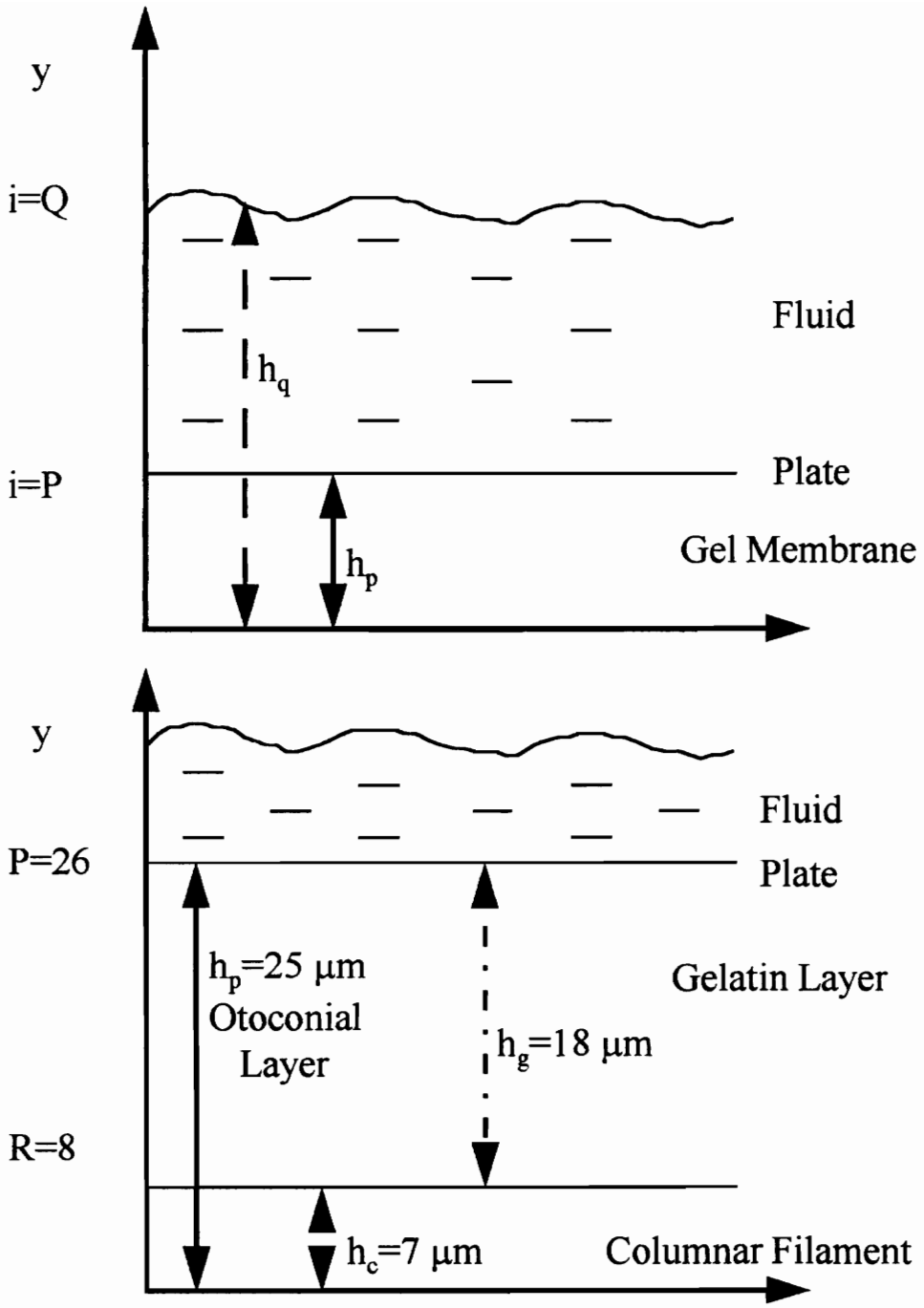

FIGURE 4.0a - **Top Figure:** Heights of the gel and fluid layers. **Bottom Figure:** Heights of the columnar filament and the gelatin layer of the gelatinous membrane.

Q must have a finite value. According to previous work of Cotton [3], Q is set to 1021 spatial steps which approximated the opposite membranous wall of the utricle or saccule. Plate and interface displacement at Q=1021 and Q=153 yield the same results for constant elasticity and viscosity. The graph is illustrated in Figures 4.0b-c. Therefore Q is set at 153 in this model since this provided much faster running time. The plate's inertia causes the plate displacement to exceed the displacement at the gel interface. Apparently, wall spacing of the utricle or saccule is not significant.

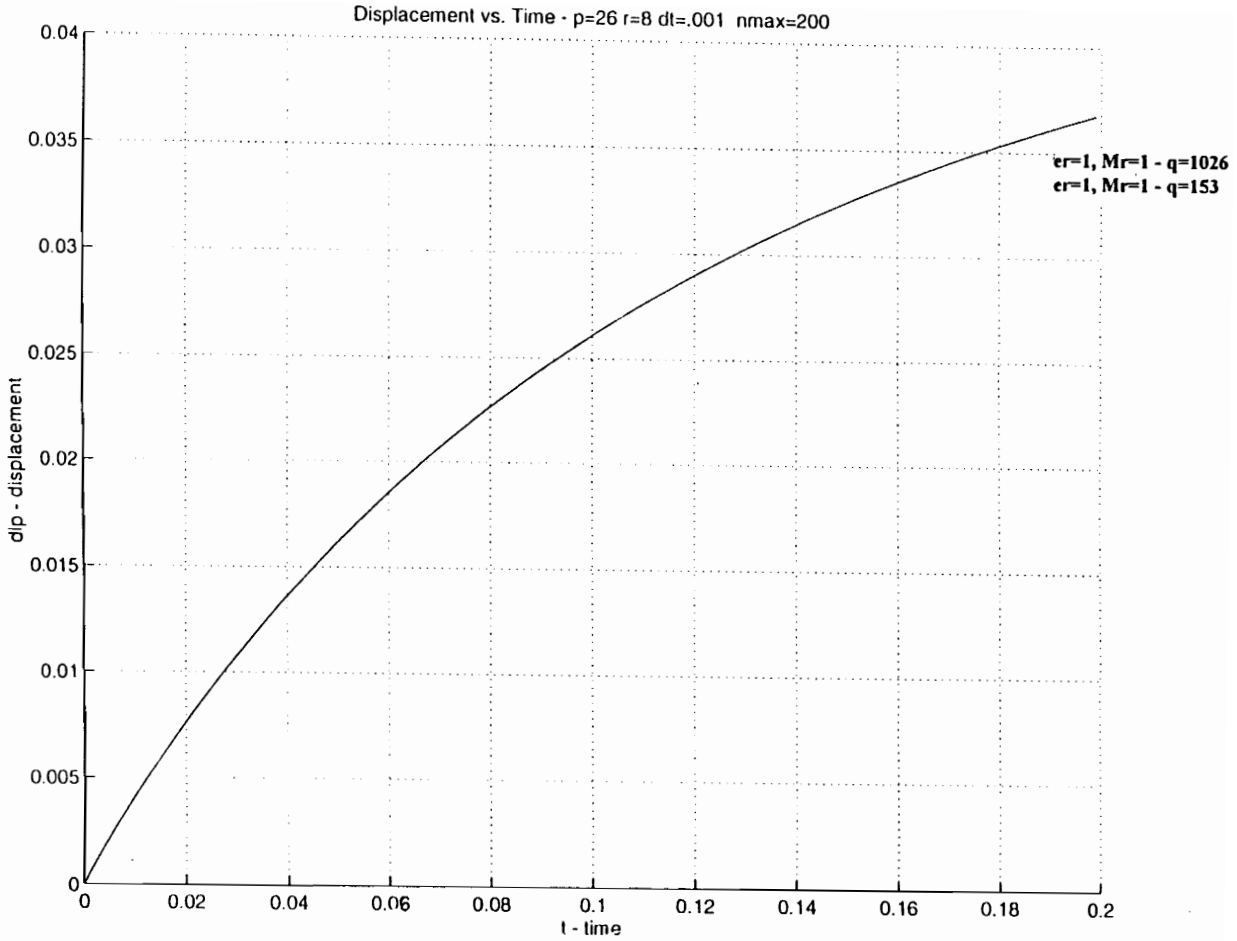

FIGURE 4.0b - Plate Displacement vs. Time Curve: Constant Elasticity and Viscosity at t=0.2

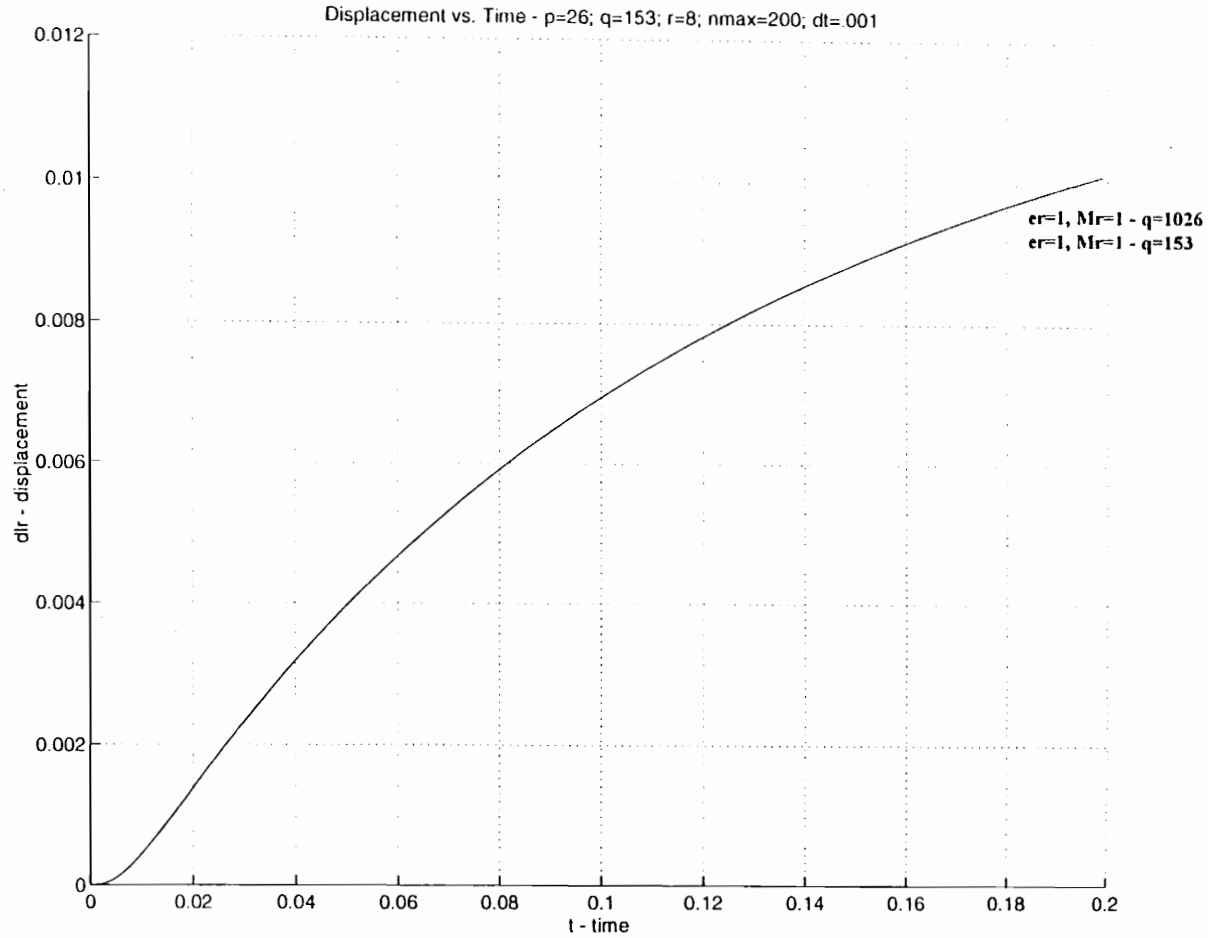

FIGURE 4.0c - Displacement at the Gelatinous Interface (Point R) vs. Time Curve: Constant Elasticity and Viscosity at t=0.2

4.1 Response to a Step Change in Velocity (Impulse in Acceleration)

When the elasticity and the viscosity of both gel layers remain constant, the results of the single-layered viscoelastic model of the human otolith organs are matched for both short and long times. These results are illustrated in Figures 4.1a-b. Constant elasticity and viscosity produce the same slope for the columnar filament and the gelatin layer. This behavior is similar to the previous model presented by Grant and Cotton [7] for gel layer of constant viscoelasticity. This result shows that this model reproduces earlier results.

Plate displacement versus time and interface displacement versus time are shown for various values of ε_r in Figures 4.1c-d. It is apparent in these Figures that the variations in elasticity produce little or no change in displacement. The interface displacement is about four times smaller than that of the plate displacement, which is to be expected.

Figures 4.1e-h show displacement profiles, while elasticity is varied. Regardless of the variation of elasticity in the lower or upper layers of the gel, the plate displacement remains the same for both layers. Despite the significant range of ε_r from .1 to 10, there is little or no change in displacement of the plate. The slope is the same for both gel layers. Therefore, changing the elasticity while the damping remains constant does not affect the plate displacement.

The dynamic plate and interface displacements are affected by viscosity. When the viscosity of the upper layer exceeds the viscosity of the lower layer, more displacement is created by the upper layer. This clearly demonstrates that damping is a controlling

element in this model. Plate displacement is greater than interface displacement. This phenomena can be seen clearly in Figures 4.1i-j.

The results of the single-layered viscoelastic gel model for constant elasticity and viscosity are reproduced in Figures 4.1k-l. In this case, elasticity and viscosity remain constant. For shorter times, a nonlinear behavior is illustrated. However, longer times demonstrate linear behavior. Both shorter and longer times for the upper and lower gel layers produce slopes that are approximately the same.

Displacement profiles for change in viscosity and constant elasticity are illustrated in Figures 4.1m-n . The upper layer having a higher viscosity than the lower layer, produces more displacement. For shorter times, the lower layer displays linear behavior and nonlinearity is shown for the upper layer. For longer times, linearity is shown for both the upper and lower layers. Steeper slopes are produced for viscosity values of the upper layer exceeding that of the lower layer. The upper layer produces significantly more plate displacement than the lower layer.

In Figures 4.1o-p, the slopes of each layer are reversed when the lower layer viscosity exceeds that of the upper layer. These slopes for each layer are much steeper. More viscosity in the upper layer of the gel produces more plate displacement for both shorter and longer times. The increase in viscosity stiffens each layer thereby producing steeper slopes.

A viscosity ratio less than 0.90 produces instabilities in the system. Negative displacements are produced. This behavior is anatomically impossible and may be due to a numerical error of the finite difference method.

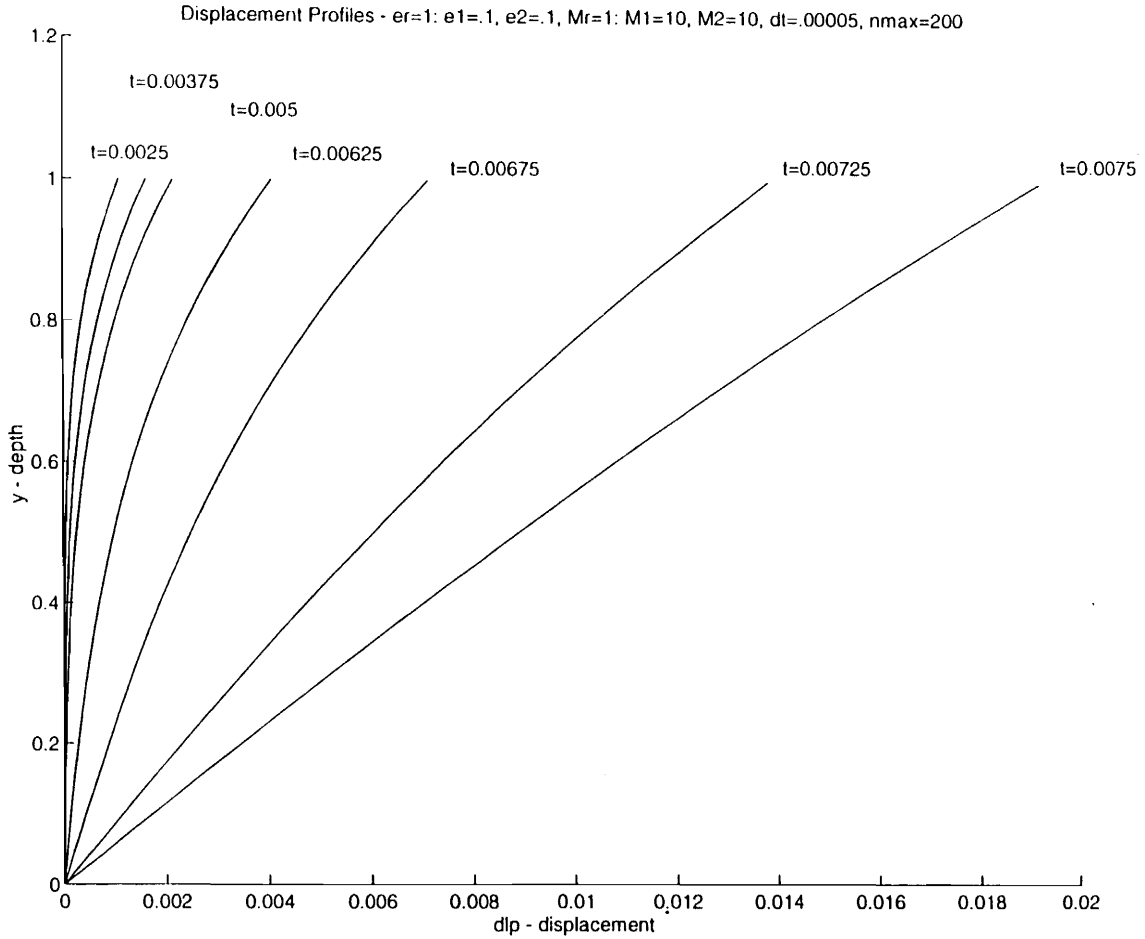

FIGURE 4.1a - Displacement Profiles: Constant Elasticity and Viscosity at t=0.01

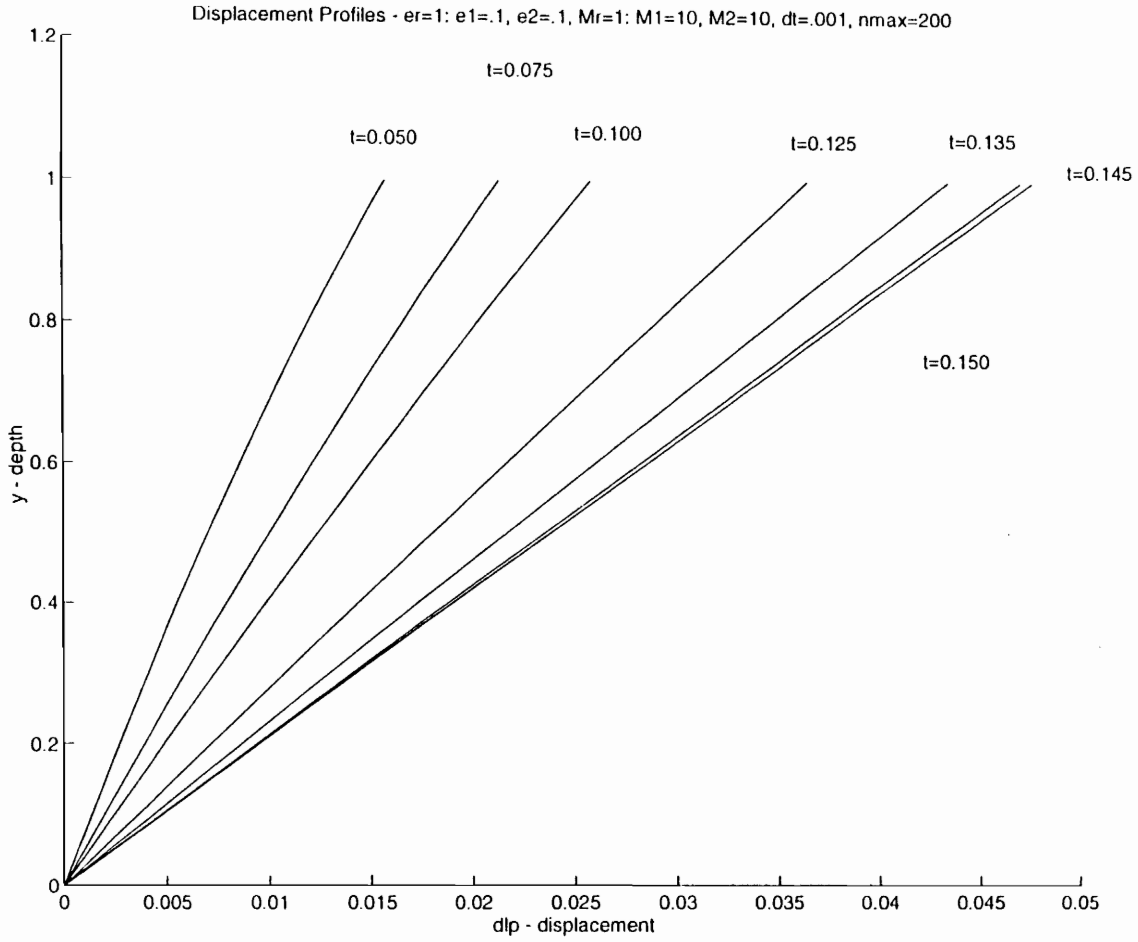

FIGURE 4.1b - Displacement Profiles: Constant Elasticity and Viscosity at t=0.2

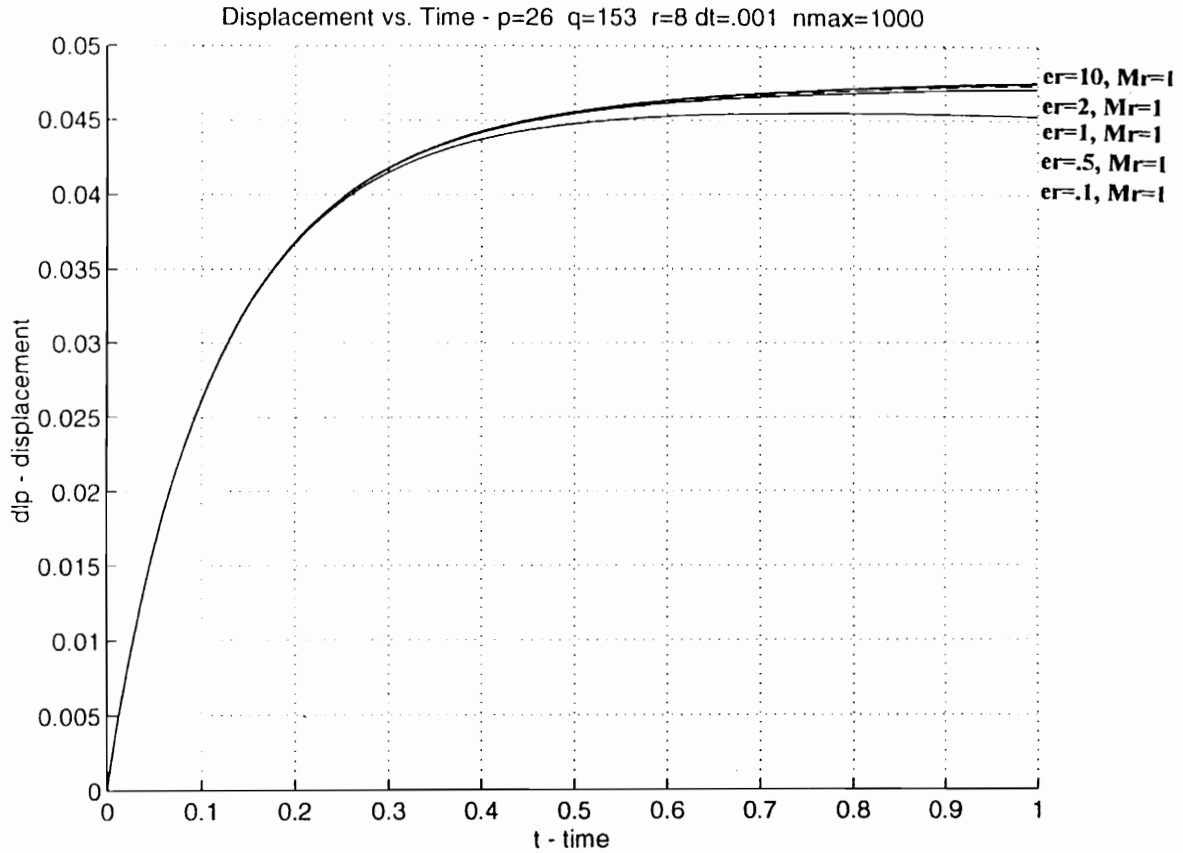

FIGURE 4.1c - Plate Displacement vs. Time Curve: Varied Elasticity and Constant Viscosity at t=1.0

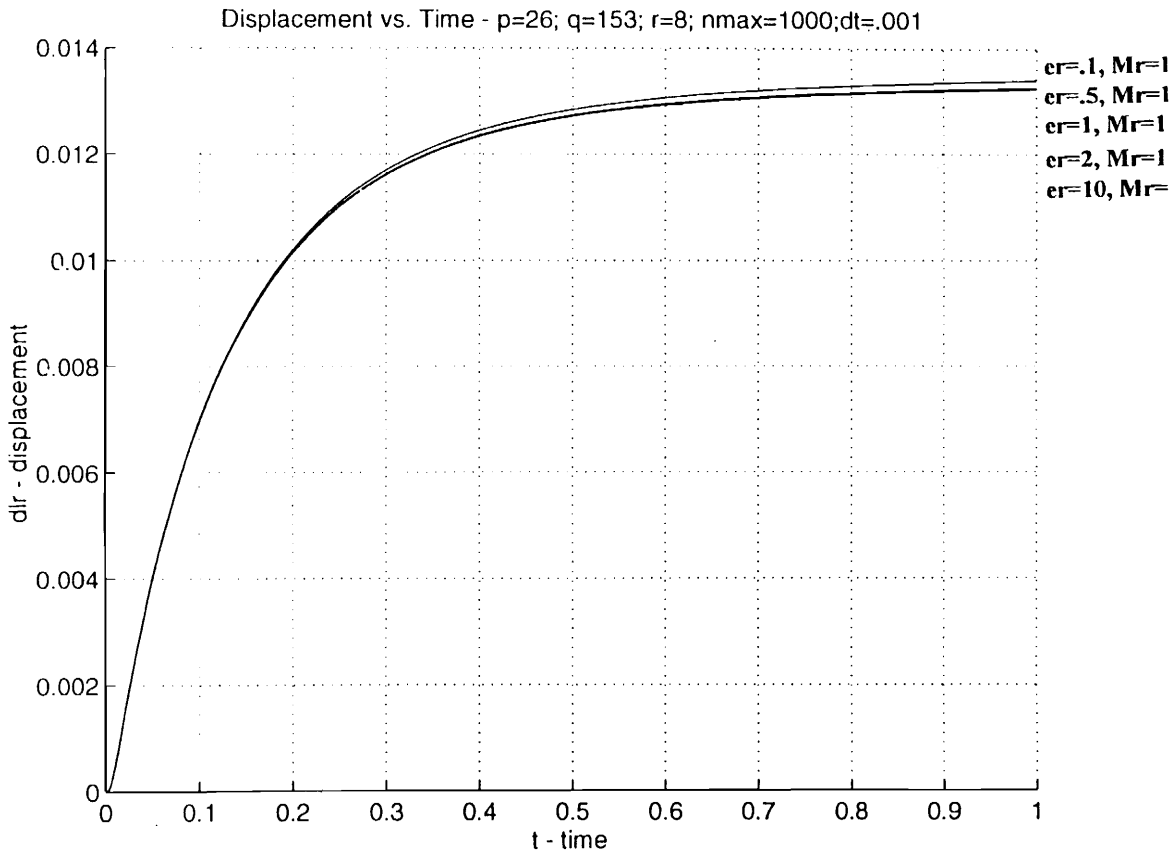

FIGURE 4.1d - Displacement at Point R vs. Time Curve: Varied Elasticity and Constant Viscosity at t=1.0

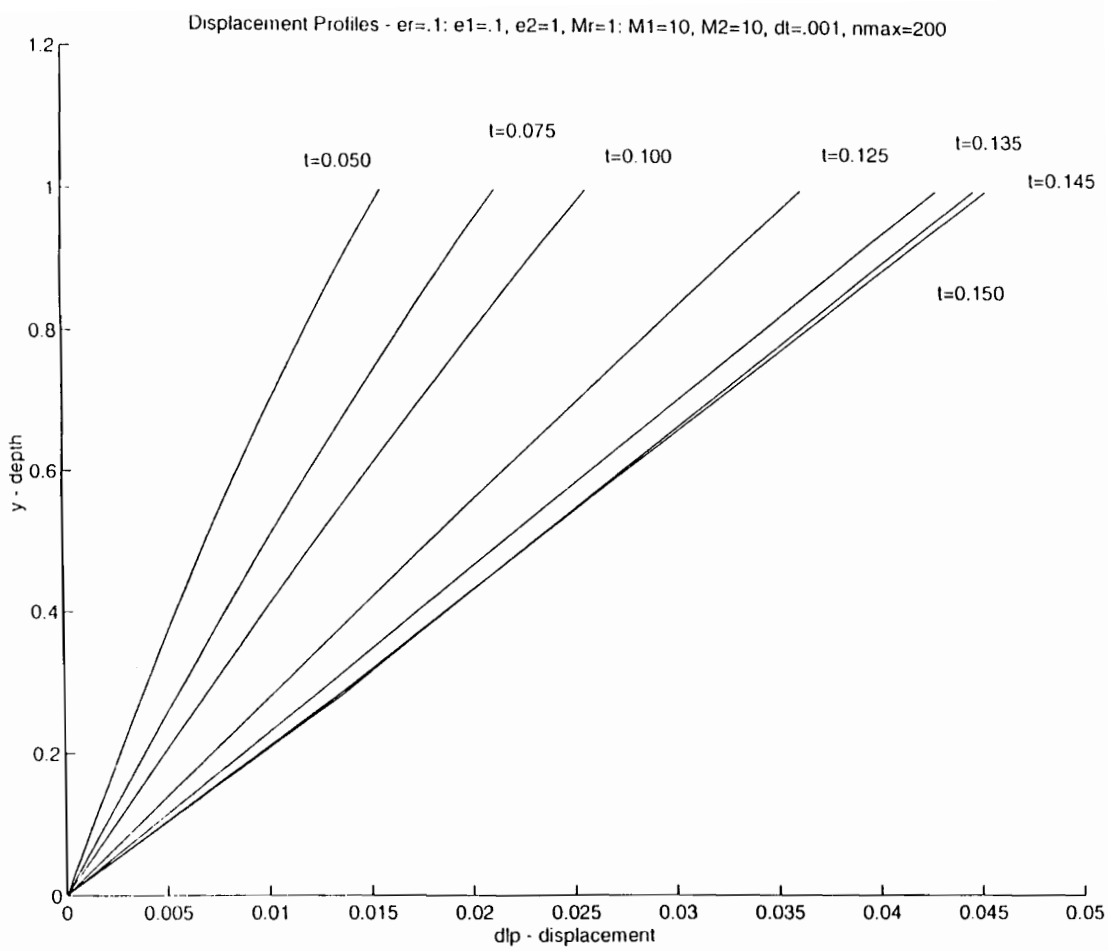

FIGURE 4.1e - Displacement Profiles: Varied Elasticity and Constant Viscosity at t=0.2

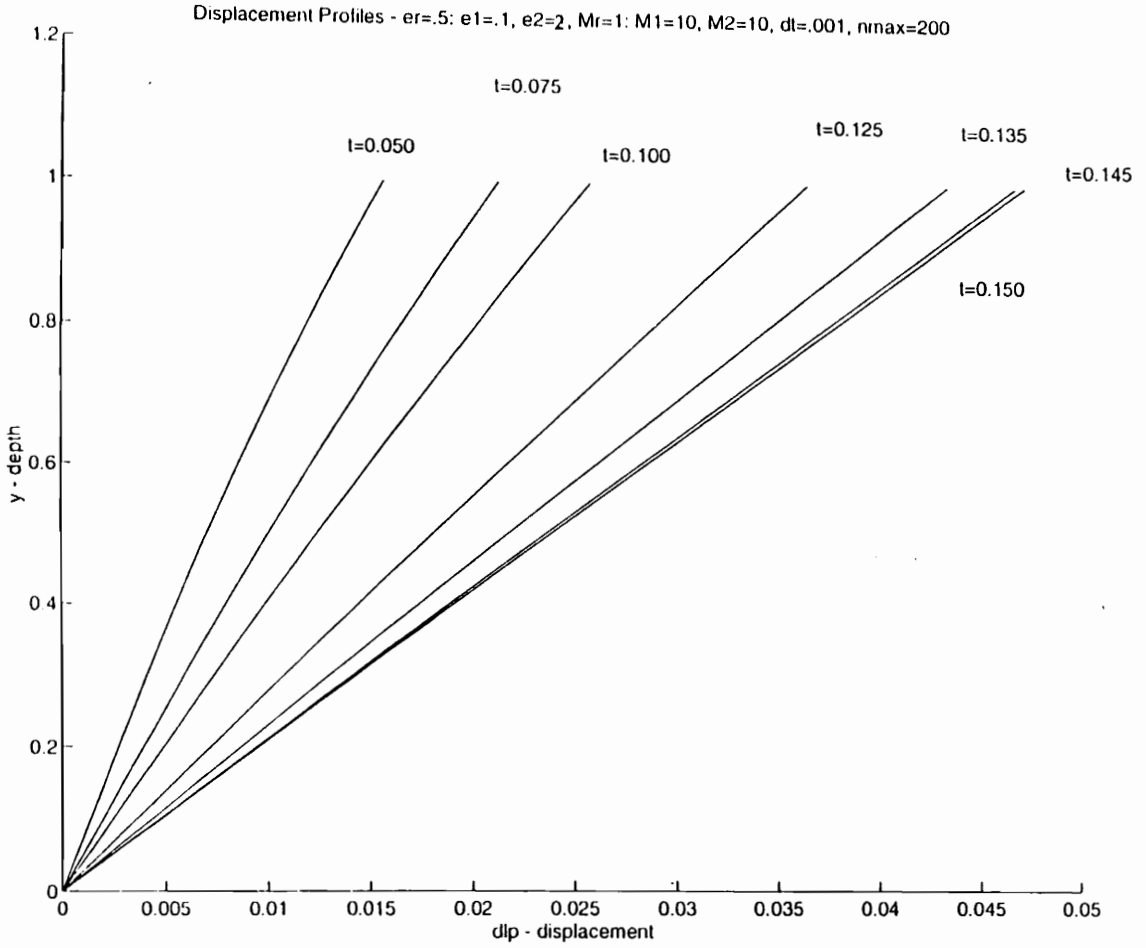

FIGURE 4.1f **- Displacement Profiles: Varied Elasticity and Constant Viscosity at t=0.2**

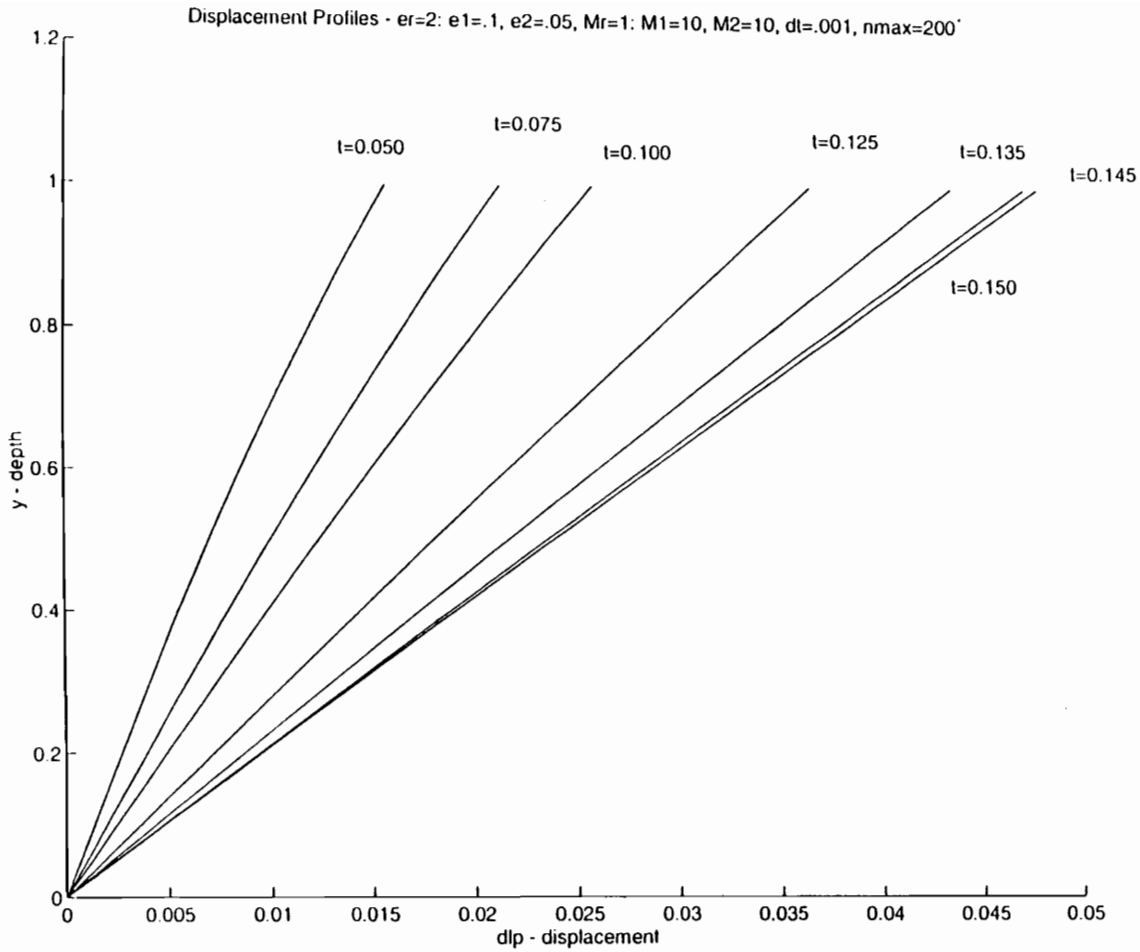

FIGURE 4.1g **- Displacement Profiles: Varied Elasticity and Constant Viscosity at t=0.2**

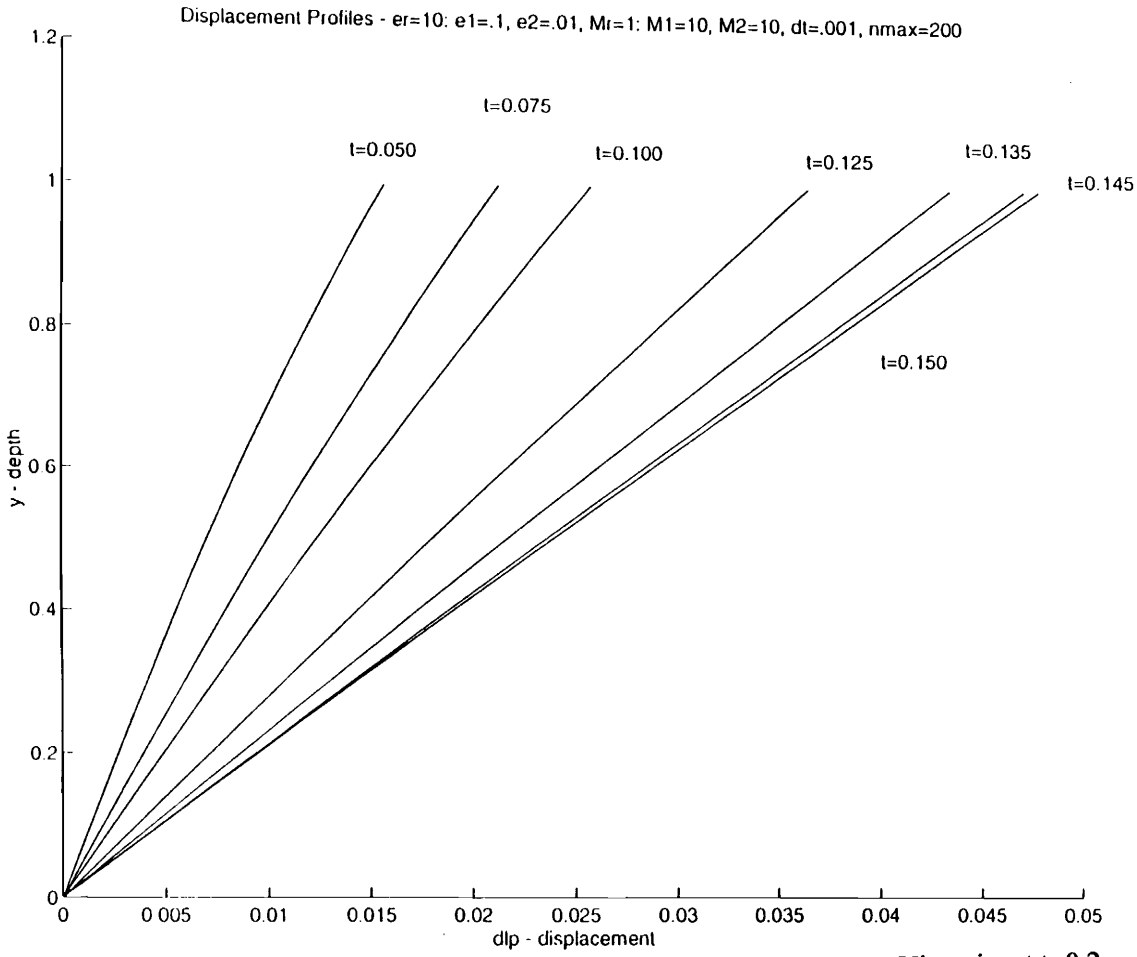

FIGURE 4.1h - Displacement Profiles: Varied Elasticity and Constant Viscosity at t=0.2

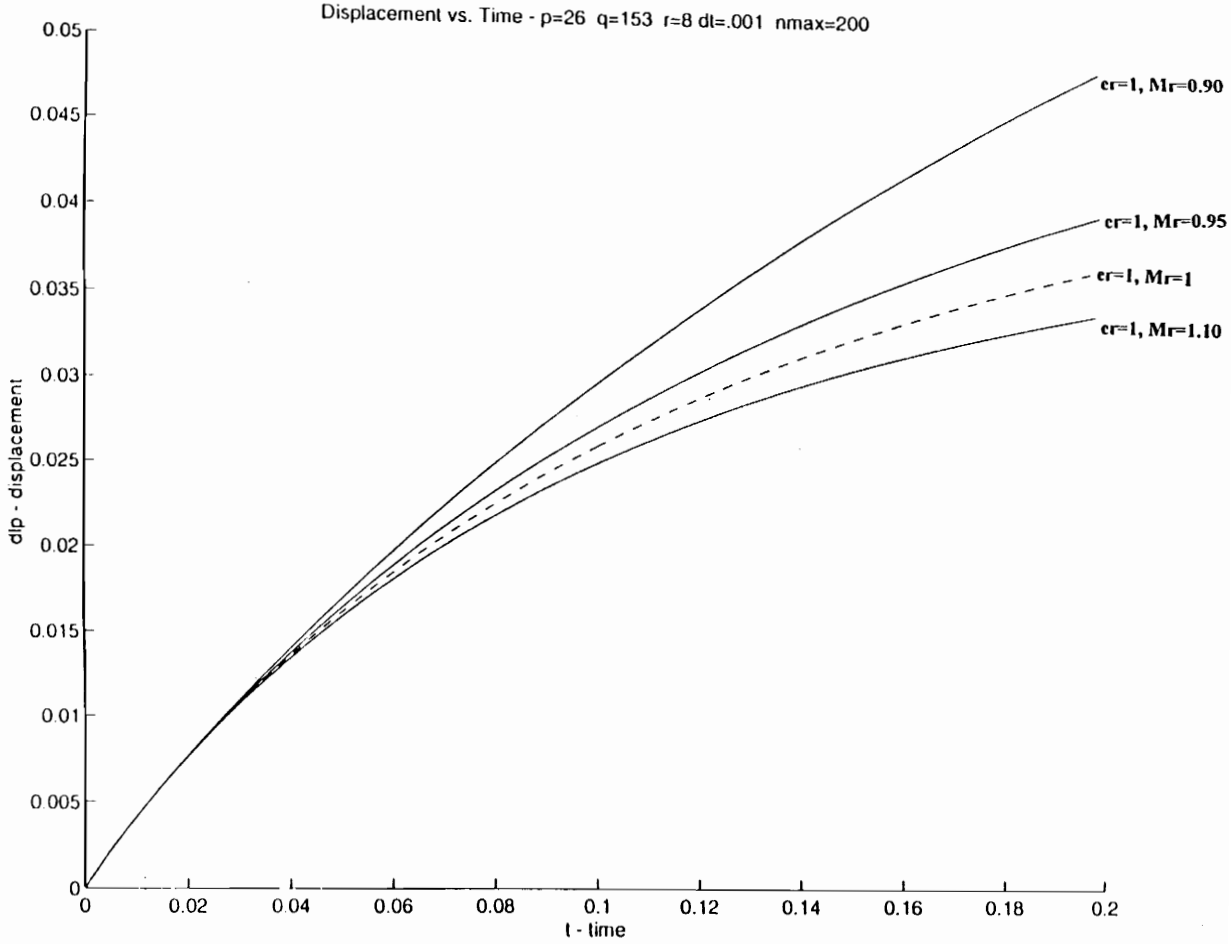

FIGURE 4.1i - Plate Displacement vs. Time Curve: Varied Viscosity and Constant Elasticity at t=0.2

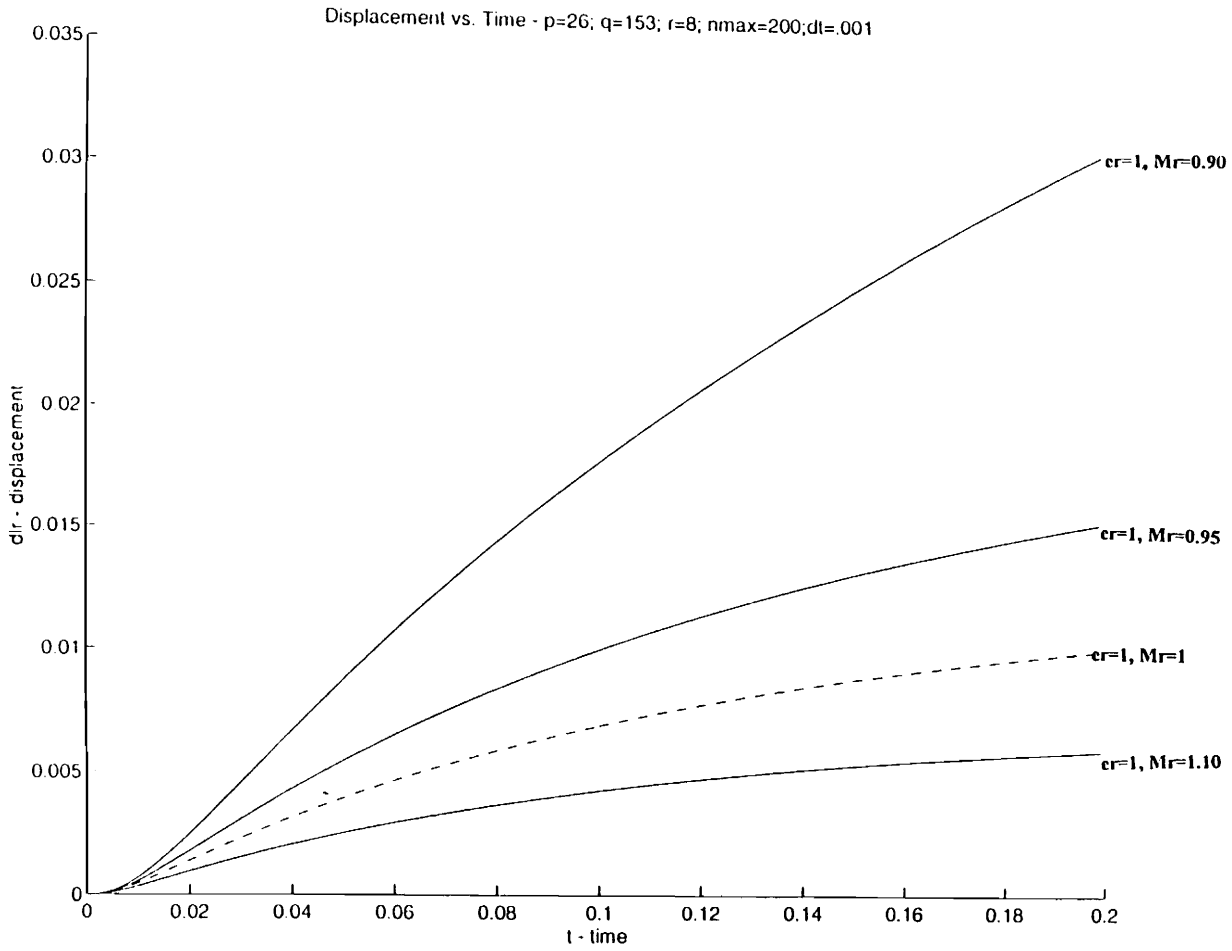

FIGURE 4.1j - Displacement at Point R vs. Time Curve: Varied Viscosity and Constant Elasticity at t=0.2

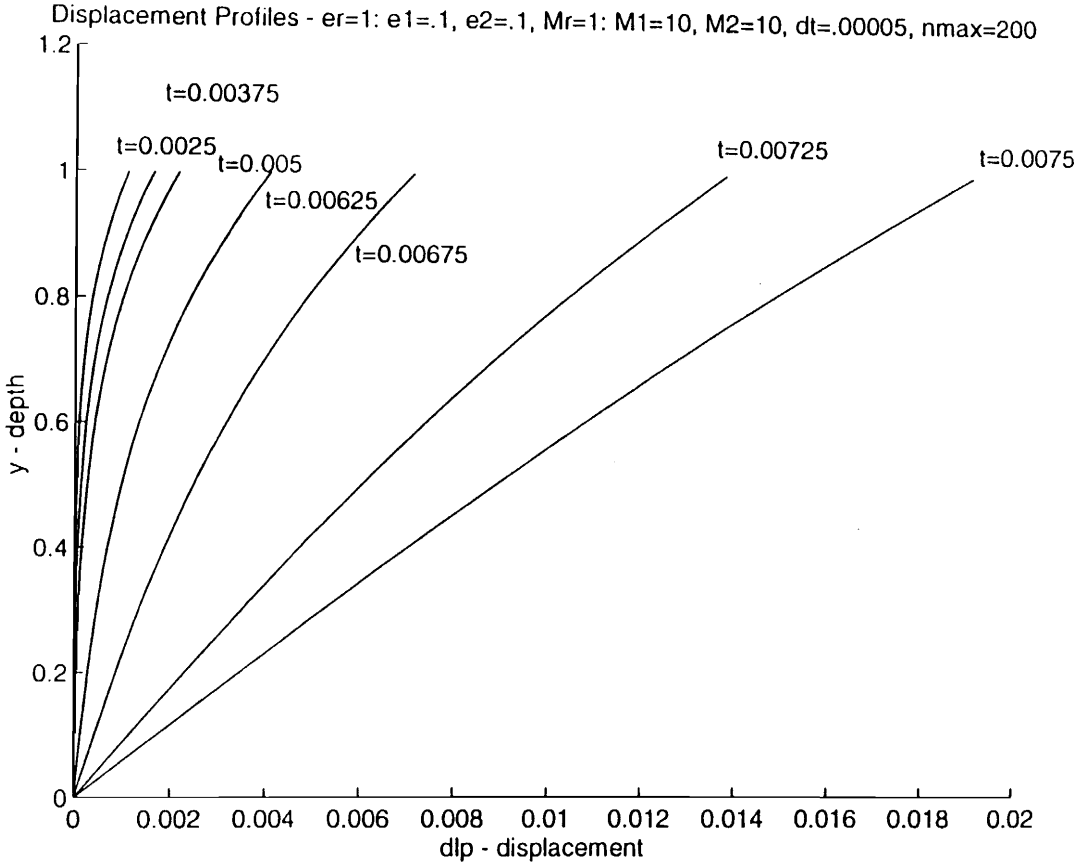

FIGURE 4.1k - Displacement Profiles: Constant Elasticity and Viscosity at t=0.01

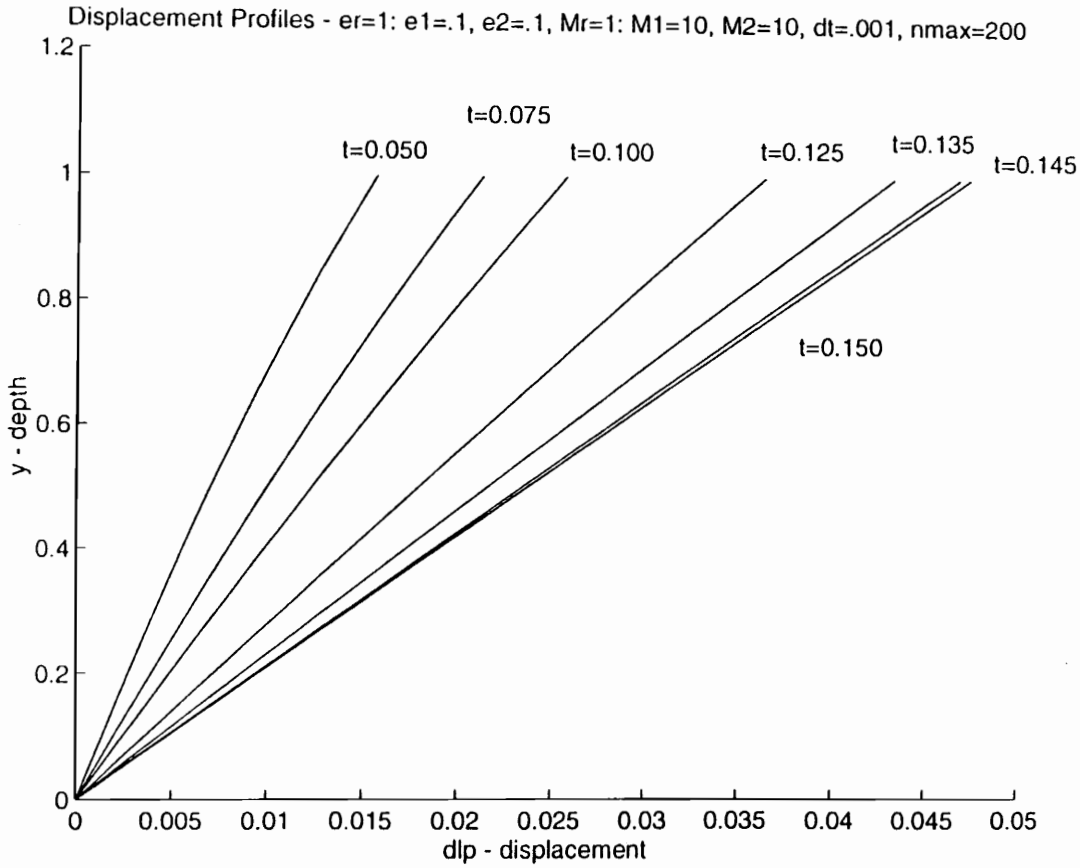

FIGURE 4.11 - Displacement Profiles: Constant Elasticity and Viscosity at t=0.2

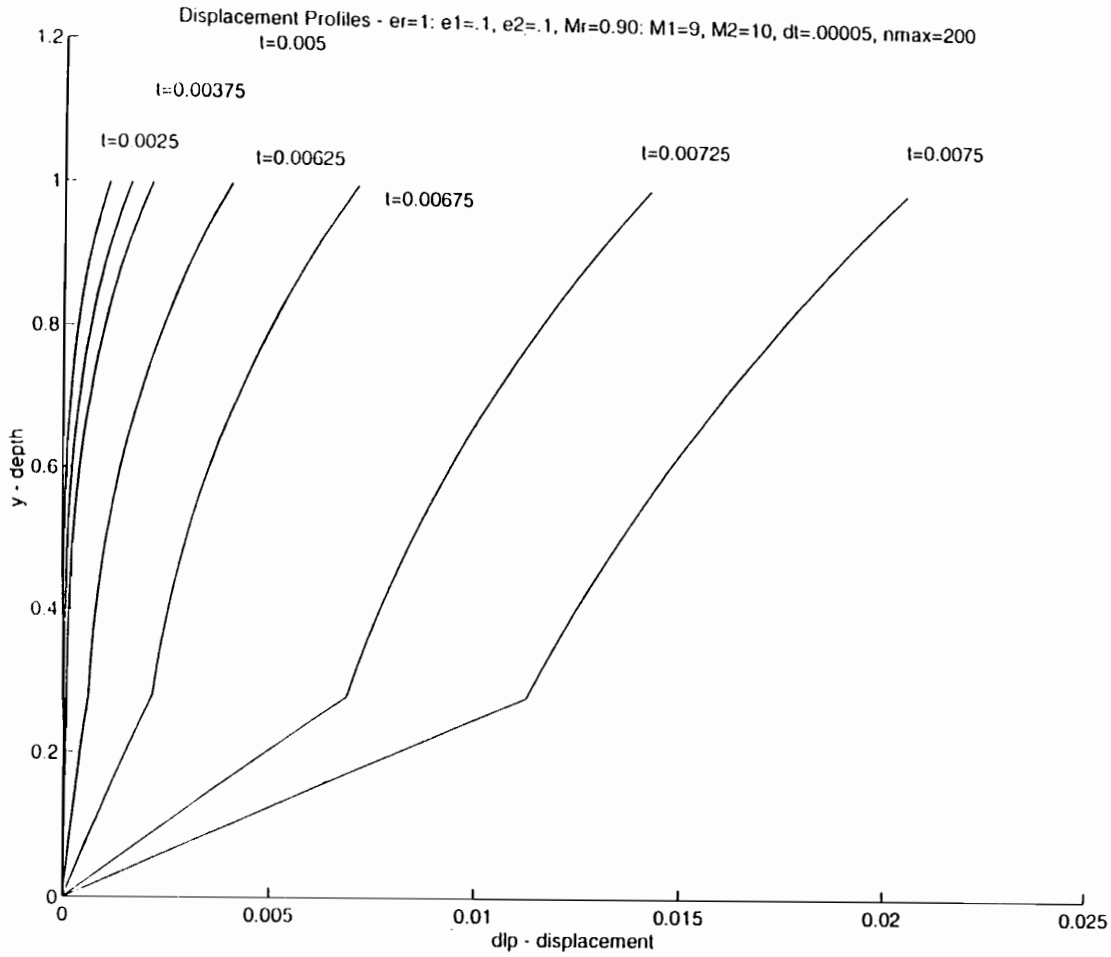

FIGURE 4.1m - Displacement Profiles: Varied Viscosity and Constant Elasticity at t=0.01

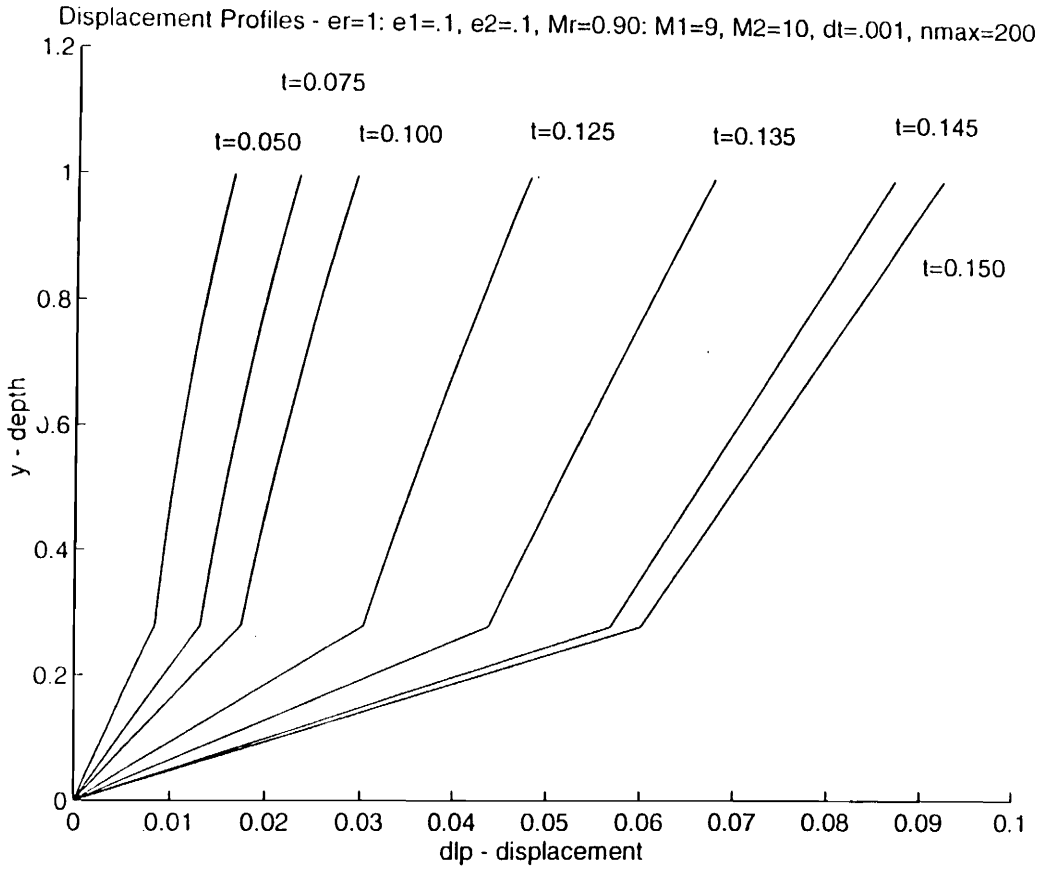

FIGURE 4.1n - Displacement Profiles: Varied Viscosity and Constant Elasticity at t=0.2

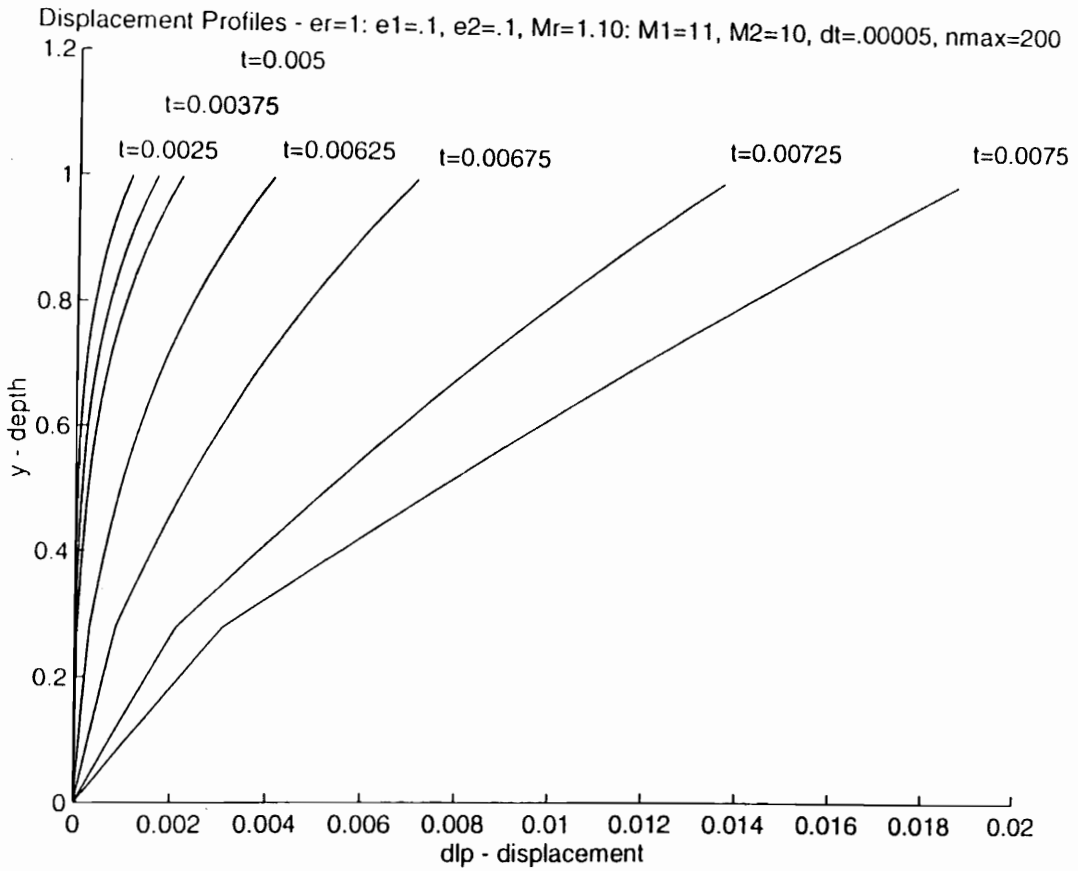

FIGURE 4.1o - Displacement Profiles: Varied Viscosity and Constant Elasticity at t=0.01

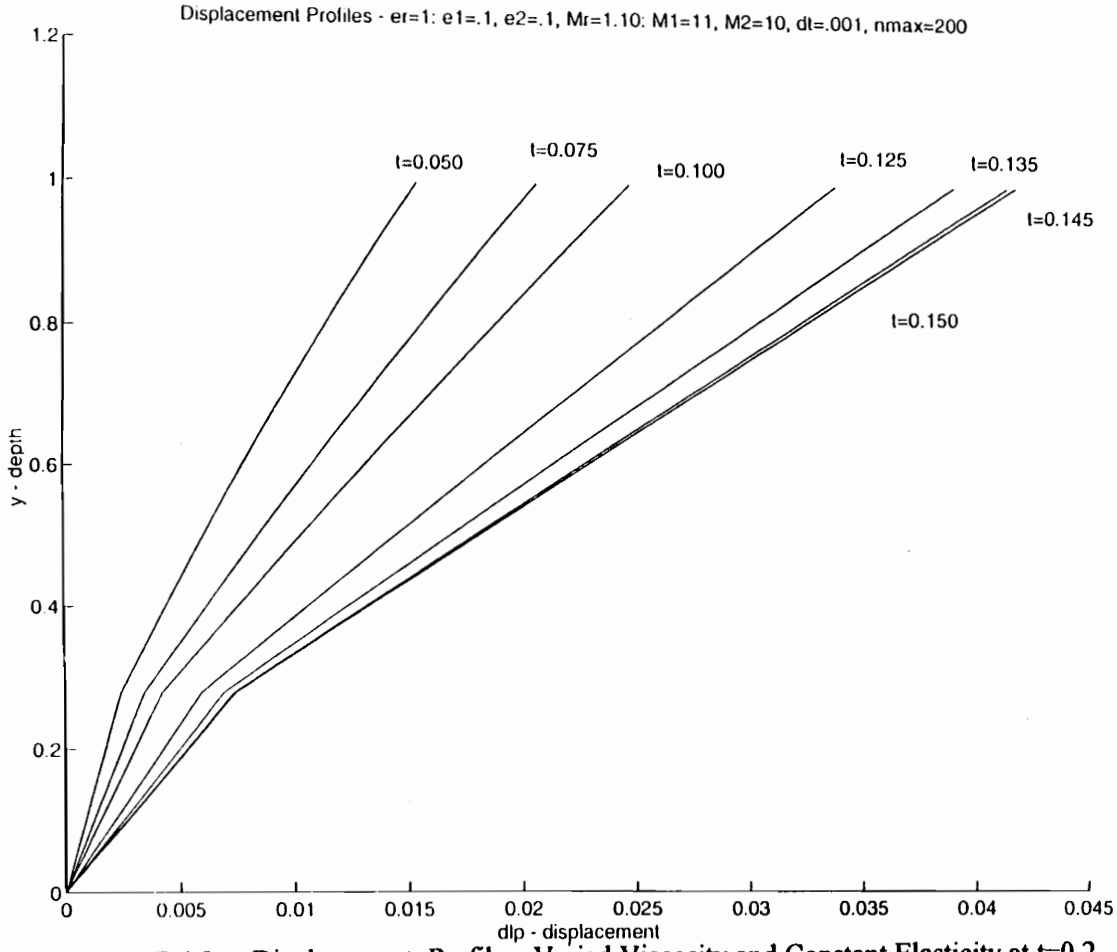

FIGURE 4.1p - Displacement Profiles: Varied Viscosity and Constant Elasticity at t=0.2

4.2 Constant Acceleration Response

The steady-state case of an otolith organ under a constant gravitational acceleration is observed. The nondimensionalized governing equation for the plate (Equation 2.4.2) loses all transient terms and the gravitational acceleration term equals the elastic term. The following equations are used to determine the time displacement profiles:

for the lower layer,

$$(1-R) = \bar{\varepsilon}_1 \frac{\partial \bar{\delta}_r}{\partial \bar{y}_r} = \bar{\varepsilon}_1 \frac{\bar{\delta}_r}{\Delta \bar{y}_r}$$

$$\text{where } \Delta \bar{y}_r = 0.28 = \frac{1}{7}$$

for the upper layer,

$$(1-R) = \bar{\varepsilon}_2 \frac{\partial \bar{\delta}}{\partial \bar{y}_p} = \bar{\varepsilon}_2 \frac{\bar{\delta}_p}{\Delta \bar{y}_p} - \bar{\delta}_r$$

$$\text{where } \Delta \bar{y}_p = 0.72 = 1 - 0.28$$

This is illustrated in Figure 4.2a. The values of ε_r range from 0.5 to 10. Constant elasticity and damping produce the same slope for the upper layer and the lower layer of the gel which is illustrated in Figure 4.2b. These results confirm the maximum plate displacement calculations.

Two different slopes in the two layers occur when the elasticity of the upper layer exceeds that of the lower layer. This phenomenon illustrated in Figure 4.2c implies that

the model works. In fact, this result produces similar results to that of the step change in skull velocity. Various ε_r values are tested. Upper layer elasticity exceeding .2 and lower layer elasticity exceeding .1 produce inaccurate results. This may be due to a numerical error in the approximation of values at infinite time.

In Figures 4.2d-f, the lower layer elasticity exceeds that of the upper layer. The elasticity ratio ranges from 2 to 10. The viscosity for the upper and lower layers of the gel is 10. These slopes become steeper for both layers. The upper layer produces more plate displacement than the lower layer. For various viscosity ratios where M_2 equals values other than 10 for both longer and shorter times, the trials yield similar results.

If the viscosity ratio of the lower layer to the upper layer is below 0.90, the system does not behave properly. For longer times, negative displacements occur initially and later result in very large positive displacements. However, there aren't any negative displacements present at shorter times.

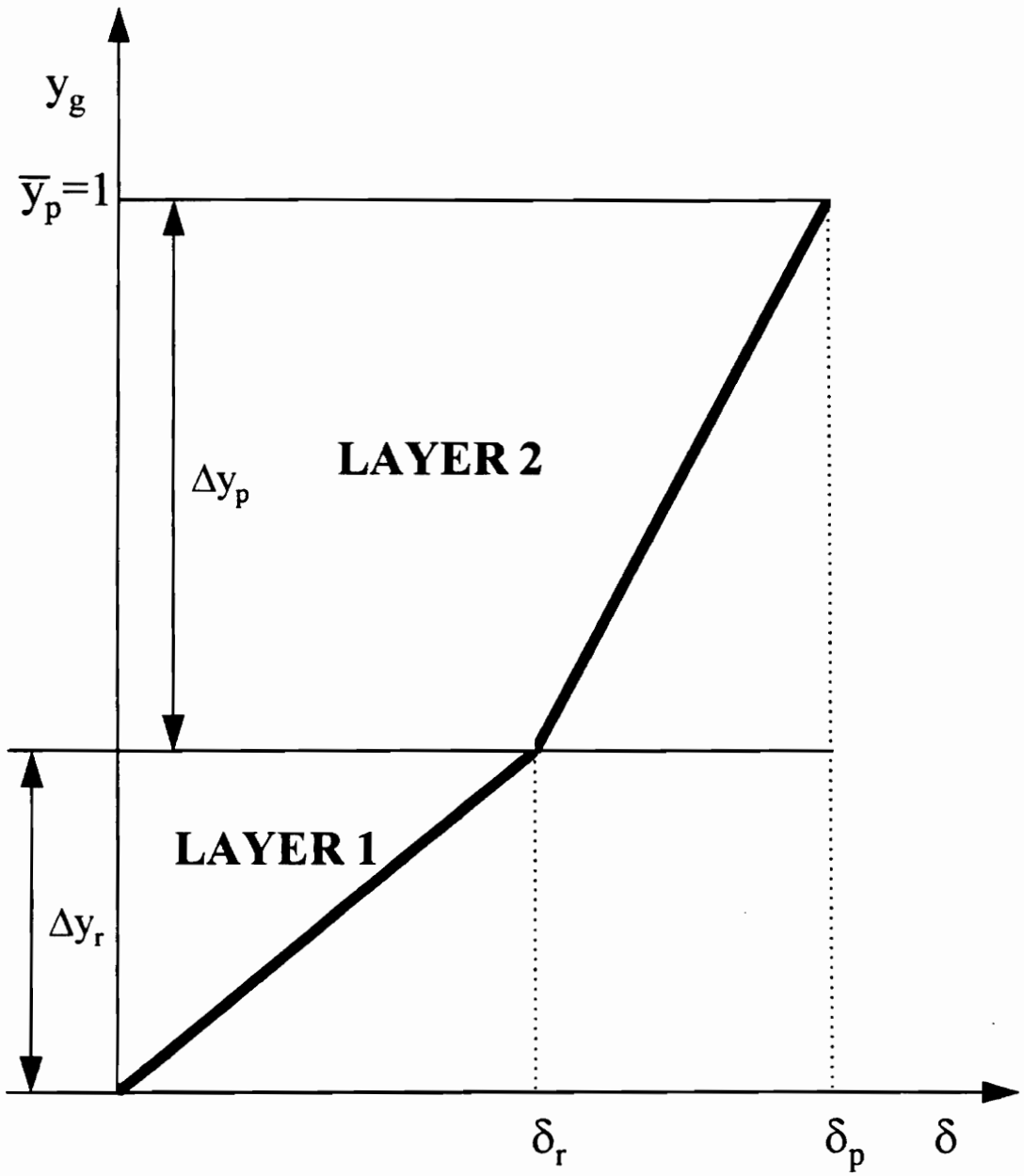

FIGURE 4.2a - Calculations for δ_r and δ_p

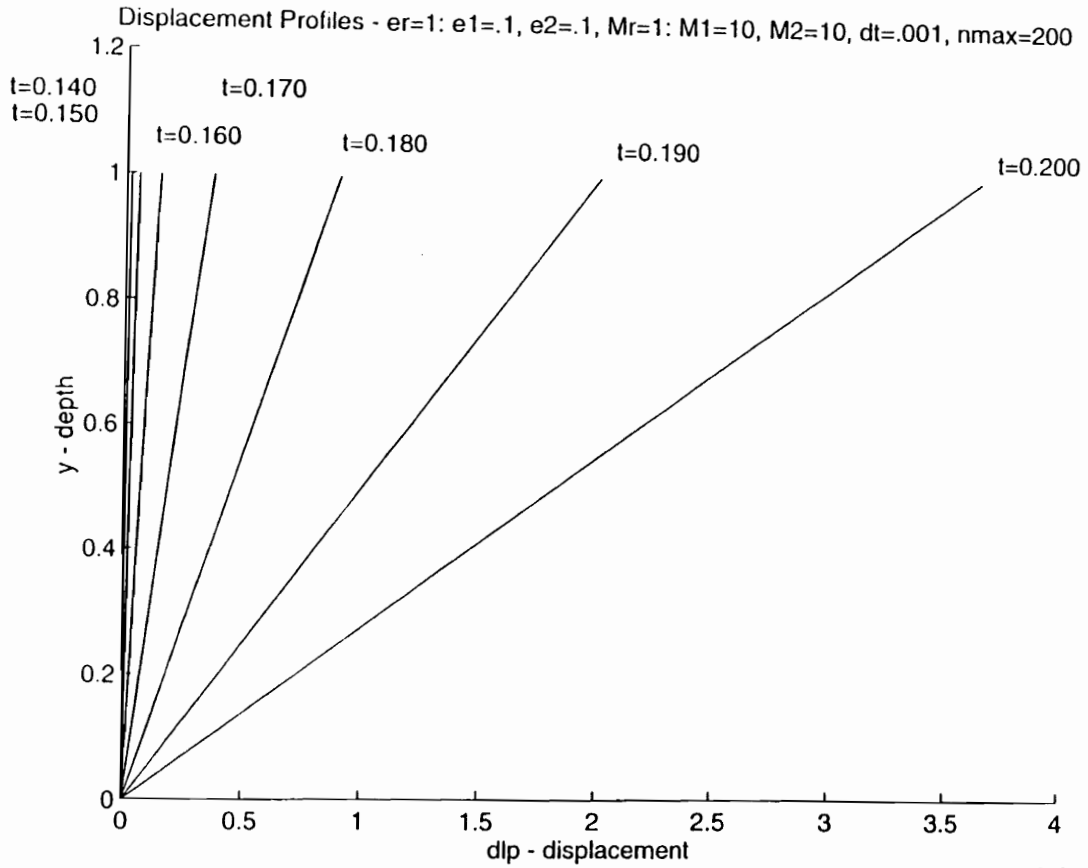

FIGURE 4.2b - Displacement Profiles: Constant Elasticity and Viscosity at t=0.2

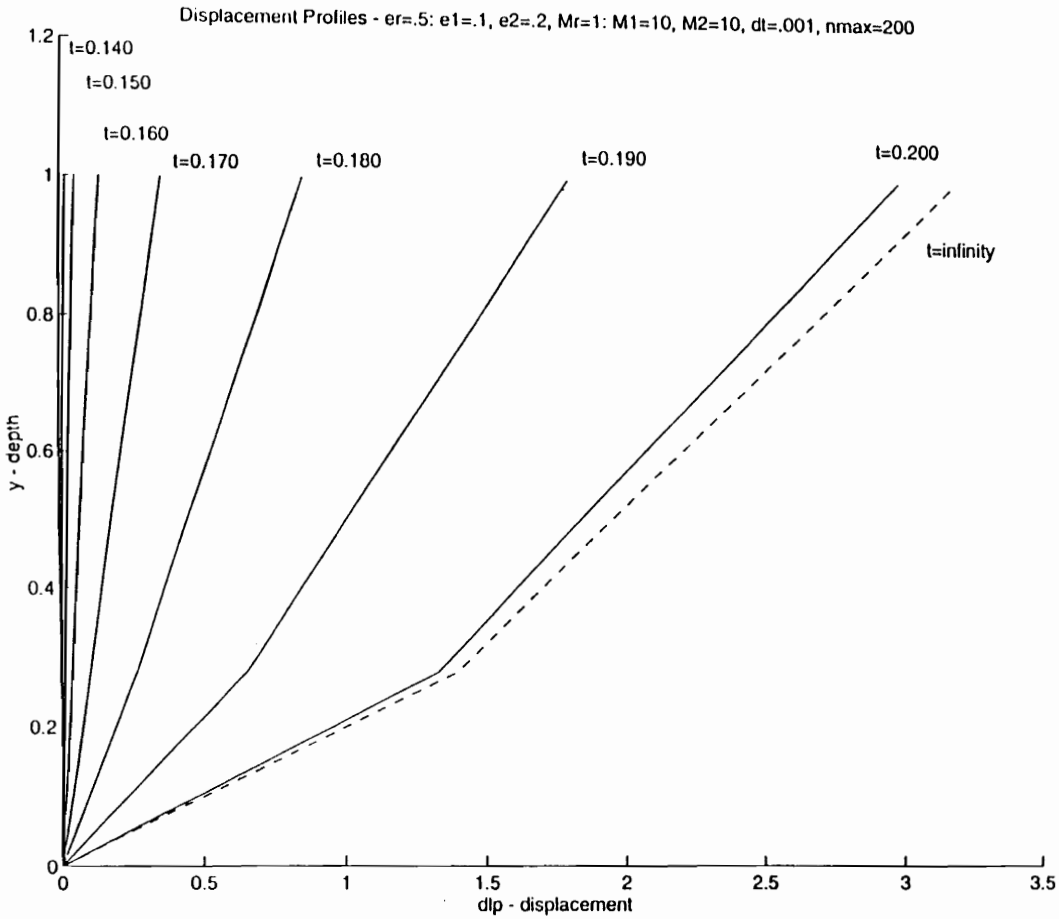

FIGURE 4.2c - Displacement Profiles: Varied Elasticity and Constant Viscosity at t=0.2

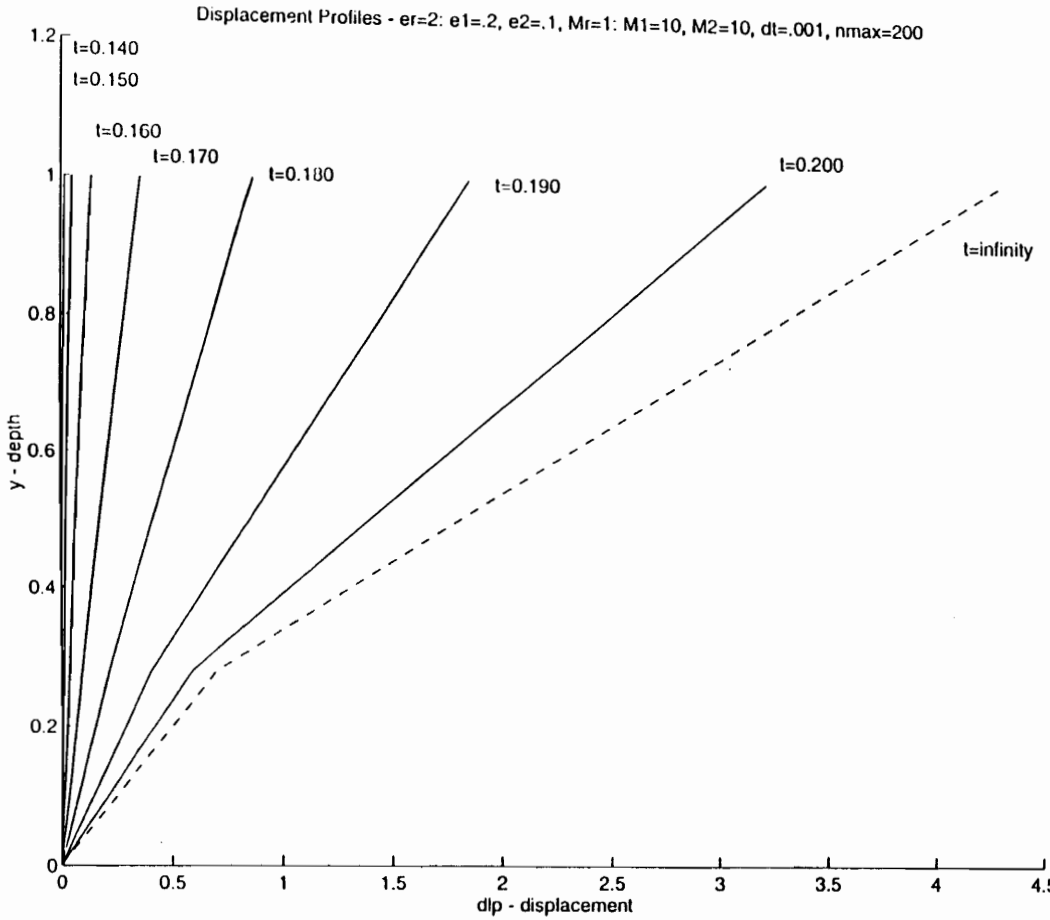

FIGURE 4.2d - Displacement Profiles: Varied Elasticity and Constant Viscosity at t=0.2

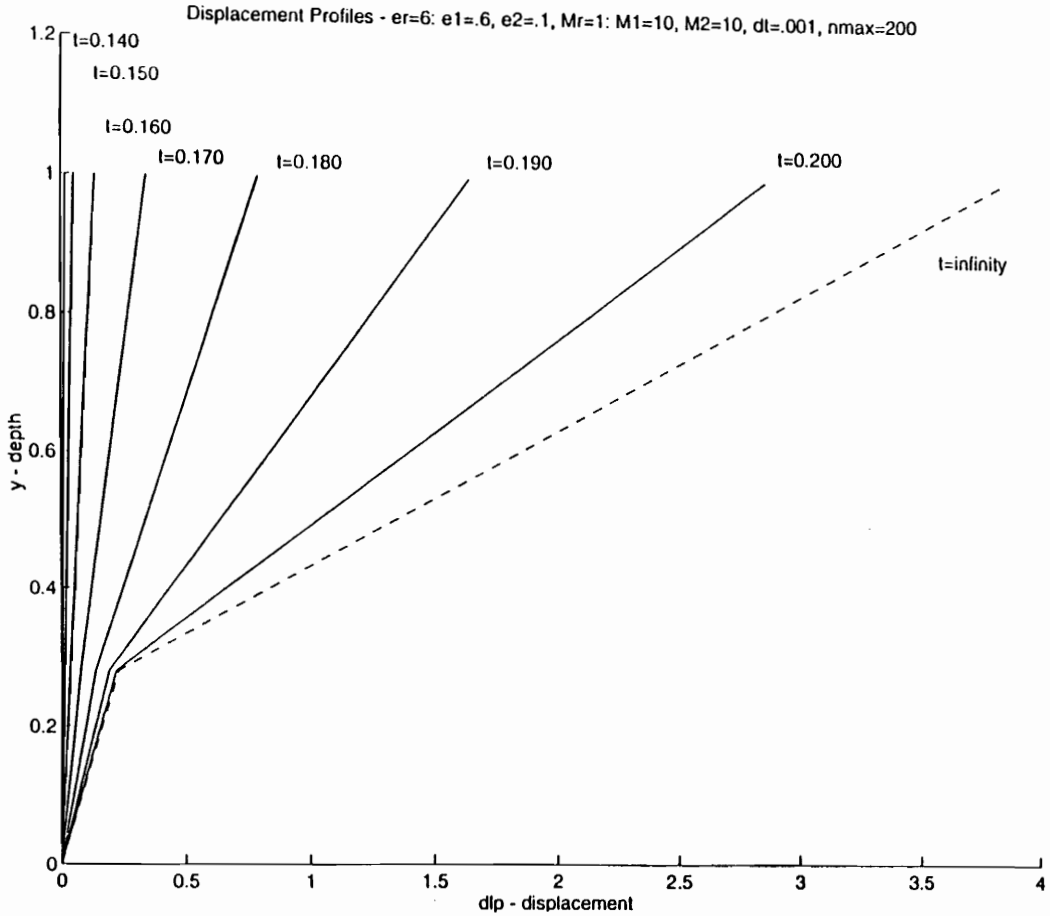

FIGURE 4.2e - Displacement Profiles: Varied Elasticity and Constant Viscosity at t=0.2

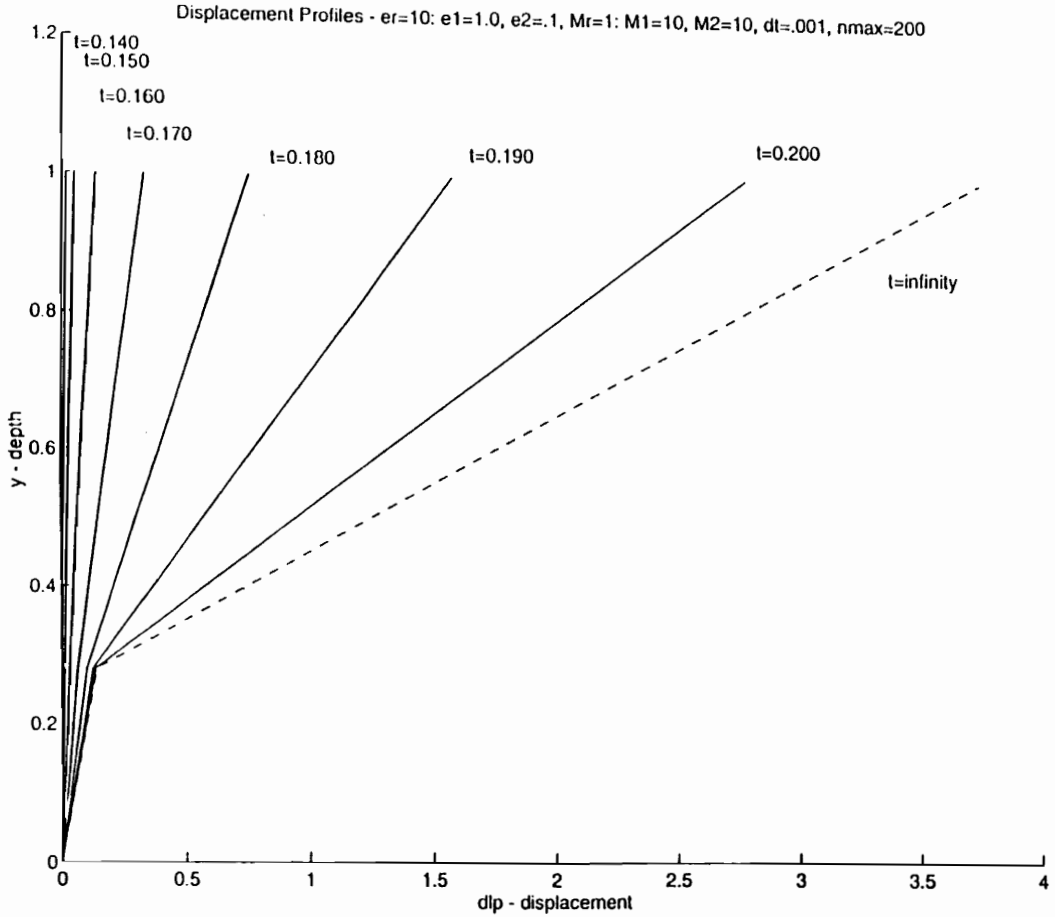

FIGURE 4.2f - Displacement Profiles: Varied Elasticity and Constant Viscosity at t=0.2

Chapter 5

Conclusions

For a step change in velocity of the skull, the otoconial membrane reaches a maximal displacement and slowly returns to its equilibrium position by the viscoelastic gelatinous membrane. In this model, changes in elasticity had little to no effect on the plate displacement with a step change in velocity (an impulse in acceleration). This result suggests that the gel's elasticity does not affect movement of the plate with this type of stimulus. However, the viscosity produces considerable changes in plate displacements. . The viscosity ratio of 0.90 and greater produces results that are anatomically correct. The upper layer of the gelatinous membrane consistently produce more plate displacements than the lower layer. This behavior is understandable since the upper layer is directly attached to the plate. Greater plate displacement is also produced when the viscosity of the upper layer exceeds that of the lower layer. This greater displacement occurs because the lower layer has less stiffness which causes movement of the hair follicles of the sensory cell base.

For the constant acceleration response, the elasticity has a significant effect on plate displacement. Elasticity ratios greater than 0.33 yield anatomically correct results. These results confirm the maximum plate displacement calculations. Less displacement is produced for the elasticity of the upper layer exceeding that of the lower layer. Obviously, the elasticity can limit the maximum displacement.

For constant viscosity and elasticity, the results of the single-layered viscoelastic model and the bi-layered gel model match considerably. Both the single-layered gel and the gel bi-layered models are illustrated in Figure 5.0a. Notice that the upper layer has a higher displacement than the lower layer. This behavior is due to the higher viscosity of the upper gel layer. More importantly, the nondimensional displacement of the single-layered gel is only 0.047, whereas the nondimensional displacement of the bi-layered gel model is double this value. At the interface, the displacement of the bi-layered gel model is approximately five times greater than the displacement of the single-layered gel model. By simply adding another the bi-layered gel structure to this model, the plate displacement is increased significantly.

To further explain this phenomena it is necessary to consider the composition and function of the otolith organ. During changes in acceleration, the differences in densities between the endolymph fluid, viscoelastic gelatinous membrane, and the otoconial membrane cause the gelatinous membrane to shear. The denser otoconial membrane mass lags behind the sensory cell base due to its inertia and this motion results in deformation of the bi-layered gelatinous membrane. This amorphous and fibrillar gelatinous layer consists of small holes. The gelatinous layer is composed of mucopolysaccharides and glycoproteins. The viscous nature of the gelatinous layer is caused by its content of acidic mucopolysaccharides. Kachar [12] states that the upper gelatinous layer (gelatin layer) has a more closely packed structure and is therefore more viscous. This finding suggests that the lower gelatinous layer (columnar filament) is more loosely structured. Because of

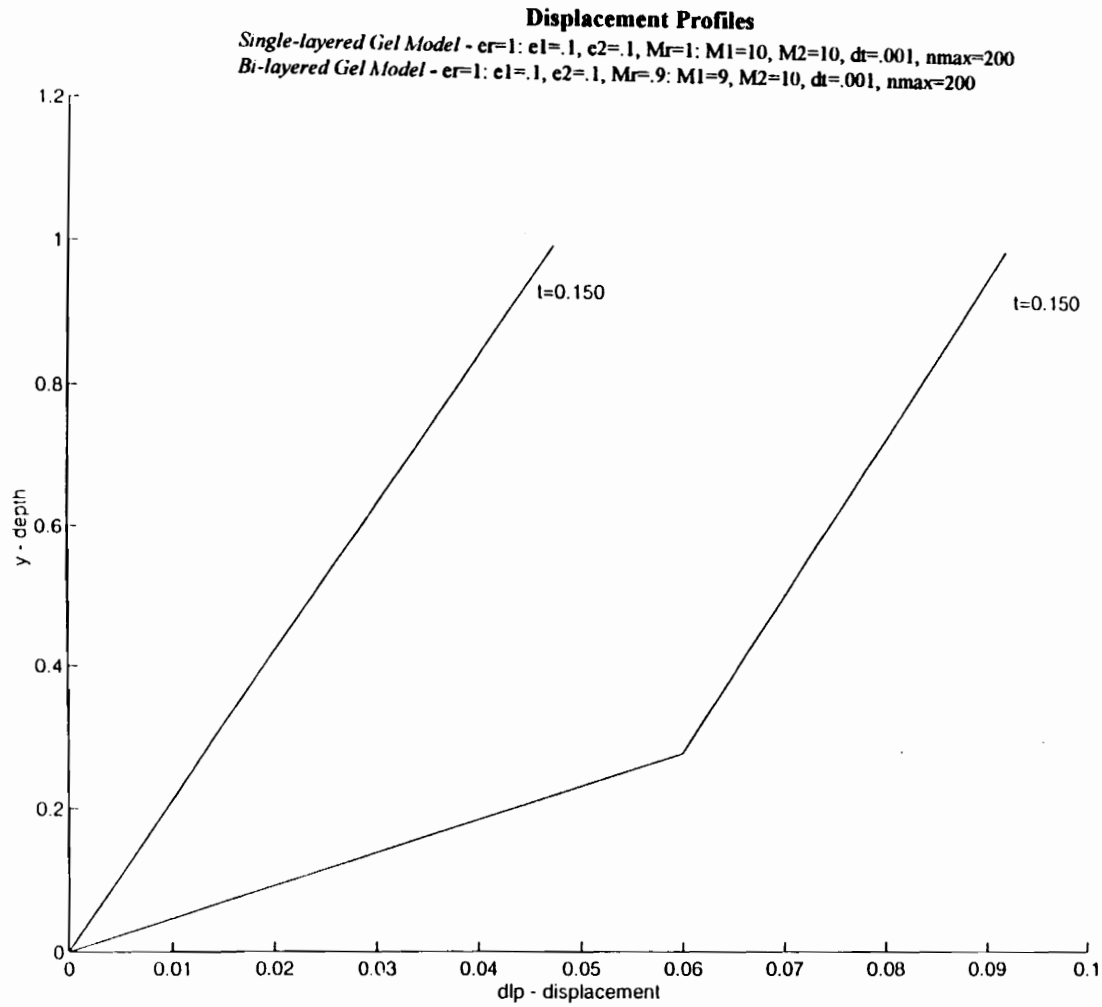

FIGURE 5.0a - Displacement Profiles: **Left**-Single-layered Gel Model and **Right**-Bi-layered Gel Model at t=0.2

the fewer number of mucopolysaccharides and significant number of holes in this loosely arranged structure, the addition of this lower layer allows for less viscous dissipation. The lower layer of the gelatinous membrane deforms more easily in shear than its upper layer. The shearing of the gel's lower layer bends the ciliary bundles of the sensory cell base. These ciliary bundles are connected by protein links. When the ciliary bundles bend, the protein links break allowing ions from the surrounding extracellular fluid to flow into the hair cells changing their polarity. The hair cells send signals to the Central Nervous System to the brain where these signals are used to provide changes in postural control and visual fixation.

Figure 5.0b shows plate displacement at viscosity ratios less than 0.90. The upper layer provides more displacement than the lower layer. The constant increase of displacement at increasing times indicates that there is no oscillatory behavior. However, at longer times negative displacements are produced and the upper layer creates less displacement than the lower layer. This model does not work for viscosity ratios less than 0.90. The cause of this behavior is uncertain. Perhaps it is caused by a numerical problem. However, for constant viscosity and elasticity, the results of the single-layered viscoelastic model and this model match considerably.

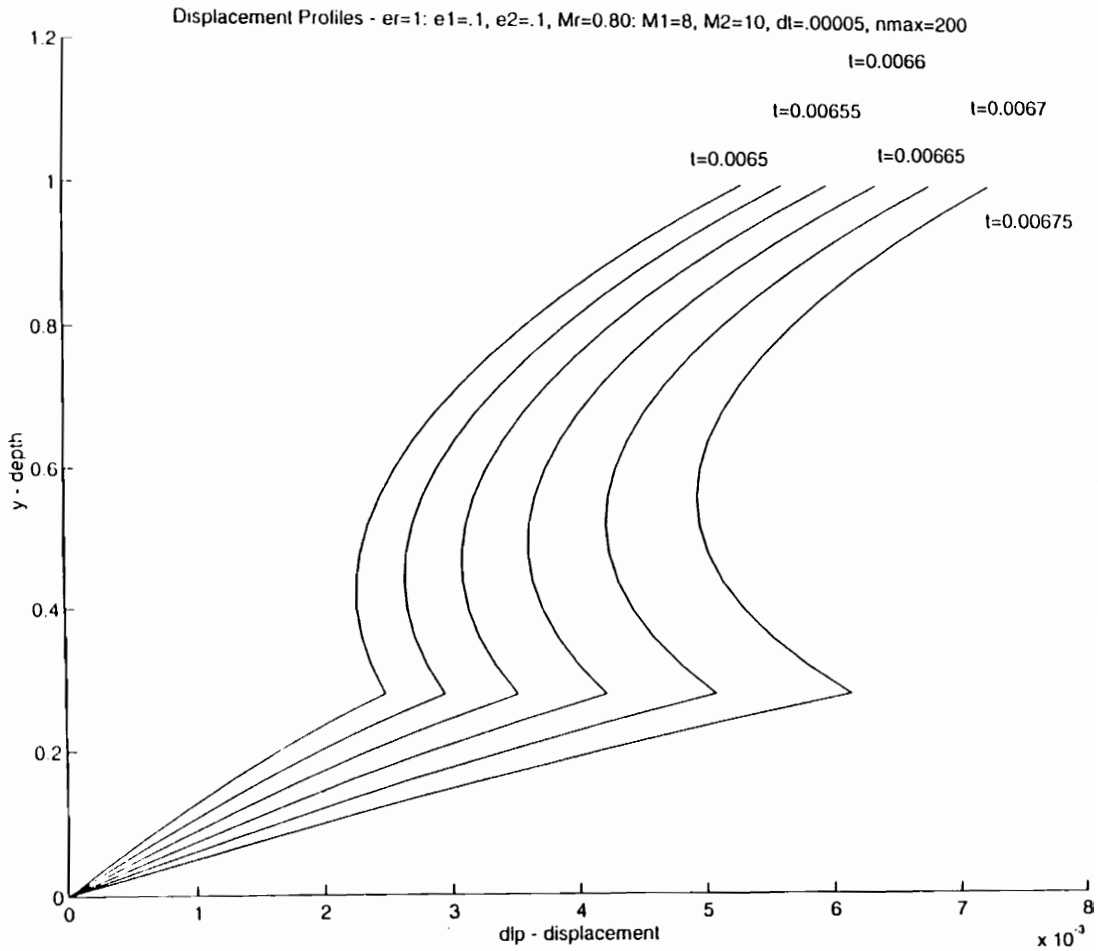

FIGURE 5.0b - Displacement Profiles: Instabilities at Viscosity Ratio=0.80 and Constant Elasticity at t=0.01

Chapter 6

Summary

The otolith organs are responsible for sensing linear motion in the inner ear. They comprise an overdamped second order system and respond to gravity and skull acceleration. This work models the otolith organ as a three material system; endolymph (fluid), otoconial membrane (rigid plate) and the bi-layered gelatinous membrane (viscoelastic gel). Each layer of the gel is modeled as a Kelvin-Voigt viscoelastic material. Each layer possesses different elastic and viscous properties. The governing equations for the fluid and the plate are derived and nondimensionalized. The shear stresses acting at the surface of the bi-layered gel are nondimensionalized and equated to develop the governing equation. These governing equations are solved for a step change in velocity and a constant acceleration stimulus.

The addition of this bi-layered structure produces more plate displacement than the single layered viscoelastic model for both a step change in velocity and a constant acceleration stimulus. In fact, the gel's lower layer (columnar filament), where the hair follicles are located, produce even greater displacement. The movement of these hair follicles send two distinct types of sensory signals to the hair cells which ultimately transmits a signal to the Central Nervous System, where these signals are utilized to provide changes in visual fixation and postural control.

References

1 Ballantyne, J., "Anatomy of the Ear". Ultrastructure Atlas of the Inner Ear. Butterworths, London, 1984.

2 Carlstrom, D., "Crystallographic Studies of the Vertebrae Otoliths". *Biological Bulletin*. 125:441-463, 1963.

3 Cotton, J., "A viscoelastic Model for the Response to a Step Change in Velocity of the Human Otolith Organs", Masters Thesis, Virginia Polytechnic Institute and State University, June 1984.

4 DeVries H. L., "Mechanics of the Labyrinth Organs". *Acta Otolaryngol.* 38:262-73, 1950.

5 Grant, J.W., W. A. Best, R. LoNigro R., "Governing Equations of Motion for the Otolith Organs and Their Response to a Step Change in Velocity of the Skull". *Journal of Biomechanical Engineering*. 106:302-8, 1984.

6 Grant, J.W., W. A. Best, "Otolith Organ Mechanics: Lumped Parameter Model and Dynamic Response". *Avia. Space Environ. Med.* 58:970-6, 1987.

7 Grant, J.W. and J. Cotton, "A Model for Otolith Dynamic Response with a Viscoelastic Gel Layer". *Journal of Vestibular Research.* 1:139-51, 1991.

8 Grant, J.W., "Vestibular Mechanics". *Handbook of Biomedical Engineering*. 39:517-27, 1995.

9 Graybiel, A., "The Importance of the Otolith Organs in Man Based Upon a Specific Test for Utricular Function". *Ann. Otol.* 65:470, 1956.

10 Graybiel, A., "Oculogravic Illusion". *Arch. Opthal.* 48:605, 1952.

11 Graybiel, A., "Otolith Function and Human Performance". *Adv. Oto-Rhino-Laryng*. 20:485-519, 1973.

12 Kachar, B., M. Parakkal, J. Fex., "Structural Basis for Mechanical Transduction in the frog Vestibular Sensory Apparatus: I. The Otolithic Membrane". *Hearing Researc*h. 45:179-90, 1989.

13 Lim, D., "The Development and Structure of the Otoconia". *Ultrastructural Atlas of the Inner Ear*. Butterworths, London, 1984.

14 Mach, E., "Grundlinien der Lehre von den Bewegungsempfindungen", Leipzing: Wilhelm Engelmann, 1875.

15 Miller, E. F. II, A. Graybiel, "A Comparison of Occular Counterolling Movements between Normal persons and Deaf subjects with Bilateral Labyrinthine defects". *Ann. Otol.* 72: 885-83, 1963.

16 Miller, E. F. II, "Evaluation of Otolith Organ Function by Means of Occular Counterolling Measurements". Vestibular Function on Earth and in Space. J. Stahle, Ed., Oxford, England:1970.

17 Spoendlin, H. H., "Ultrastructural Studies of the Labyrinth in Squirrel Monkeys". *The First Symposium on the Role of the Vestibular Organ in the Space Exploration*: NASA SP-77:7-22, 1965.

18 Von Rosenberg, D. U., *Methods for the Numerical Solution Partial Differential Equations*, p.113. Gerald Farrar and Assoc., Inc., Publishing Division, Tulsa, 1969.

19 Wersäll, J. and P.G. Lundquist, "Morphological Polarization of the Mechanoreceptors of the Vestibular and Acoustic Systems", *Second Symposium on the Role of the Vestibular Organs in Space Exploration*: NASA SP-115: 57-71, 1966.

20 Young, L. R. et. al., "Occular Torsion on Earth and in Weightlessness". *Annals of the New York Academy of Science*. 374:80-92, 1981.

21 Young, L. R. and J. L. Meiry, "A Revised Dynamic Otolithic Model". *Aerospace Med.* 39:606-8, 1968.

Appendix A


```
%Solutions of the Distributed Otolith problem using Finite Differences
%Version: dl(i,n+1)=dl(i,n)+(u(i,n+1))dt
%        First order correct derivatives for the otoconial layer

  %i=spatial index; n=time index - n=1:t=0; n=2:t=dt; n=3:t=2*dt; ...
  %p=solid otoconial layer location, q=fluid boundary location; q>p+1;
  %Note: The gov. eqns are designed for point  p  to be 1 unit above 0
  %     ex.: for dys=0.05 and p=21 there are 20  space steps between 1 & p
  %nmax=number of time steps
p=26; q=153; r=8; nmax=200;
  %Constants
R=0.5;
e1=.1; M1=17; k=1;
e2=.1;  M2=20;
dyf=0.04;  dys=dyg=0.04;
dt=.00005;

   %sizing matrices
u=zeros(q,nmax);
dl=zeros(p,nmax);
%*******************
dlp=zeros(1,nmax);
%*******************
a=zeros(1,q);
b=zeros(1,q);
c=zeros(1,q);
d=zeros(1,q);
t=zeros(1,nmax);
  %InitialConditions
u(p,2)=1-R;
%Time step loop
for n=2:nmax,

 %Difference Equations

    %GEL LAYER 1
 b(2)=R*dys*dys/dt+2*e1*dt+2*M1;
 c(2)=-(e1*dt+M1);
 d(2)=(R*dys*dys/dt)*u(2,n)+e1*(dl(1,n)-2*dl(2,n)+dl(3,n));
 for i=3:r-1,
   a(i)=-(e1*dt+M1);
   b(i)=R*dys*dys/dt+2*e1*dt+2*M1;
   c(i)=-(e1*dt+M1);
   d(i)=(R*dys*dys/dt)*u(i,n)+e1*(dl(i-1,n)-2*dl(i,n)+dl(i+1,n));
 end
```

```
    % i=r, INTERMEDIATE GEL LAYER
   a(r)=-2*(e1*dt+M1);
    b(r)=2*(R*dys*dys/dt+2*e1*dt+2*M1);
   c(r)=-2*(e2*dt+M2);
   d(r)=2*(R*dys*dys/dt)*u(r,n)+(2*e1)*dl(r-1,n)-2*(e1+e2)*dl(r,n)+(2*e2)*dl(r+1,n);

    % GEL LAYER 2
 for i=r+1:p-1,
   a(i)=-(e2*dt+M2);
    b(i)=R*dys*dys/dt+2*e2*dt+2*M2;
   c(i)=-(e2*dt+M2);
   d(i)=(R*dys*dys/dt)*u(i,n)+e2*(dl(i-1,n)-2*dl(i,n)+dl(i+1,n));
 end

    %PLATE
  a(p)=(-e2*dt-M2);
  b(p)=dys/dt+k*dys/dyf+e2*dt+M2;
  c(p)=(-k*dys/dyf);
  d(p)=(dys/dt)*u(p,n)-e2*(dl(p,n)-dl(p-1,n));
%a(p)=(-2*e2*dt-2*M2);
%b(p)=2*dys/dt+2*k*dys/dyf+R*dys/dt*(dyf+dys)+2*e2*dt+2*M2;
%c(p)=(-2*k*dys/dyf);
%d(p)=(2*dys/dt+R*k*dys*dyf/dt+R*dys*dys/dt)*u(p,n)+e2(-2*dl(p,n)+2*dl(p-1,n));

    %FLUID
 for i=p+1:q-2,
  a(i)=-k;
  b(i)=R*dyf*dyf/dt+2*k;
  c(i)=-k;
  d(i)=(R*dyf*dyf/dt)*u(i,n);
end
  a(q-1)=-k;
  b(q-1)=R*dyf*dyf/dt+2*k;
  d(q-1)=(R*dyf*dyf/dt)*u(q-1,n);

 %Solution by Thomas Algorithm
bt(2)=b(2);
ga(2)=d(2)/b(2);
for i=3:q-1,
 bt(i)=b(i)-a(i)*c(i-1)/bt(i-1);
 ga(i)=(d(i)-a(i)*ga(i-1))/bt(i);
end
 %back substitution step
u(q-1,n+1)=ga(q-1);
for j=q-2:-1:2,
```

```
    u(j,n+1)=ga(j)-c(j)*u(j+1,n+1)/bt(j);
  end
  for i=2:p,
    dl(i,n+1)=dl(i,n)+u(i,n+1)*dt;
  end
%**********************
 dlp(n+1)=dl(p,n+1);
%**********************
 t(n+1)=t(n)+dt;
 if n>=100
   dt=1.1*dt;
 end
 end

%Otoconaial Layer Displacement print out
hold on
%****************
%plot(t,dlp,'-')
%****************
grid

%Save displacements to another file
%**********************
%save dsp10.mat t dlp10
%**********************
%Velocity Profile print out
%ys(1)=0;
%for i=2:q
%  ys(i)=ys(i-1)+dys;
%end
%for i=1:q
%  us2(i)=u(i,2);
%  us10(i)=u(i,10);
%  us50(i)=u(i,50);
%  us100(i)=u(i,100);
%end
%plot(ys,us2,ys,us10,ys,us50,ys,us100);
%grid

%Displacement Profile print out
ys(1)=0;
for i=2:p
  ys(i)=ys(i-1)+dys;
end
for i=1:p
   %dlp1(i)=dl(i,1);
```

```
    %dlp2(i)=dl(i,2);
    %dlp3(i)=dl(i,3);
    %dlp4(i)=dl(i,4);
    %dlp5(i)=dl(i,5);
    %dlp6(i)=dl(i,6);
    %dlp7(i)=dl(i,7);
    %dlp8(i)=dl(i,8);
    %dlp9(i)=dl(i,9);
    %dlp10(i)=dl(i,10);
    %dlp15(i)=dl(i,15);
    %dlp20(i)=dl(i,20);
    %dlp25(i)=dl(i,25);
    dlp50(i)=dl(i,50);
    dlp75(i)=dl(i,75);
    dlp100(i)=dl(i,100);
    dlp125(i)=dl(i,125);
    dlp135(i)=dl(i,135);
    dlp145(i)=dl(i,145);
    dlp150(i)=dl(i,150);
    %dlp160(i)=dl(i,160);
    %dlp170(i)=dl(i,170);
    %dlp180(i)=dl(i,180);
    %dlp190(i)=dl(i,190);
    %dlp200(i)=dl(i,200);
end
hold on

%plot(dlp1,ys,dlp2,ys,dlp3,ys,dlp4,ys,dlp5,ys,dlp6,ys,dlp7,ys,dlp8,ys,dlp9,ys,dlp10,ys);
 plot(dlp50,ys,dlp75,ys,dlp100,ys,dlp125,ys,dlp135,ys,dlp145,ys,dlp150,ys);
%plot(dlp150,ys,dlp160,ys,dlp170,ys,dlp180,ys,dlp190,ys,dlp200,ys);
grid


 gtext('t=0.0025');gtext('t=0.00375');gtext('t=0.005');gtext('t=0.00625');gtext('t=0.00675');gtext('t=0.00725')
%gtext('dlp150');gtext('dlp160');gtext('dlp170');gtext('dlp180');gtext('dlp190');gtext('dlp200');

title('Displacement Profiles - cr=1: c1=.1, c2=.1, Mr=0.85: M1=17, M2=20, dt=.00005, nmax=200')
xlabel('dlp - displacement')
ylabel('y - depth')
```

Appendix B


```
%Solutions of the Distributed Otolith problem using Finite Differences
%Version: dl(i,n+1)=dl(i,n)+(u(i,n+1))dt
%       First order correct derivatives for the otoconial layer

 %i=spatial index; n=time index - n=1:t=0; n=2:t=dt; n=3:t=2*dt; ...
 %p=solid otoconial layer location, q=fluid boundary location; q>p+1;
 %Note: The gov. eqns are designed for point  p  to be 1 unit above 0
 %     ex.: for dys=0.05 and p=21 there are 20  space steps between 1 & p
 %nmax=number of time steps
p=26; q=153; r=8; nmax=200;
 %Constants
R=0.5;
e1=.1; M1=17; k=1;
e2=.1;  M2=20;
dyf=0.04; dys=dyg=0.04;
dt=.00005;

  %sizing matrices
u=zeros(q,nmax);
dl=zeros(p,nmax);
%*******************
dlp=zeros(1,nmax);
%*******************
a=zeros(1,q);
b=zeros(1,q);
c=zeros(1,q);
d=zeros(1,q);
t=zeros(1,nmax);
 %InitialConditions
u(p,2)= u(p,3);
%Time step loop
for n=2:nmax,

%Difference Equations

   %GEL LAYER 1
 b(2)=R*dys*dys/dt+2*e1*dt+2*M1;
 c(2)=-(e1*dt+M1);
 d(2)=(R*dys*dys/dt)*u(2,n)+e1*(dl(1,n)-2*dl(2,n)+dl(3,n));
 for i=3:r-1,
  a(i)=-(e1*dt+M1);
  b(i)=R*dys*dys/dt+2*e1*dt+2*M1;
  c(i)=-(e1*dt+M1);
  d(i)=(R*dys*dys/dt)*u(i,n)+e1*(dl(i-1,n)-2*dl(i,n)+dl(i+1,n));
end
```

```
    % i=r, INTERMEDIATE GEL LAYER
   a(r)=-2*(e1*dt+M1);
    b(r)=2*(R*dys*dys/dt+2*e1*dt+2*M1);
   c(r)=-2*(e2*dt+M2);
   d(r)=2*(R*dys*dys/dt)*u(r,n)+(2*e1)*dl(r-1,n)-2*(e1+e2)*dl(r,n)+(2*e2)*dl(r+1,n);

    % GEL LAYER 2
 for i=r+1:p-1,
   a(i)=-(e2*dt+M2);
    b(i)=R*dys*dys/dt+2*e2*dt+2*M2;
   c(i)=-(e2*dt+M2);
   d(i)=(R*dys*dys/dt)*u(i,n)+e2*(dl(i-1,n)-2*dl(i,n)+dl(i+1,n));
 end

    %PLATE
  a(p)=(-e2*dt-M2);
  b(p)=dys/dt+k*dys/dyf+e2*dt+M2;
  c(p)=(-k*dys/dyf);
  d(p)=(dys/dt)*u(p,n)-e2*(dl(p,n)-dl(p-1,n));
%a(p)=(-2*e2*dt-2*M2);
%b(p)=2*dys/dt+2*k*dys/dyf+R*dys/dt*(dyf+dys)+2*e2*dt+2*M2;
%c(p)=(-2*k*dys/dyf);
%d(p)=(2*dys/dt+R*k*dys*dyf/dt+R*dys*dys/dt)*u(p,n)+e2(-2*dl(p,n)+2*dl(p-1,n))+Δys(1-R);

    %FLUID
 for i=p+1:q-2,
  a(i)=-k;
   b(i)=R*dyf*dyf/dt+2*k;
  c(i)=-k;
   d(i)=(R*dyf*dyf/dt)*u(i,n);
end
  a(q-1)=-k;
   b(q-1)=R*dyf*dyf/dt+2*k;
   d(q-1)=(R*dyf*dyf/dt)*u(q-1,n);

 %Solution by Thomas Algorithm
bt(2)=b(2);
ga(2)=d(2)/b(2);
for i=3:q-1,
 bt(i)=b(i)-a(i)*c(i-1)/bt(i-1);
 ga(i)=(d(i)-a(i)*ga(i-1))/bt(i);
end
  %back substitution step
u(q-1,n+1)=ga(q-1);
for j=q-2:-1:2,
```

```
   u(j,n+1)=ga(j)-c(j)*u(j+1,n+1)/bt(j);
  end
  for i=2:p,
   dl(i,n+1)=dl(i,n)+u(i,n+1)*dt;
  end
 %**********************
 dlp(n+1)=dl(p,n+1);
 %**********************
 t(n+1)=t(n)+dt;
 if n>=100
   dt=1.1*dt;
 end
 end

 %Otoconaial Layer Displacement print out
 hold on
 %****************
 %plot(t,dlp,'-')
 %****************
 grid

 %Save displacements to another file
 %**********************
 %save dsp10.mat t dlp10
 %**********************
 %Velocity Profile print out
 %ys(1)=0;
 %for i=2:q
 %  ys(i)=ys(i-1)+dys;
 %end
 %for i=1:q
 %  us2(i)=u(i,2);
 %  us10(i)=u(i,10);
 %  us50(i)=u(i,50);
 %  us100(i)=u(i,100);
 %end
 %plot(ys,us2,ys,us10,ys,us50,ys,us100);
 %grid

 %Displacement Profile print out
 ys(1)=0;
 for i=2:p
   ys(i)=ys(i-1)+dys;
 end
 for i=1:p
    %dlp1(i)=dl(i,1);
```

```
    %dlp2(i)=dl(i,2);
    %dlp3(i)=dl(i,3);
    %dlp4(i)=dl(i,4);
    %dlp5(i)=dl(i,5);
    %dlp6(i)=dl(i,6);
    %dlp7(i)=dl(i,7);
    %dlp8(i)=dl(i,8);
    %dlp9(i)=dl(i,9);
    %dlp10(i)=dl(i,10);
    %dlp15(i)=dl(i,15);
    %dlp20(i)=dl(i,20);
    %dlp25(i)=dl(i,25);
    dlp50(i)=dl(i,50);
    dlp75(i)=dl(i,75);
    dlp100(i)=dl(i,100);
    dlp125(i)=dl(i,125);
    dlp135(i)=dl(i,135);
    dlp145(i)=dl(i,145);
    dlp150(i)=dl(i,150);
    %dlp160(i)=dl(i,160);
    %dlp170(i)=dl(i,170);
    %dlp180(i)=dl(i,180);
    %dlp190(i)=dl(i,190);
    %dlp200(i)=dl(i,200);
end
hold on

%plot(dlp1,ys,dlp2,ys,dlp3,ys,dlp4,ys,dlp5,ys,dlp6,ys,dlp7,ys,dlp8,ys,dlp9,ys,dlp10,ys);
 plot(dlp50,ys,dlp75,ys,dlp100,ys,dlp125,ys,dlp135,ys,dlp145,ys,dlp150,ys);
%plot(dlp150,ys,dlp160,ys,dlp170,ys,dlp180,ys,dlp190,ys,dlp200,ys);
grid


 gtext('t=0.0025');gtext('t=0.00375');gtext('t=0.005');gtext('t=0.00625');gtext('t=0.00675');gtext('t=0.00725');
%gtext('dlp150');gtext('dlp160');gtext('dlp170');gtext('dlp180');gtext('dlp190');gtext('dlp200');

title('Displacement Profiles - er=1: e1=.1, e2=.1, Mr=0.85: M1=17, M2=20, dt= 00005, nmax=200')
xlabel('dlp - displacement')
ylabel('y - depth')
```

Appendix C


```
%Solutions of the Distributed Otolith problem using Finite Differences
%Version: dl(i,n+1)=dl(i,n)+(u(i,n+1))dt
%         First order correct derivatives for the otoconial layer

  %i=spatial index; n=time index - n=1:t=0; n=2:t=dt; n=3:t=2*dt; ...
  %p=solid otoconial layer location, q=fluid boundary location; q>p+1;
  %Note: The gov. eqns are designed for point  p  to be 1 unit above 0
  %      ex.: for dys=0.05 and p=21 there are 20  space steps between 1 & p
  %nmax=number of time steps
p=26; q=153; r=8; nmax=500;
  %Constants
R=0.5;
e1=.1; M1=18; k=1;
e2=.1;  M2=20;
dyf=0.04; dys=dyg=0.04;
dt=.001;

    %sizing matrices
u=zeros(q,nmax);
dl=zeros(p,nmax);
%******************
dlp=zeros(1,nmax);
%******************
a=zeros(1,q);
b=zeros(1,q);
c=zeros(1,q);
d=zeros(1,q);
t=zeros(1,nmax);
   %InitialConditions
u(p,2)=1-R;
%Time step loop
for n=2:nmax,

  %Difference Equations

      %GEL LAYER 1
  b(2)=R*dys*dys/dt+2*e1*dt+2*M1;
  c(2)=-(e1*dt+M1);
  d(2)=(R*dys*dys/dt)*u(2,n)+e1*(dl(1,n)-2*dl(2,n)+dl(3,n));
  for i=3:r-1,
    a(i)=-(e1*dt+M1);
    b(i)=R*dys*dys/dt+2*e1*dt+2*M1;
    c(i)=-(e1*dt+M1);
    d(i)=(R*dys*dys/dt)*u(i,n)+e1*(dl(i-1,n)-2*dl(i,n)+dl(i+1,n));
  end

      % i=r, INTERMEDIATE GEL LAYER
    a(r)=-2*(e1*dt+M1);
    b(r)=2*(R*dys*dys/dt+2*e1*dt+2*M1);
    c(r)=-2*(e2*dt+M2);
    d(r)=2*(R*dys*dys/dt)*u(r,n)+(2*e1)*dl(r-1,n)-2*(e1+e2)*dl(r,n)+(2*e2)*dl(r+1,n);

      % GEL LAYER 2
  for i=r+1:p-1,
    a(i)=-(e2*dt+M2);
    b(i)=R*dys*dys/dt+2*e2*dt+2*M2;
```

```
    c(i)=-(e2*dt+M2);
    d(i)=(R*dys*dys/dt)*u(i,n)+e2*(dl(i-1,n)-2*dl(i,n)+dl(i+1,n));
  end

      %PLATE
    a(p)=(-e2*dt-M2);
    b(p)=dys/dt+k*dys/dyf+e2*dt+M2;
    c(p)=(-k*dys/dyf);
    d(p)=(dys/dt)*u(p,n)-e2*(dl(p,n)-dl(p-1,n));
%a(p)=(-2*e2*dt-2*M2);
%b(p)=2*dys/dt+2*k*dys/dyf+R*dys/dt*(dyf+dys)+2*e2*dt+2*M2;
%c(p)=(-2*k*dys/dyf);
%d(p)=(2*dys/dt+R*k*dys*dyf/dt+R*dys*dys/dt)*u(p,n)+e2(-2*dl(p,n)+2*dl(p-1,n));

      %FLUID
  for i=p+1:q-2,
    a(i)=-k;
    b(i)=R*dyf*dyf/dt+2*k;
    c(i)=-k;
    d(i)=(R*dyf*dyf/dt)*u(i,n);
  end
    a(q-1)=-k;
    b(q-1)=R*dyf*dyf/dt+2*k;
    d(q-1)=(R*dyf*dyf/dt)*u(q-1,n);

    %Solution by Thomas Algorithm
  bt(2)=b(2);
  ga(2)=d(2)/b(2);
  for i=3:q-1,
    bt(i)=b(i)-a(i)*c(i-1)/bt(i-1);
    ga(i)=(d(i)-a(i)*ga(i-1))/bt(i);
  end
    %back substitution step
  u(q-1,n+1)=ga(q-1);
  for j=q-2:-1:2,
    u(j,n+1)=ga(j)-c(j)*u(j+1,n+1)/bt(j);
  end
  for i=2:p,
    dl(i,n+1)=dl(i,n)+u(i,n+1)*dt;
  end
%**********************
 dlp(n+1)=dl(p,n+1);
%**********************
 t(n+1)=t(n)+dt;
 %if n>=100
   %dt=1.1*dt;
 %end
 end

%Otoconaial Layer Displacement print out
hold on
%***************
plot(t,dlp,'-')
%***************
grid

%Save displacements to another file
```

```
%**********************
%save dsp10.mat t dlp10
%**********************
%Velocity Profile print out
%ys(1)=0;
%for i=2:q
%  ys(i)=ys(i-1)+dys;
%end
%for i=1:q
%  us2(i)=u(i,2);
%  us10(i)=u(i,10);
%  us50(i)=u(i,50);
%  us100(i)=u(i,100);
%end
%plot(ys,us2,ys,us10,ys,us50,ys,us100);
%grid

%Displacement Profile print out
%ys(1)=0;
%for i=2:p
  % ys(i)=ys(i-1)+dys;
%end
%for i=1:p
    %dlp5(i)=dl(i,5);
    %dlp6(i)=dl(i,6);
    %dlp7(i)=dl(i,7);
    %dlp8(i)=dl(i,8);
    %dlp9(i)=dl(i,9);
    %dlp10(i)=dl(i,10);
    %dlp15(i)=dl(i,15);
    %dlp20(i)=dl(i,20);
    %dlp25(i)=dl(i,25);
    %dlp50(i)=dl(i,50);
    %dlp75(i)=dl(i,75);
    %dlp100(i)=dl(i,100);
    %dlp125(i)=dl(i,125);
    %dlp135(i)=dl(i,135);
    %dlp145(i)=dl(i,145);
    %dlp150(i)=dl(i,150);
    %dlp160(i)=dl(i,160);
    %dlp170(i)=dl(i,170);
    %dlp180(i)=dl(i,180);
    %dlp190(i)=dl(i,190);
    %dlp200(i)=dl(i,200);
%end
%hold on
%plot(dlp50,ys,dlp75,ys,dlp100,ys,dlp125,ys,dlp135,ys,dlp145,ys,dlp150,ys);
%plot(dlp5,ys,dlp6,ys,dlp7,ys,dlp8,ys,dlp9,ys,dlp10,ys);
%dlp25,ys,dlp50,ys,dlp75,ys);
%plot(dlp150,ys,dlp160,ys,dlp170,ys,dlp180,ys,dlp190,ys,dlp200,ys);
%grid

gtext('er=1, Mr=0.90');
title('Displacement vs. Time - p=26  q=153  r=8 dt=.001  nmax=500')
ylabel('dlp - displacement')
xlabel('t - time')
```

Appendix D


```
%Solutions of the Distributed Otolith problem using Finite Differences
%Version: dl(i,n+1)=dl(i,n)+(u(i,n+1))dt
%        First order correct derivatives for the otoconial layer

 %i=spatial index; n=time index - n=1:t=0; n=2:t=dt; n=3:t=2*dt; ...
 %p=solid otoconial layer location, q=fluid boundary location; q>p+1;
 %Note: The gov. eqns are designed for point  p  to be 1 unit above 0
 %     ex.: for dys=0.05 and p=21 there are 20  space steps between 1 & p
 %nmax=number of time steps
p=26; q=153; r=8; nmax=500;
 %Constants
R=0.5;
e1=.1; M1=10; k=1;
e2=1;  M2=10;
dyf=0.04; dys=dyg=0.04;
dt=.001;

  %sizing matrices
u=zeros(q,nmax);
dl=zeros(p,nmax);
%*******************
dlr=zeros(1,nmax);
%*******************
a=zeros(1,q);
b=zeros(1,q);
c=zeros(1,q);
d=zeros(1,q);
t=zeros(1,nmax);
 %InitialConditions
u(p,2)=1-R;
%Time step loop
for n=2:nmax,

%Difference Equations

   %GEL LAYER 1
 b(2)=R*dys*dys/dt+2*e1*dt+2*M1;
 c(2)=-(e1*dt+M1);
 d(2)=(R*dys*dys/dt)*u(2,n)+e1*(dl(1,n)-2*dl(2,n)+dl(3,n));
 for i=3:r-1,
  a(i)=-(e1*dt+M1);
  b(i)=R*dys*dys/dt+2*e1*dt+2*M1;
  c(i)=-(e1*dt+M1);
  d(i)=(R*dys*dys/dt)*u(i,n)+e1*(dl(i-1,n)-2*dl(i,n)+dl(i+1,n));
 end
```

```
    % i=r, INTERMEDIATE GEL LAYER
   a(r)=-2*(e1*dt+M1);
    b(r)=2*(R*dys*dys/dt+2*e1*dt+2*M1);
   c(r)=-2*(e2*dt+M2);
   d(r)=2*(R*dys*dys/dt)*u(r,n)+(2*e1)*dl(r-1,n)-2*(e1+e2)*dl(r,n)+(2*e2)*dl(r+1,n);

    % GEL LAYER 2
 for i=r+1:p-1,
   a(i)=-(e2*dt+M2);
    b(i)=R*dys*dys/dt+2*e2*dt+2*M2;
   c(i)=-(e2*dt+M2);
   d(i)=(R*dys*dys/dt)*u(i,n)+e2*(dl(i-1,n)-2*dl(i,n)+dl(i+1,n));
 end

    %PLATE
  a(p)=(-e2*dt-M2);
  b(p)=dys/dt+k*dys/dyf+e2*dt+M2;
  c(p)=(-k*dys/dyf);
  d(p)=(dys/dt)*u(p,n)-e2*(dl(p,n)-dl(p-1,n));
%a(p)=(-2*e2*dt-2*M2);
%b(p)=2*dys/dt+2*k*dys/dyf+R*dys/dt*(dyf+dys)+2*e2*dt+2*M2;
%c(p)=(-2*k*dys/dyf);
%d(p)=(2*dys/dt+R*k*dys*dyf/dt+R*dys*dys/dt)*u(p,n)+e2(-2*dl(p,n)+2*dl(p-1,n));

    %FLUID
 for i=p+1:q-2,
  a(i)=-k;
  b(i)=R*dyf*dyf/dt+2*k;
  c(i)=-k;
  d(i)=(R*dyf*dyf/dt)*u(i,n);
end
  a(q-1)=-k;
  b(q-1)=R*dyf*dyf/dt+2*k;
  d(q-1)=(R*dyf*dyf/dt)*u(q-1,n);

 %Solution by Thomas Algorithm
bt(2)=b(2);
ga(2)=d(2)/b(2);
for i=3:q-1,
 bt(i)=b(i)-a(i)*c(i-1)/bt(i-1);
 ga(i)=(d(i)-a(i)*ga(i-1))/bt(i);
end
  %back substitution step
u(q-1,n+1)=ga(q-1);
for j=q-2:-1:2,
```

```
   u(j,n+1)=ga(j)-c(j)*u(j+1,n+1)/bt(j);
  end
  for i=2:p,
   dl(i,n+1)=dl(i,n)+u(i,n+1)*dt;
  end
%**********************
 dlr(n+1)=dl(r,n+1);
%**********************
 t(n+1)=t(n)+dt;
 %if n>=100
  %dt=1.1*dt;
 %end
 end

%Otoconaial Layer Displacement print out
hold on
%****************
plot(t,dlr,'-')
%****************
grid

%Save displacements to another file
%**********************
%save dsp10.mat t dlp10
%**********************
%Velocity Profile print out
%ys(1)=0;
%for i=2:q
%  ys(i)=ys(i-1)+dys;
%end
%for i=1:q
%  us2(i)=u(i,2);
%  us10(i)=u(i,10);
%  us50(i)=u(i,50);
%  us100(i)=u(i,100);
%end
%plot(ys,us2,ys,us10,ys,us50,ys,us100);
%grid

%Displacement Profile print out
%ys(1)=0;
%for i=2:p
  % ys(i)=ys(i-1)+dys;
%end
%for i=1:p
   %dlp5(i)=dl(i,5);
```

```
    %dlp6(i)=dl(i,6);
    %dlp7(i)=dl(i,7);
    %dlp8(i)=dl(i,8);
    %dlp9(i)=dl(i,9);
    %dlp10(i)=dl(i,10);
    %dlp15(i)=dl(i,15);
    %dlp20(i)=dl(i,20);
    %dlp25(i)=dl(i,25);
    %dlp50(i)=dl(i,50);
    %dlp75(i)=dl(i,75);
    %dlp100(i)=dl(i,100);
    %dlp125(i)=dl(i,125);
    %dlp135(i)=dl(i,135);
    %dlp145(i)=dl(i,145);
    %dlp150(i)=dl(i,150);
    %dlp160(i)=dl(i,160);
    %dlp170(i)=dl(i,170);
    %dlp180(i)=dl(i,180);
    %dlp190(i)=dl(i,190);
    %dlp200(i)=dl(i,200);
%end
%hold on
 %plot(dlp50,ys,dlp75,ys,dlp100,ys,dlp125,ys,dlp135,ys,dlp145,ys,dlp150,ys);
%plot(dlp5,ys,dlp6,ys,dlp7,ys,dlp8,ys,dlp9,ys,dlp10,ys);
%dlp25,ys,dlp50,ys,dlp75,ys);
%plot(dlp150,ys,dlp160,ys,dlp170,ys,dlp180,ys,dlp190,ys,dlp200,ys);
%grid

gtext('er=.1,Mr=1');
title('Displacement vs. Time - p=26; q=153; r=8; nmax=500;dt=.001')
ylabel('dlr - displacement')
xlabel('t - time')
```

Vita

Name: **Mirtis Denise Coggins**

Place of Birth: **Washington, D.C.**

Education:

Virginia Polytechnic and State University, 1996
M.S., Engineering Science and Mechanics with
Biomechanics Concentration

Delaware State University, 1994
B.S., Physics with Engineering Emphasis and Mathematics

Work Experience:

Graduate Teaching Assistant, 1994-1996
Virginia Polytechnic and State University
Blacksburg, Virginia

Neuroscience Research Assistant, 1994
National Institutes of Health
Bethesda, Maryland

Science Demonstrator, 1992-1994
National Air & Space Museum
Southwest, Washington, D.C.